DETONATION HAZARD CLASSIFICATION BASED ON THE CRITICAL ORIFICE PLATE DIAMETER FOR DETONATION PROPAGATION

by

Mitchell Cross

A thesis submitted to the Department of Mechanical and Materials Engineering

In conformity with the requirements for

the degree of Master of Applied Science

Queen's University

Kingston, Ontario, Canada

(August, 2015)

Abstract

Accidental explosions in the chemical, oil & gas industry are a serious problem. The ultimate objective of this thesis is to establish a new parameter/process that can be used to categorize the relative detonation explosion hazard of a fuel that can be measured in a smaller, more practical apparatus. Experiments were carried out in an apparatus consisting of a 6.1 m long (composed of 2 equal length sections), 100 mm inner-diameter tube. A detonation was initiated in the first half of the tube using an acetylene-oxygen driver ignited by a weak spark. The second half of the tube contained orifice plates equally spaced at the tube diameter. Six different orifice plate diameters between 38.1 mm (1.5″) and 76.2 mm (3″), in increments of 6.4 mm (1/4″) were used in the study. The average combustion front velocity was obtained from time-of-arrival measurements deduced from ionization probe signals. The critical (minimum) orifice plate diameter required for successful transmission of a detonation from a smooth tube was measured for different stoichiometric fuel-air mixtures. The ratio of the critical orifice plate diameter (d) and the mixture detonation cell size (λ) varies strongly with the orifice plate blockage ratio (BR), with a value approaching unity ($d/\lambda \rightarrow 1$) with decreasing blockage ratio. It is proposed that the critical orifice plate diameter could be used to categorize the detonation hazard potential of single or multi-component fuels. Additional experiments were performed in same apparatus to measure the Deflagration to Detonation Transition (DDT) and detonation propagation limits (distinguished by the method of initiation). Both the propagation and the DDT limits narrow with increasing BR, more significantly for the DDT limits. The narrowing of the limits with increasing BR also corresponds to a larger deviation from the $d/\lambda=1$ detonation limit criterion. These results indicate that the beneficial effects of the orifice plate in providing a reflection surface diminishes with increased BR due to the increased effect of shock wave weakening by the diffraction process. Novel use of soot foils showed that the structure of the detonation wave is very non-uniform and highly unsteady, characterized by local detonation initiation and failure.

Acknowledgements

I would like to start by thanking my supervisor, Gaby Ciccarelli, for his constant support making this whole process as successful and enjoyable as it has been.

Next I would like to thank my friends and colleagues, Mark Kellenberger, JD MacLean, and Andrew House for their support and encouragement on a daily basis.

Access to the McLaughlin Hall machine shop and its staff was a priceless asset in the design and machining of my apparatus. They have consistently gone above and beyond when asked for assistance throughout this project. For that I would like to thank Andy Bryson, Corey Fowler, Derek Hodgson, and Paul Moreland. I would also like to acknowledge Onno Oosten for his constant technical support.

Last but not least, I would like to thank my family and fiancé, Aven Allen, for their unwavering support and love. I could not have done this without you all.

Table of Contents

List of Figures

List of Tables

Nomenclature and Symbols

Abbreviations

ANSI	American National Standards Institute
ASME	American Society of Mechanical Engineers
BR	Blockage Ratio
CJ	Chapman Jouguet
DAQ	Data Acquisition
DC	Direct Current
DDT	Deflagration to Detonation Transition
DME	Dimethyl Ether
NI	National Instruments
ZND	Zeldovich, von Neumann, and Döring

Symbols

A	Arrhenius Constant
a	Speed of Sound
C_p	Constant Pressure Specific Heat
C_v	Constant Volume Specific Heat
D	Tube Diameter
d	Orifice Plate Diameter
d_c	Critical Tube/Orifice Diameter
E_a	Activation Energy

E_c	Critical Initiation Energy
h	Enthalpy
h_f°	Heat of Formation
IP	Ionization Probe
k	Ratio Specific Heats
L	Characteristic Size (created by Dorofeev et al.)
L_c	Cell Length
l_i	Induction Zone Length
M	Mach Number
M_{CJ}	Mach Number at CJ state
P	Pressure
q	Heat Transfer (release)
$\overline{q}$	Rate of Heat Transfer
R	Universal Gas Constant
s	Entropy
S	Obstacle Spacing
T	Temperature
u	Velocity
V	Voltage
Δ	Reaction zone length
λ	Cell Width
ρ	Density
Φ	Equivalence Ratio: Air – Fuel ratio

Chapter 1

Introduction

1.1 Project Overview

There are two distinct modes of combustion. Deflagration (commonly referred to as a flame) represents the subsonic mode of combustion that is governed by the diffusion process of mass and heat. The supersonic combustion mode is detonation, and it is governed by adiabatic shock heating. Deflagrations typically propagate at a rate of only a few meters per second, whereas detonations commonly propagate in the range of a couple of thousand meters per second [1]. The detonation mode of combustion presents a large risk from an industrial safety point of view due to the extremely high shock overpressure associated with the high propagation velocity. The energy required to initiate a direct detonation of a gaseous fuel is also relatively large. The measured order of magnitude required for direct detonation initiation of a free cloud is 10 – 1000 kJ for Hydrogen-air mixtures of varying equivalence ratio. A deflagration can be ignited within a similar mixture, with as little as a few millijoules [2]. This is why industrial explosions typically start from a weak ignition source, such as static discharge producing a slow moving deflagration. Although static discharge is common, there are an abundance of possible weak ignition sources. The transition from a subsonic deflagration to a supersonic detonation is possible through the process of flame acceleration and is often referred to as deflagration-to-detonation transition (DDT). The flame acceleration leading up to DDT is highly dependent on the fuel mixture composition as well as the surrounding geometry and has been thoroughly studied over past century.

The study of flame acceleration and the detonation phenomenon goes back to the work of Mallard and Le Chatelier [3]. Their work stemmed from the prevalence of coal mine explosions in the late 1800s due to the high demand for the popular fuel source. The continuous increase in

the world demand for energy and the push towards environmentally friendly sources has resulted in the emergence of alternative fuels. These alternative fuels, such as methanol and ethanol, pose an unknown explosion hazard in their production, transportation, storage, and use. The current methodology of characterizing detonation sensitivity developed by Peraldi et al. and Dorofeev et al. respectively, provide a reasonable estimation of the detonation propagation limits of a fuel in an obstacle filled tube [4, 5]. However, the application of these criteria is limited by the reliability of the detonation cell size (to be defined in the next chapter) as a scaling parameter for a fixed range of mixtures and initial conditions [2]. Detonation cell-size data is available for common fuels but has an inherent uncertainty associated with its measurement. This uncertainty can be as large a ±50% of the measured value [6]. The large uncertainty associated with cell size measurements makes the application of these criteria inappropriate for industrial safety applications. A new parameter is required that can be used to categorize detonation explosion hazard of a fuel and the improvement of industrial explosion safety codes.

This multi-part project involves the measurement of DDT and Detonation Propagation limits of various fuels in an obstacle filled tube. In the first part of the study the objective was to look more closely at the DDT limits in an obstacle filled tube. Specifically, to determine if the measured detonation composition limits are dictated by the DDT event, or by the detonation wave propagation requirements. This was done by comparing the composition limits obtained from the classical flame acceleration and DDT obstacle filled tube experiment and a new approach, where a steady detonation wave is transmitted from a smooth tube into an obstacle filled tube. For both set-ups, the limit for successful transmission from the obstacle-section into the smooth tube was also obtained in order to gain insight into the propagation mechanism of the detonation wave in the obstacle section. Additionally, the soot-foil technique was used to provide insight into the detonation wave propagation mechanism in the obstacle filled tube. This soot-foil method will be

discussed in a later chapter.These tests were done with several fuel-air mixtures in order to confirm the universality of the results.

In the second part of this study a new methodology was developed to characterize the detonation sensitivity of a fuel-air mixture. As part of this methodology, a new experimentally measured parameter was developed called the critical (minimum) orifice plate diameter. The parameter represents the smallest orifice plate diameter for which a detonation wave can propagate through an orifice plate filled tube. These tests were done using the method described above, where for a given stoichiometric fuel-air mixture a detonation wave is transmitted from a smooth tube into an obstacle filled tube where the orifice plate diameter is increased until the detonation wave successfully propagates. This detonation sensitivity method is desirable for the reasons it does not require a large-scale apparatus or use of controlled solid explosives, like existing approaches. These tests were run with a number of different test fuels such as Hydrogen, Ethylene, Acetylene, Propane, Dimethyl ether (DME), and Methane, in order to classify them in terms of their relative detonation hazard . These fuels were chosen based on concurrent research in the Queen's University Combustion Lab and popularity in the combustion research field.

The principal contribution of this project is the large quantity of flame acceleration and detonation propagation data that was produced for several different fuel-air mixtures and orifice plate diameters. This data can be used to characterize the detonation sensitivity of a fuel that is more practical than existing approaches. The novel application of the soot foil technique increases understanding of the propagation mechanism of a detonation wave in an obstacle filled tube.

Chapter 2

Detonation Theory

This chapter provides a concise review of theory relevant to the current study. The objective is to provide the reader with the necessary information to understand the motivation for this work.

2.1 Introduction

Combustion can occur in one of two different modes, e.g., a deflagration or detonation. Deflagration represents the subsonic mode of combustion that is more prevalent in common engineering applications. Deflagrations are governed by the molecular transport of heat and mass, which limits the one-dimensional laminar burning velocity (flame velocity relative to unburned gas velocity) to typically less than 1m/s for fuel-air mixtures at atmospheric conditions [3]. When a flame is ignited at the closed-end of a channel it will propagate at a flame speed higher than the laminar burning velocity due to the expansion of the combustion products (products have a lower density than the unreacted gas). The flame velocity increases with increased flame surface associate with a non-uniform velocity profile in the unburned gas, as well as with the presence of turbulence. Bulk velocity and non-uniformities and turbulence are generated when a flame propagates in a duct equipped with obstacles. Expansion of the combustion products induces a flow in the unburned gas ahead of the flame. The larger the flame area the higher the volumetric burning rate, which translates into a higher unburned gas velocity that translates to a higher flame velocity. This positive feedback mechanism between the unburned gas velocity and the flame area results in flame acceleration. Flame acceleration can result in velocities as high as the speed of sound in the combustion products, i.e., around 1000 m/s for stoichiometric hydrogen-air. A deflagration travelling at this velocity is termed a “fast” or “choked” flame.

Detonation represents the less commonly experienced supersonic mode of combustion (unburned gas velocity relative to the combustion wave is supersonic). A detonation wave is characterized by a propagating lead shock and a coupled trailing-reaction zone travelling up to a couple of thousand meters per second for fuel-air mixtures. Detonations are able to propagate at a constant velocity well above the speed of sound in the unburned gas through the mechanism of adiabatic shock heating. This mechanism describes the adiabatic compression of the unburned mixture by the shock wave. Adiabatic compression of the reactants initiates the rapid chemical reaction or auto-ignition necessary for the system to propagate at a constant velocity that depends on the energy content of the fuel. This propagating wave system can generate overpressures of around 20 bars [7]. The pressure rise across a detonation wave presents a significant hazard for the safe storage, transportation and use of reactive gases and is the main reason why detonations are studied for industrial safety applications. The focus of this review will be on the detonative mode of combustion, including the transition from a deflagration to a detonation.

2.2 Combustion Propagation Regimes

As discussed above, there are two general modes of combustion, detonation and deflagration. These modes are very general titles which can be broken down into more specific categories based on the strength of the detonation/deflagration and the boundary conditions of the system. Figure 2.1 shows typical average flame velocity measurements made at the end of an obstacle filled tube (following flame acceleration) for different hydrogen-air mixture compositions.

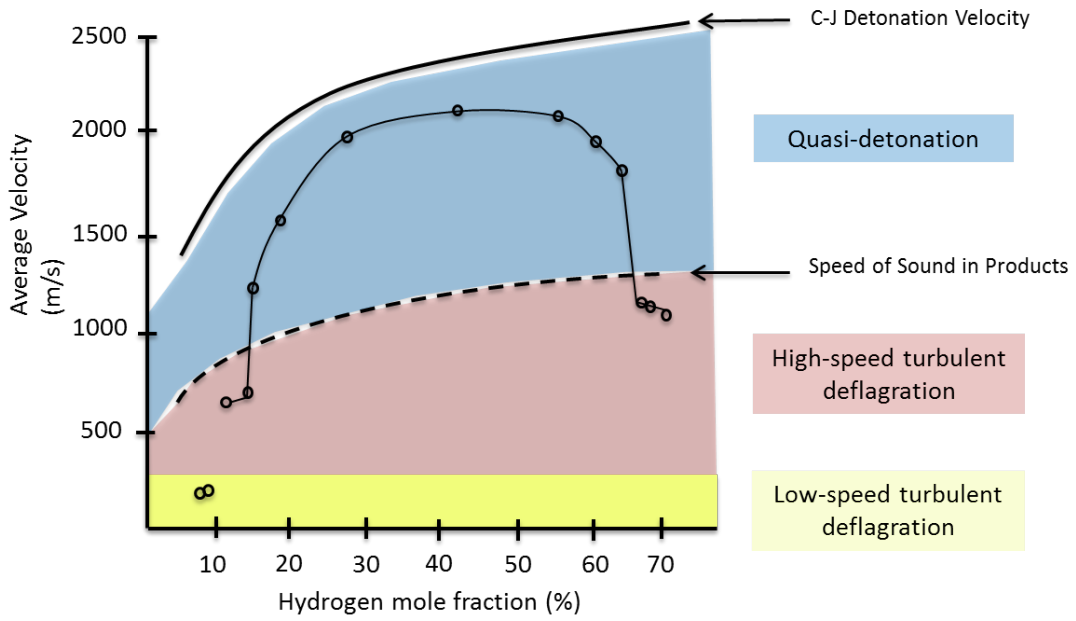

Figure 2.1: A typical velocity versus mole fraction curve for DDT tests in an obstacle filled tube. The Chapman-Jouguet (CJ) detonation velocity and speed of sound in the products are shown for reference.

Once the flame reaches a quasi-steady velocity in the obstacle section, three quasi-steady propagation regions are possible: low-speed turbulent deflagration, high-speed turbulent deflagration, and quasi-detonation. Low-speed deflagrations propagate at subsonic velocity typically below 200 m/s; high-speed deflagrations propagate at a velocity between the speed of sound of the unburned and burned gas (calculated based on adiabatic constant pressure combustion); quasi-detonations propagate at a velocity between the burned gas speed of sound and the theoretical detonation velocity. A quasi detonation propagates at a velocity deficit from the theoretical detonation velocity due to the failure and re-initiation of the detonation wave between obstacles. The size of this deficit depends largely on the reactivity of the mixture and the obstacle geometry. These propagation regimes will be discussed in more detail later in this thesis.

2.3 One Dimensional Detonation Wave

The pioneering work of Mallard and Le Châtelier [8] demonstrated the possibility of two modes of combustion in the same gaseous mixture. This was the first significant study of detonation waves where a transition from deflagration to detonation was observed and marked the discovery of the detonation phenomenon. After the discovery of the detonation phenomenon Chapman [9] and Jouguet [10] independently introduced a quantitative theory used to predict the detonation velocity of an explosive gas mixture. This theory is known as the Chapman-Jouguet (CJ) Theory.

The CJ theory is used to find the unique solution to the one-dimensional conservation equations across the detonation front. The theory assumes an equilibrium is reached downstream of the wave and that all the energy released in the detonation wave occurred instantaneously across the shock, i.e., neglecting the presence of a reaction zone. Based on this a one-dimensional thermodynamic model was developed, where mass, momentum, and energy were balanced across a control volume surrounding the detonation wave front. The control volume shown in Figure 2.2 surrounds the entire detonation wave where the unburned reactants enter the control volume at the detonation wave velocity, indicated by state 1, and exit as combustion products at state 2.

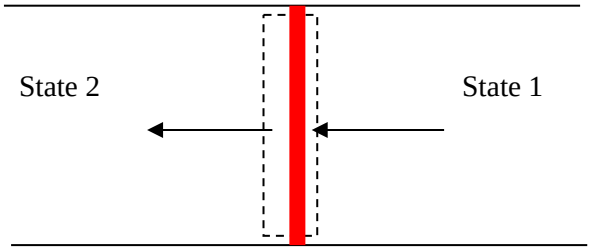

Figure 2.2: CJ one-dimensional thermodynamic model. Steady-state combustion occurs within the control volume and equilibrium is achieved at state 2 [11].

The one-dimensional, steady conservation equations are

Conservation of mass

$$\rho_1 u_1 = \rho_2 u_2 \qquad \textbf{(2.1)}$$

Conservation of momentum

$$P_2 - P_1 = \rho_1 u_1 (u_1 - u_2) \quad \textbf{(2.2)}$$

Conservation of Energy

$$\frac{{u_1}^2}{2} + h_1 = \frac{{u_2}^2}{2} + h_2 \quad \textbf{(2.3)}$$

Assuming a perfect gas provides the following two additional equations

$$P = \rho R T \quad \textbf{(2.4)}$$

$$h = h_f^\circ + c_p (T - T^\circ) \quad \textbf{(2.5)}$$

where T°= 298K and h_f^o represents the heat of formation at standard conditions

Applying Equations (2.4) & (2.5) to (2.3), the energy equation becomes

$$\frac{{u_1}^2}{2} + c_{p_1} T_1 + q = \frac{{u_2}^2}{2} + c_{p_2} T_2 \quad \textbf{(2.6)}$$

Where q is the chemical energy per unit mass

$$q = h_{f_1}^\circ + h_{f_2}^\circ \quad \textbf{(2.7)}$$

This system of equations has 5 unknowns (P_2, ρ_2, T_2, u_2, u_1) and only 4 equations.

The Rayleigh equation is obtained by combining the conservation of mass and momentum, Equations (2.1) & (2.2) respectively.

$$\frac{P_2}{P_1} = -\left(\frac{\rho_1 {u_1}^2}{P_1}\right)\frac{\rho_1}{\rho_2} + \left(1 + \frac{\rho_1 {u_1}^2}{P_1}\right) \quad \textbf{(2.8)}$$

The Hugoniot equation is obtained by combining the conservation of momentum and energy, Equations (2.2) & (2.3) respectively.

$$c_p T_2 - \left(c_p T_1 + q\right) = \frac{1}{2}(P_2 - P_1)\left(\frac{1}{\rho_1} + \frac{1}{\rho_2}\right) \quad \textbf{(2.9)}$$

Assuming constant specific heat across the detonation wave, i.e., $k_1 = k_2 = k$

$$\left(\frac{k}{k-1}\right)\left[\left(\frac{\rho_1}{\rho_2}\right)\left(\frac{P_2}{P_1}\right)-1\right]-\frac{\rho_1 q}{P_1}=\frac{1}{2}\left(\frac{P_2}{P_1}-1\right)\left(1+\frac{\rho_1}{\rho_2}\right) \qquad \textbf{(2.10)}$$

Where the chemical energy released can be defined as a function of initial sensible energy content, Equation (2.11). When applied to the case of a shock wave, where there is no chemical reaction (q = 0), one gets

$$\left(\frac{k}{k-1}\right)\left[\left(\frac{\rho_1}{\rho_2}\right)\left(\frac{P_2}{P_1}\right)-1\right]-\frac{(k-1)q}{c_v T_1}=\frac{1}{2}\left(\frac{P_2}{P_1}-1\right)\left(1+\frac{\rho_1}{\rho_2}\right) \qquad \textbf{(2.11)}$$

This equation, often referred to as the Hugoniot equation, gives all the possible end-states for a specified heat release. The blue colored curve in Figure 2.3 represents the Shock Hugoniot obtained from Equation (2.11) with no heat release (q = 0). The red colored curve represents the Equilibrium Hugoniot where there is chemical reaction resulting in heat release ($q \neq 0$). The CJ state is the unique solution corresponding to the point where the Rayleigh line, Equation (2.8), is tangent to the Hugoniot curve (Equation (2.11)), shown graphically in Figure 2.3. It can also be shown that this state represents the minimum possible entropy rise across the detonation wave and the flow at state 2, exiting the control volume, is choked (M_2=1) [3].

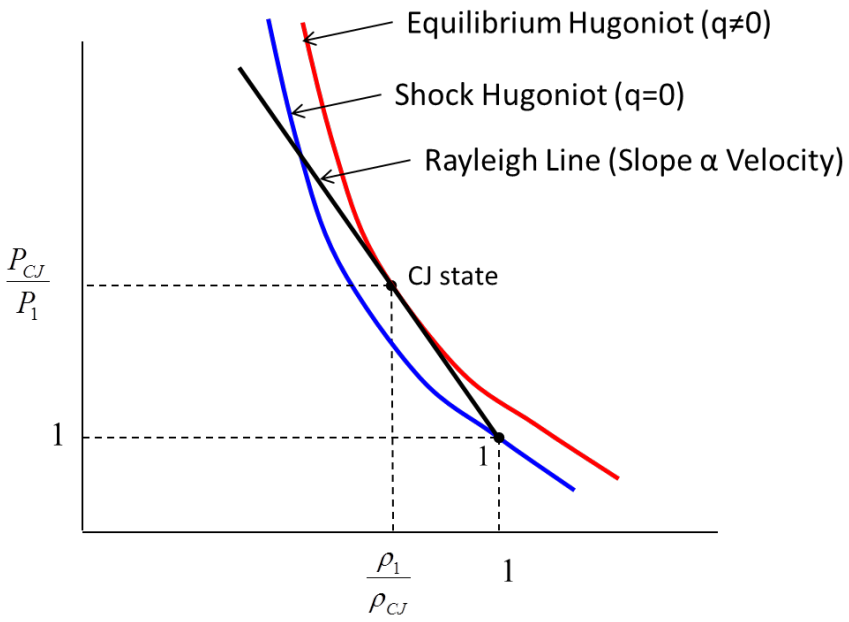

Figure 2.3: A graphical representation of the unique solution where the Rayleigh line is tangent to the Hugoniot curve. This point is referred to as the Chapman-Jouguet (CJ) state. The slope of the Rayleigh line is proportional to the detonation wave velocity. [11]

In order to solve for the CJ detonation velocity analytically, the pressure ratio in the Rayleigh and Hugoniot equations are equated to give the density ratio across the shock. The result is an equation with two possible solutions for a given incoming flow Mach number, M_1, (this also represents the wave Mach number relative to a static condition ahead of the wave) revealed by Equation (2.12).

$$\frac{\rho_1}{\rho_2} = \frac{1}{k+1}\left(k + \frac{1}{{M_1}^2}\right) \pm \sqrt{\left(\frac{1}{{M_1}^2} - 1\right)^2 - \frac{(k^2-1)2\bar{q}}{{M_1}^2}} \qquad \textbf{(2.12)}$$

Where the average heat release is given by

$$\bar{q} = \frac{q}{{c_1}^2} \qquad \textbf{(2.13)}$$

To solve for the unique CJ state solutions, the square root term is set equal to zero and M_1 is set to the CJ Mach Number, M_{CJ}, is isolated. From this a CJ velocity can be obtained.

$$\left(\frac{1}{{M_1}^2}-1\right)^2-\frac{(k^2-1)2\bar{q}}{{M_1}^2}=0 \qquad \textbf{(2.14)}$$

$$\frac{1}{{M_{CJ}}^2}=(k^2-1)\bar{q}\left\{1+\frac{1}{(k^2-1)\bar{q}}\pm\sqrt{1+\frac{2}{(k^2-1)\bar{q}}}\right\}=0 \qquad \textbf{(2.15)}$$

The two unique solutions to Equation (2.15), where the (+) and the (-) represent the detonation and deflagration solutions respectively, indicated graphically in Figure 2.4.

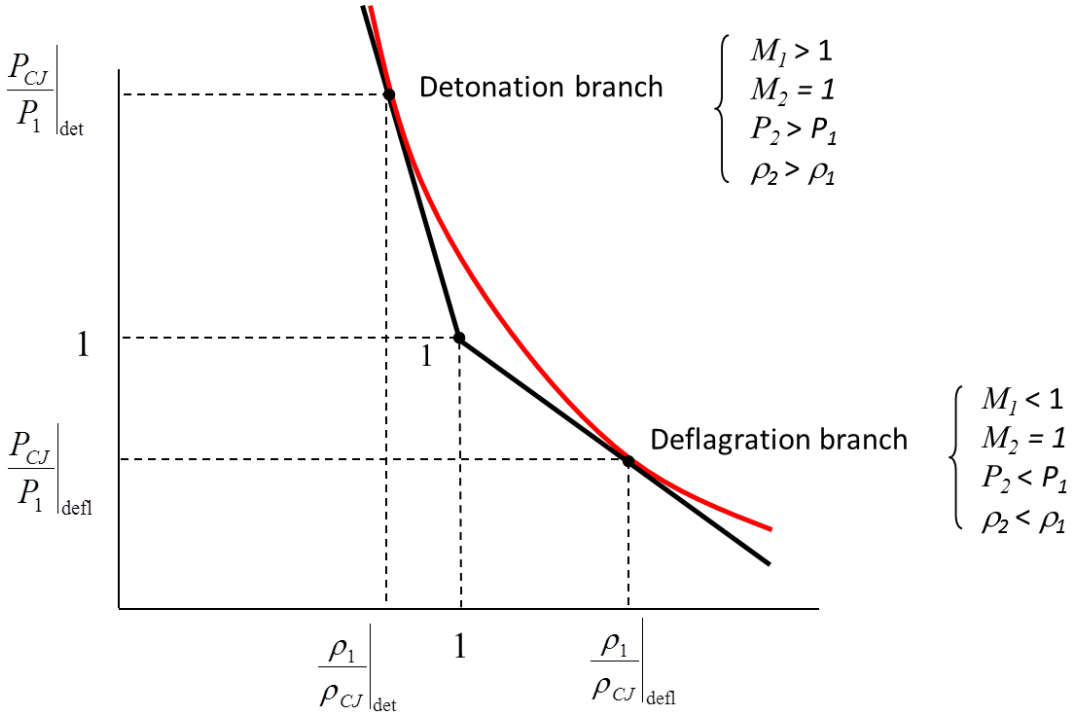

Figure 2.4: The two possible CJ state solutions indicated by the tangency of the Rayleigh line to the equilibrium Hugoniot curve. [11]

The upper branch of the Hugoniot curve includes the indicated strong CJ solution and is termed the "Detonation branch". This branch has a pressure rise across the shock typical of a detonation wave. The size of this pressure rise indicates the strength of the detonation. The lower branch of the Hugoniot curve includes the indicated weak CJ solution and is termed the "Deflagration branch". This branch has a theoretical decrease in pressure across the shock, typical of a deflagration wave. This pressure decrease (or increase in specific volume) across the

deflagration wave causes an expansion of the hot combustion products inducing a flow ahead of lead shock, observed as a critical mechanism for DDT in smooth tubes. This will be discussed further in the Deflagration to Detonation Transition section of the thesis.

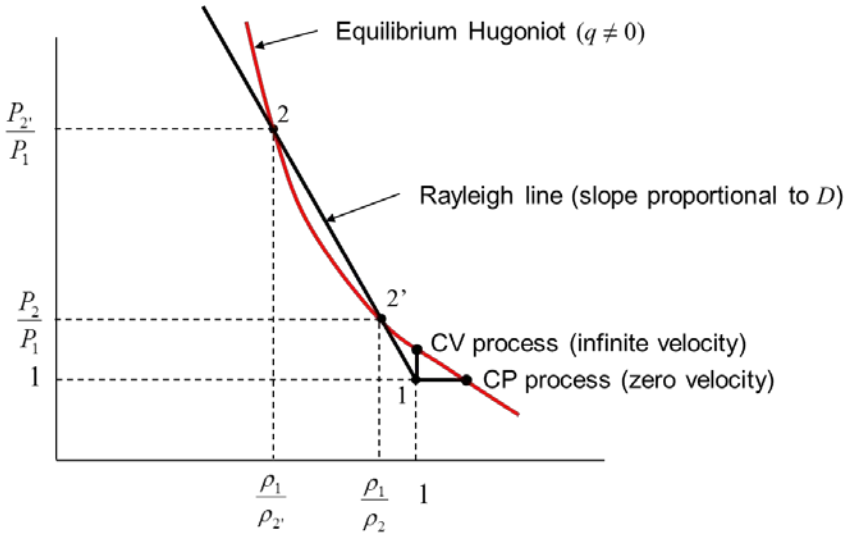

Figure 2.5: Detonation Process consists of shock compression followed by energy release. Equilibrium is attained at the end of the reaction zone. Adapted from Ciccarelli et al., [11].

The Rayleigh line generally intersects the Hugoniot curve at two points as indicated by the square root term in Equation (2.15). These two points, 2 and 2' as shown in Figure 2.5, represent the strong (overdriven) and weak detonation wave end states respectively. State 2 indicates a case where the flow in the products is subsonic relative to the detonation wave. This particular solution is unstable because the expansion waves generated at the back wall of the tube will catch up to the detonation front and weaken the lead shock wave. State 2' indicates a case where the flow in the products is supersonic relative to the wave (M_2 >1). This solution is not possible because all of the energy is released at state 2. Additionally the decrease in entropy required to achieve state 2' violates 2nd Law. This is indirectly indicated by the CJ detonation state, which represents the minimum possible entropy increase.

The CJ Theory is excellent for predicting the end state of the combustion process; however it does not accurately represent the detonation wave structure due to the absence of a reaction zone. In order to gain insight into the dynamic parameters a more detailed model is necessary. This leads to the development of the Zeldovich, von Neumann, and Döring (ZND) model which more accurately represents the internal detonation wave structure.

2.4 ZND Detonation Model

The one-dimensional ZND model was independently developed in the 1940's by Zeldovich [12], von Neumann, and Döring. They realized that the energy release after the shock wave was not instantaneous as originally assumed by Chapman and Jouguet. The ZND model introduces a finite length reaction zone that terminates at the CJ state as shown in Figure 2.6.

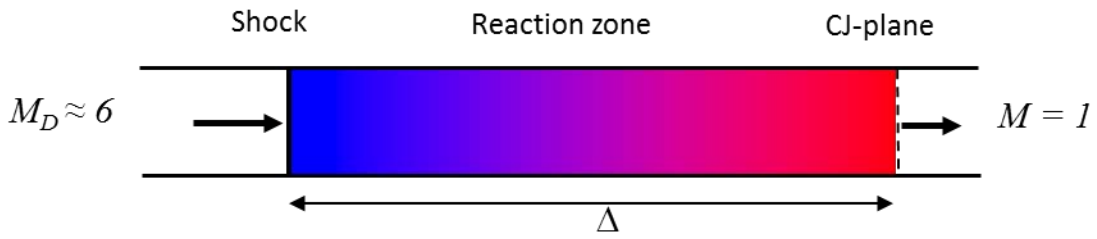

Figure 2.6: ZND detonation model [11]

The ZND model consists of a lead shock, a finite reaction zone, and a CJ plane. The reaction zone behind the lead shock consists of an initial induction zone in which the temperature and pressure remain nearly constant. The length of this induction zone is commonly defined as the distance downstream from the shock to the point where the rate of temperature increase is at a maximum, shown in Figure 2.7 [11]. The length of this induction zone is characteristic of the fuel mixture. Chemical energy is rapidly released following the induction zone increasing the temperature, asymptotically approaching the CJ state values [13]. The induction zone length is commonly used to represent the entire reaction zone length due to the asymptotic approach to chemical equilibrium shown in Figure 2.7. This rate of heat release correlates to the temperature gradient of the reaction zone.

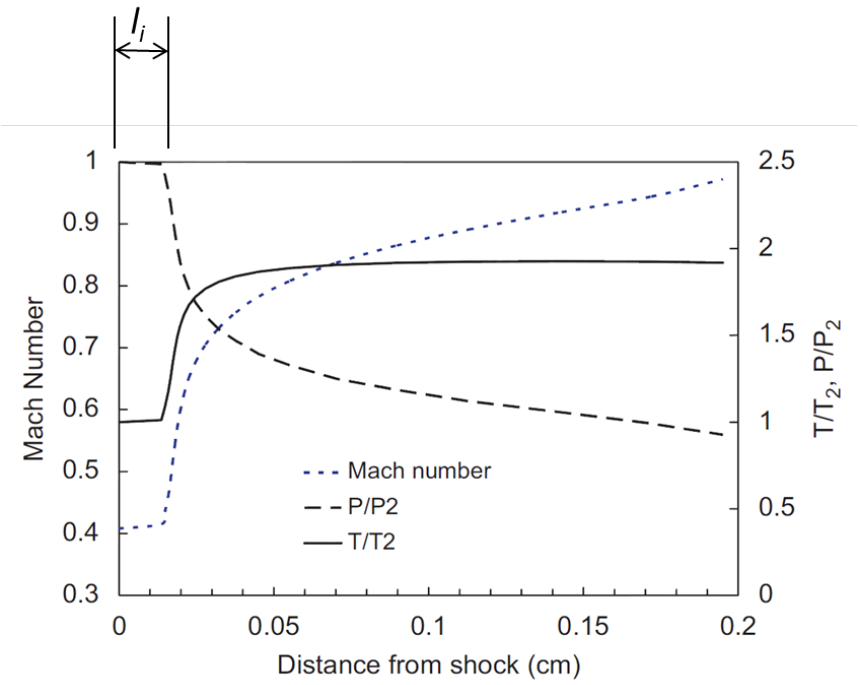

Figure 2.7: ZND detonation front structure for atmospheric hydrogen-air. The induction zone length is indicated at the point of maximum temperature change at the detonation front, l_i. Note the asymptote to unity of the post shock Mach number. [11]

In order to quantify the change in properties throughout the reaction zone, the time-dependent conservation equations and a reaction model can be integrated. Essentially this integration is carried out along the Rayleigh line defining all possible states throughout the reaction. The post shock state is obtained from the CJ theory.

To model the reaction zone properties a reaction model is necessary. Essentially a reaction model is an equation or set of equations that describes the change in chemical species with time. The most basic application is the Arrhenius rate law, Equation (2.16).

$$\frac{d}{dt}(\rho\alpha) = -k\rho\alpha\exp\left(-\frac{E_A}{RT}\right) \tag{2.16}$$

Where α is the reactant mass fraction

The induction zone chemically represents the time necessary for the formation of free radicals to initiate a chain reaction or recombination [3].

To increase the accuracy of the model a detailed reaction mechanism can be used in which a series of elementary reactions are considered for individual species. The main challenge that is in computational modeling of detonations arises for three-dimensional models. The computational power required for these computations is significant and the cost associated with these computations makes them currently impractical for this application.

2.5 Multidimensional Detonation Wave Structure

The CJ and ZND models both assume that a detonation is one-dimensional. This has proven to be accurate for determining detonation parameters; however actual detonation waves are very much three-dimensional. An actual detonation is characterized by a three-dimensional shock wave followed by a reaction zone. The detonation consists of three different waves, an incident wave, Mach stem, and transverse wave interacting in a Mach stem configuration as shown in Figure 2.8. The point of connection between these three waves is referred to as a triple point. An actual detonation wave captured using Schlieren photography is shown in Figure 2.8 where it can be seen clearly that the detonation front is not planar.

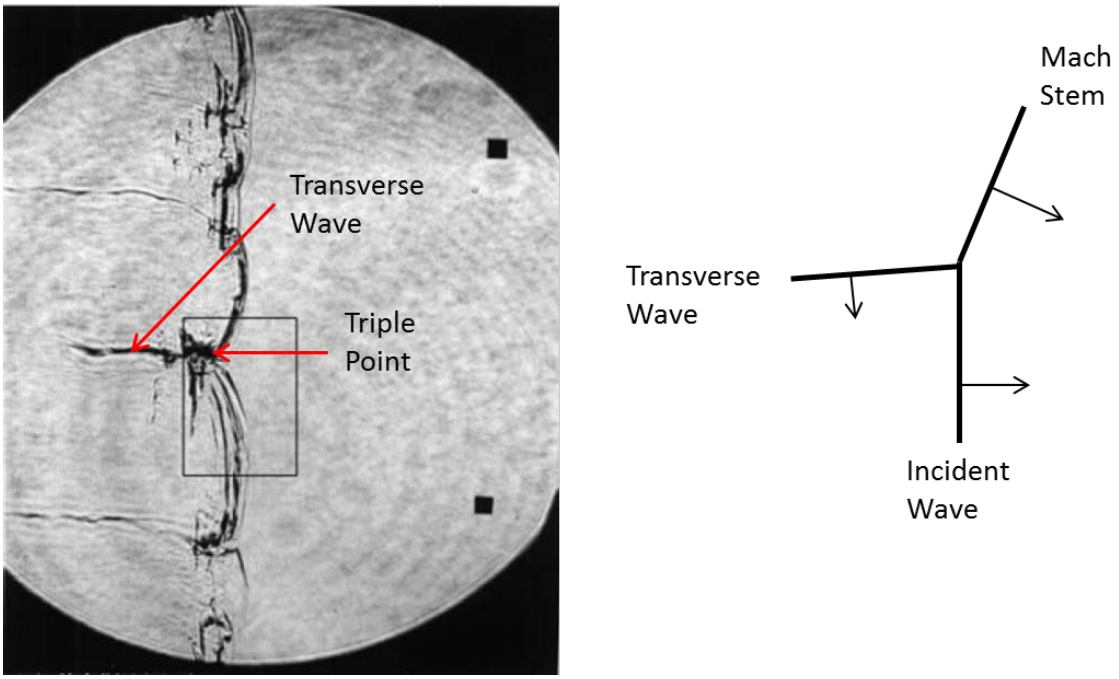

Figure 2.8: Schlieren photograph of three-Dimensional detonation front propagating from left to right in $2H_2$-O_2-$3.5N_2$, P_1 = 20 kPa in a narrow channel adapted from Austin [14].

The detonation front consists of a series of triple points propagating transversely along the detonation front. As the detonation propagates these triple points generate a cellular detonation wave pattern similar to that of "fish scales" shown in Figure 2.9 [7]. The average transverse width of the cells is characteristic of the reactivity of the mixture and is referred to as the detonation cell size, λ

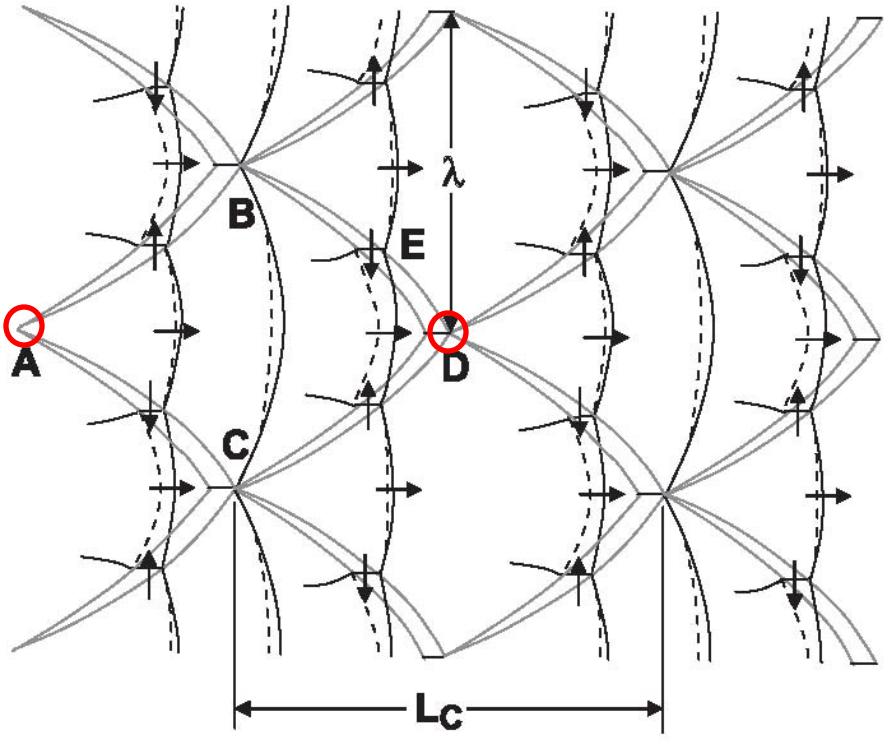

Figure 2.9: Schematic of cellular detonation wave front showing the trajectories of the triple points. The dynamic parameters detonation cell size, λ and cell length, L_c are shown. [7]

It is important to understand the mechanism by which a detonation propagates. For example, the collision of two transverse waves at location A of Figure 2.9, results in the generation of a local explosion and a strong shock wave that propagates toward location D decaying in strength. This strong shock is referred to as a "Mach stem" in the first half of the cell and is responsible for initiating chemical reaction. However, as the Mach stem begins to decay and the reaction zone length increases significantly it becomes the "incident wave" in the second half of the cell. The incident wave fully decouples from its reaction zone at the end of the cell propagating as a decoupled shock wave and deflagration. As the incident wave approaches the end of the cell the transverse waves from each triple point collide causing a local explosion that generates a new Mach stem at location D. This new Mach stem propagates into the next cell continuing the process. Similar collisions can be seen at locations B and C from the collision of

neighboring triple points. A more detailed schematic of this process is shown in Figure 2.10 isolating two connected cells.

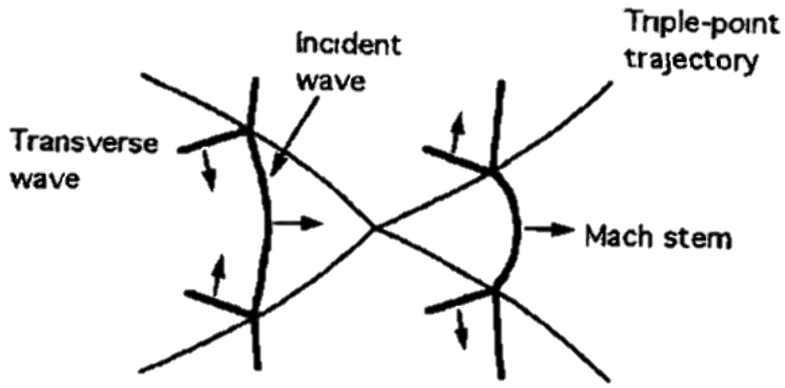

Figure 2.10: Schematic of time evolution of detonation wave front adapted from Ciccarelli et al. [15] showing the decaying incident wave and the subsequent collision results in the generation of a new Mach stem.

This propagation method characterized by a collision, decay, and re-initiation is responsible for the highly time dependent, unstable propagation of a detonation. As the Mach stem decays, there is notable difference in wave velocity from the beginning of the cell to the end. The velocity along the centerline at the beginning of the cell was found to be approximately 1.6 times the CJ velocity [16]. Conversely the velocity of the decaying incident wave was found to be only 0.6 times the CJ velocity at the end of the cell [16]. That being said, the average velocity across the cell corresponds to the CJ velocity as specified by the CJ theory conservation equations.

2.5.1 Cell Size Measurements

A record of cellular detonation structure is generally available for common fuels [17, 15, 18, 19, 5, 20, 21]. These records have been collected using the soot foil technique. This method involves covering a thin “foil” (metal sheet) with carbon soot from a kerosene lamp. The foil,

with soot on the inside, is placed in inside a tube in the path of a propagating detonation wave. As the detonation passes over the foil the cellular structure is etched into the soot. The mechanism by which the triple point displaces the soot is not well defined in the literature, but is thought to be related to the high vorticity at the triple point [22]. The result is a history of the wave propagation along the length of the foil as shown in Figure 2.11.

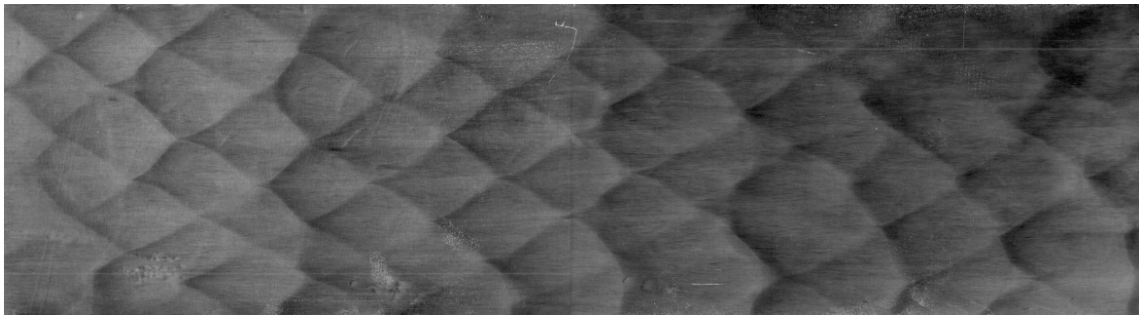

Figure 2.11: Side wall soot foil of 85% Ar-diluted stoichiometric H_2-O_2 mixture. This particular mixture displays high regularity in cellular structure from Pintgen et al. [23]

Difficulty arises in interpreting the three-dimensional cellular structure from a two-dimensional soot foil record. The measurement of cell size from a soot foil record can be problematic depending on the degree of irregularity in the cellular structure. Strehlow [24] originally demonstrated this variation in cellular structure for different fuel mixtures shown in Figure 2.12.

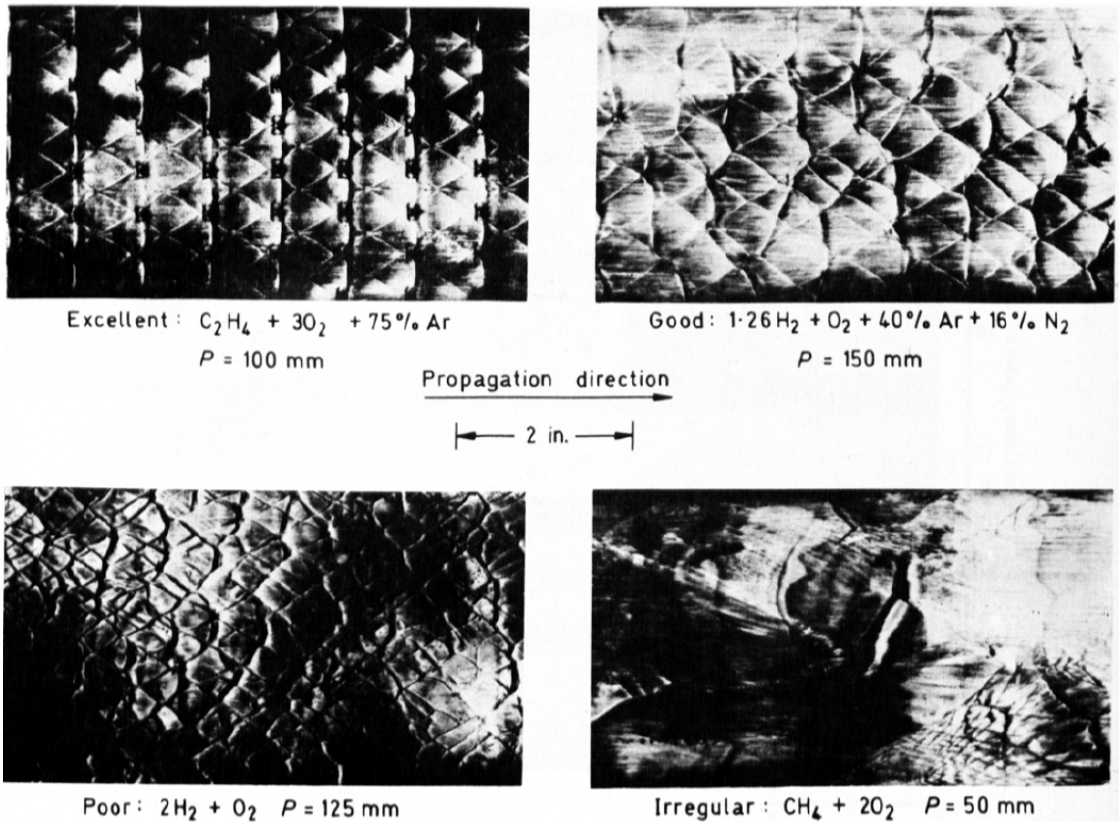

Figure 2.12: Soot foil records obtained by Strehlow [24] in a 31/4" x 1 1/2" detonation tube for different mixtures at different initial pressure, units are mm mercury. The degree of cell structure regularity is expressed qualitatively for each mixture. The addition of Argon gas to a mixture has proven to stabilize the cell pattern as seen in the top left record.

The regularity of the cell structure is specified based on the observation of two characteristics. The first is the degree of regularity of cell size defined by the triple point spacing along the foil. The larger the variation in cell size the more irregular the resultant structure will be. The second characteristic sign of cellular irregularity is the presence of "substructure" within the dominant structure. Substructure is produced by the transverse motion of weaker triple points along the detonation front inside of a cell. These less prominent waves do not play a role in the overall propagation of the detonation and often do not follow the same direction as the dominant structure. Substructure is inherent of the unstable nature of a detonation, but is most prominent in hydrocarbon-air mixtures [15]. The presence of substructure typically appears at the beginning of

a cell and decays towards the latter half. This can be explained by the variation from CJ velocity from the beginning to the end of the cell previously discussed. The local explosion caused by the collision of two triple points generates a Mach stem that is originally "overdriven" propagating at a velocity of roughly 1.6 times the CJ value [16]. The result is the generation of very small cells that grow in size as the wave decays toward the latter half of the cell as shown in Figure 2.13. As the wave approaches CJ velocity within the cell, the substructure caused by the temporarily overdriven detonation disappears.

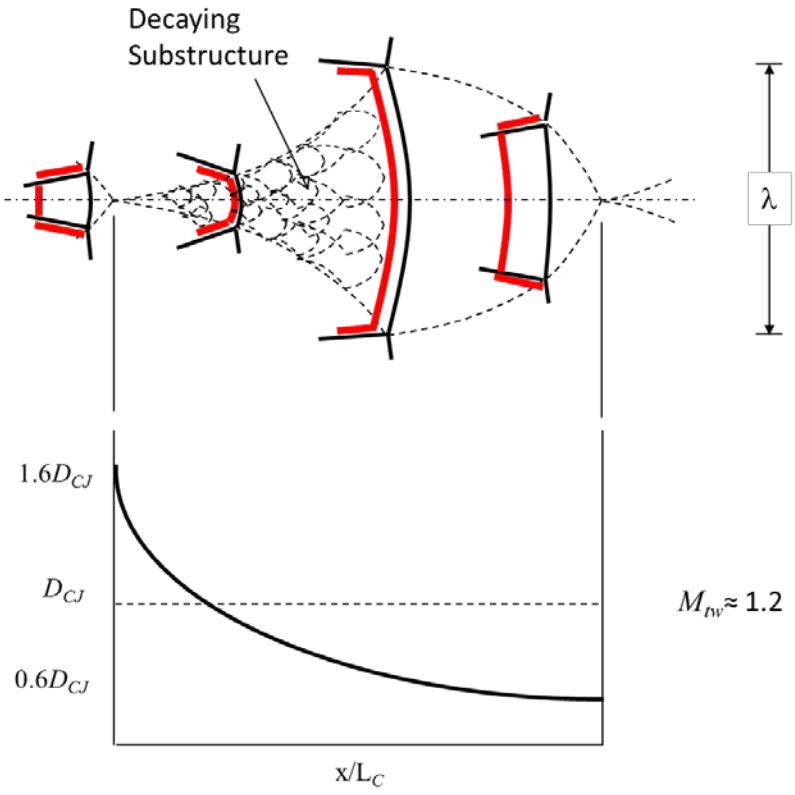

Figure 2.13: Schematic of variation of velocity along the length of a cell displaying presence of substructure adapted from Ciccarelli [11].

It is common to have substructure and cell irregularity in soot foil traces due to the unstable nature of the detonation phenomenon. This variation in cell-size found in literature can be attributed to the difficulty in choosing the correct or dominant triple point traces on the foil. This introduces significant subjectivity resulting in an associated error of ± 50% of the measured

value [19]. This uncertainty can be quantified by increasing the quantity of data collected and determining an average cell size based on a larger number of measurements. A method described by Moen et al. [25] called the “dominant mode method” is commonly used to systematically measure the average detonation cell size. In this method the cell size is based on the average spacing between triple point trajectories on the foil. The longest most prominent lines are chosen as representative of the structure. This method is described in actual application by Ciccarelli et al. [15]. The foil is removed from the detonation tube after a test and is sprayed with a clear coat to protect the record. The most dominant lines are traced on an overlaid clear Mylar, plastic sheet and measured using calibres. A minimum of three cells are necessary to provide an accurate representation of the entire structure.

2.6 Flame Acceleration in Obstructed Channels

The flame acceleration process in obstructed and non-obstructed channels has been studied extensively through the application of shadowgraph, Schlieren, and other high-speed photography methods and is qualitatively well understood. The process of flame acceleration can lead to DDT under the right conditions and has been the focus of many studies due to its importance to industrial explosion safety.

2.6.1 Deflagration to Detonation Transition

In order for a detonation wave to form, not only does an ignition source need to exist, but also obstacles must be present to produce turbulence in the unburned gas ahead of the flame. If the flame is able to accelerate to a velocity on the order of a 1000 m/s, a detonation wave can be initiated. This process is referred to as DDT. Chapman and Wheeler [26] were one of the first to perform experiments to investigate the effect of the presence of obstacles on flame acceleration. Starting in the early 1980s flame acceleration leading to DDT has been investigated primarily in round tubes equipped with repeated orifice plates [3]. Peraldi et al. [4] showed that in this configuration a quasi-steady explosion front can propagate at a velocity between the speed of

sound of the combustion products (isobaric process) and the CJ detonation wave velocity. This type of wave was referred to as a "quasi-detonation". For a given tube diameter and orifice plate blockage ratio (BR) the quasi-detonation regime is defined by the lean and rich composition limits. These DDT limits represent the initial mixture condition required to achieve flame acceleration leading to hot spot generation and transition to detonation.

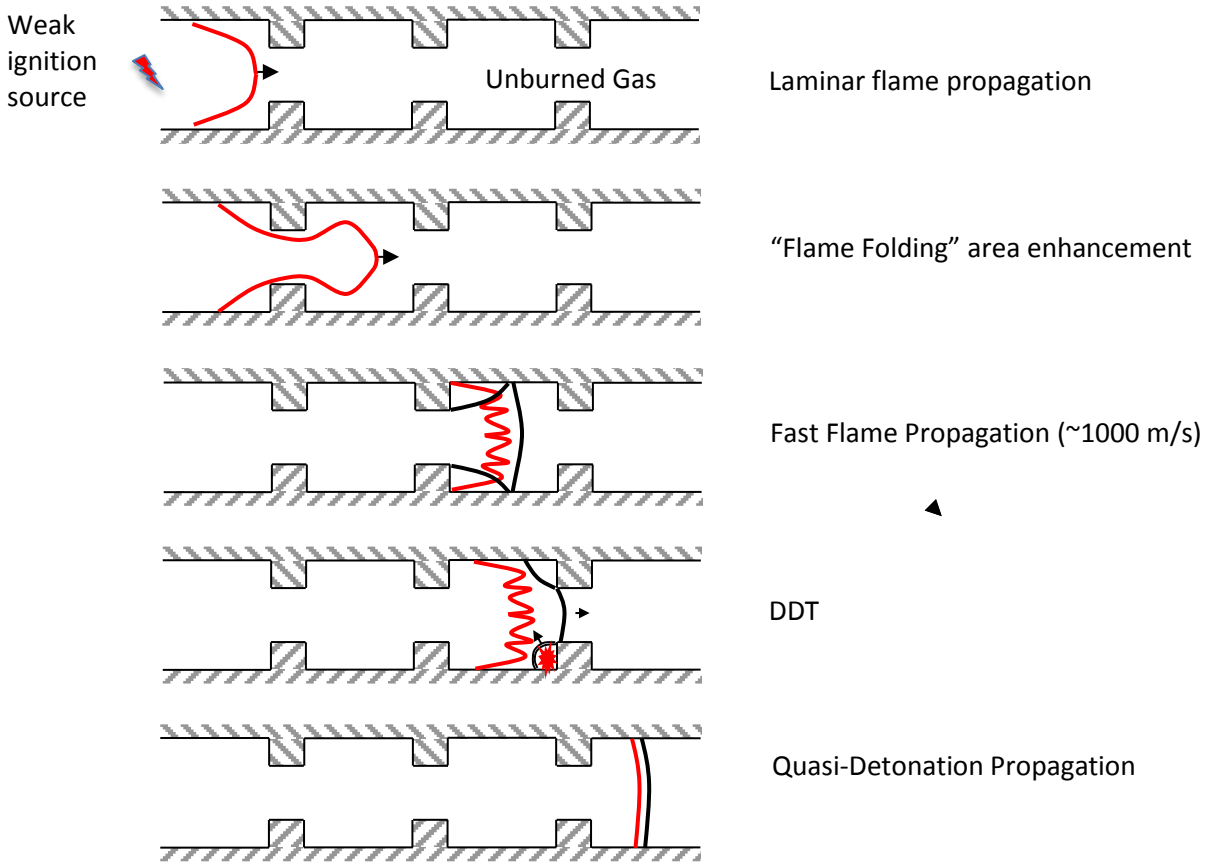

Figure 2.14: Typical schematic showing flame acceleration and transition to detonation in an obstacle filled tube, adapted from Ciccarelli [11].

The energy required to get a direct detonation initiation is very large. Explosions typically start with a weak ignition source such as static discharge. The weak ignition generates a flame that accelerates aided by obstacles to a critical velocity at which detonation can occur. The schematic in Figure 2.14, shows the typical flame acceleration and DDT process in an obstacle filled tube. In order of occurrence, a flame is generated from a weak ignition source and a laminar

flame begins to accelerate down the tube pushing the cold unburned gas ahead of it. As the flame encounters the first obstacles the laminar flame is distorted by the unburned gas flow field generated by the obstacle. This leads to an increase in surface area of the flame, and thus the volumetric burning rate, which increases the flow velocity of the unburned gas. This feedback mechanism greatly enhances the acceleration of the flame. As the flame accelerates to approximately ~300m/s (speed of sound in unburned gas) compression waves form and coalesce into a lead shockwave in front of the flame. When the flame reaches a velocity of around the combustion products speed of sound (approximately 1000 m/s), the shock/flame complex is referred to as a fast (or choked) flame. If the flame reaches this critical velocity then transition to detonation can occur resulting in a propagating quasi-detonation, Figure 2.14.

2.7 Quasi-Detonation Propagation

Quasi-detonations are highly unsteady, with large swings in instantaneous velocity as the wave propagates past individual obstacles. Using high-speed schlieren photography Teodorcyk et al. [27] showed that in the quasi-detonation regime the large CJ detonation velocity deficit (difference between measured average wave velocity and the CJ detonation velocity) can be attributed to intermittent detonation initiation and failure during diffraction around obstacles, shown schematically in Figure 2.15.

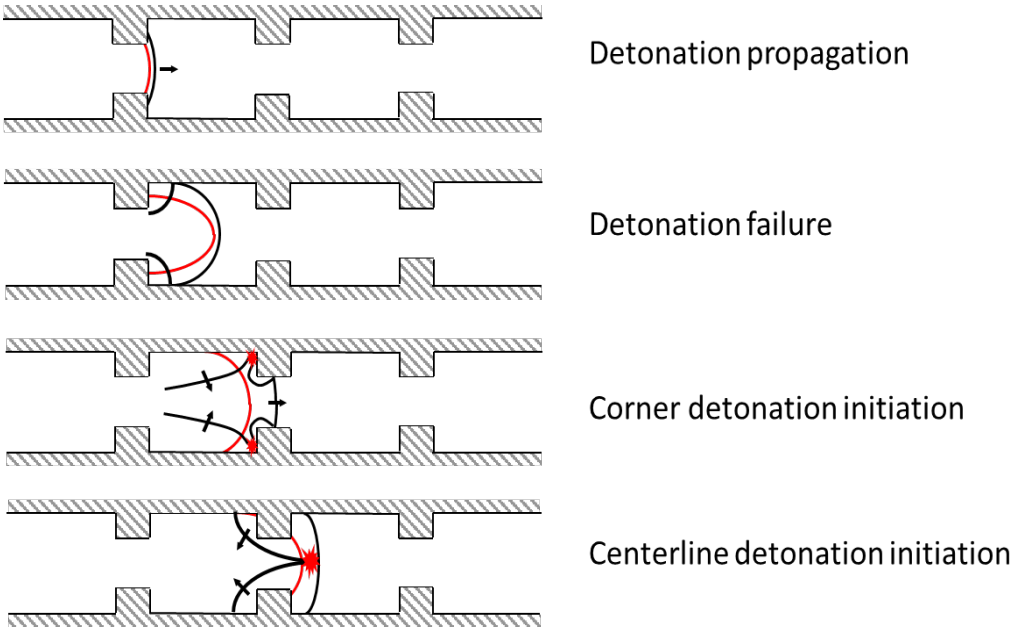

Figure 2.15: Schematic of propagating quasi-detonation. Detonation re-initiation is shown due to shock reflection of the obstacle face resulting in a strong shock collision at the channel centerline.

In recent experiments performed with sub-atmospheric hydrogen-oxygen in an optically accessible channel equipped with top and bottom surface mounted fence-type obstacles Kellenberger and Ciccarelli [28] captured the fast flame and quasi-detonation propagation modes using high-speed schlieren photography.

Chapter 3

Literature Review

Several methods of categorizing the detonation hazard associated with gaseous fuels exist in the literature. This section will introduce the dynamic parameters associated with gaseous detonations and the experimental methods used to measure these parameters. A full review of the relevant theory necessary to understand these methods is provided in the following sections of this chapter.

3.1 Dynamic Parameters

Dynamic parameters require information about the internal turbulent structure of the detonation and the related chemical reactions rates. This is why they are referred to as dynamic detonation parameters, as opposed to the static equilibrium states of the CJ theory [7]. These dynamic parameters include but are not limited to the detonation cell size λ, critical tube diameter d_c, and critical initiation energy E_c. The large range in temporal and spatial scales that need to be resolved, as well as the complex multi-step reactions, make direct numerical simulation in three-dimensions economically impractical [29, 30]. The dynamic parameters are determined exclusively through experimental measurement.

Extensive experimental data on cell size, critical tube diameter, and critical activation energy has been collected over the past century. The majority of this data is focused around common fuel mixtures such as hydrogen-air and small hydrocarbons [6, 31, 32, 33, 19]. There is to-date very little data for less common fuels due to the large cost associated with running these scale of tests. To mention just one of these projects, a large scale project was carried out by Knystautas et al., 1983 to systematically produce experimental measurements of several dynamics parameters. Detonation cell size and estimates of critical tube diameter, critical initiation energy, and detonability limits for various hydrocarbon-air mixtures (H_2, C_2H_2, C_2H_4,

C_2H_6, C_2H_8, and C_4H_{10}) were obtained [19]. These experiments were carried out over a range of fuel concentrations in three different tubes of diameters 5, 15, and 30 cm. This project represents the largest single collection of dynamic property data and was largely used to verify the universality of several detonation sensitivity correlations developed on the principle of these dynamic parameters. The Knystautas et al. study will be referred to often due to the commonality in fuel-air mixtures used with the present study. A collection of data from this study, along with other recognized studies of dynamic properties are effectively organized in the Caltech Detonation Database [34].

3.1.1 Detonation Cell Size, λ

Detonation cell size represents a characteristic length scale associated with a detonation wave's characteristic "fish-scale" structure. This scale has been fundamental to the development of several important correlations that categorize the reactivity of a fuel. Large quantities of experimental cell-size data have been collected by several prominent researchers for common fuels using the soot foil technique. Knystautas et al. measured the cell size of a variety of common hydrocarbon fuels over a complete range of compositions using this soot foil technique [19]. As previously mentioned, this study represents only one of several important studies in determining the universality of λ as a parameter for ranking the detonation sensitivity of gaseous fuels. Detonation cell size, λ is typically plotted as a function of fuel-air mixture equivalence ratio resulting in a U-shaped curve as shown in Figure 3.1 [35]. As expected for the range of fuels, the smallest cell size commonly occurs at roughly an equivalence ratio of one ($\Phi \approx 1$). This can be expected since stoichiometric mixture corresponds to the most reactive mixture. Based on this, the various fuels sensitivity can be ranked based on their minimum detonation cell size. Referring to Figure 3.1, it is straight-forward to determine the relative explosion hazard of each mixture. Based on this method of ranking fuels, it is safe to say that acetylene (C_2H_2) is the most sensitive of the mixtures tested and methane (CH_4) is the least. This method cannot give an

absolute measurement of sensitivity but is valuable in giving a relative measurement to other common fuels and has been used in combination with other dynamic parameters to give a more finite measurement.

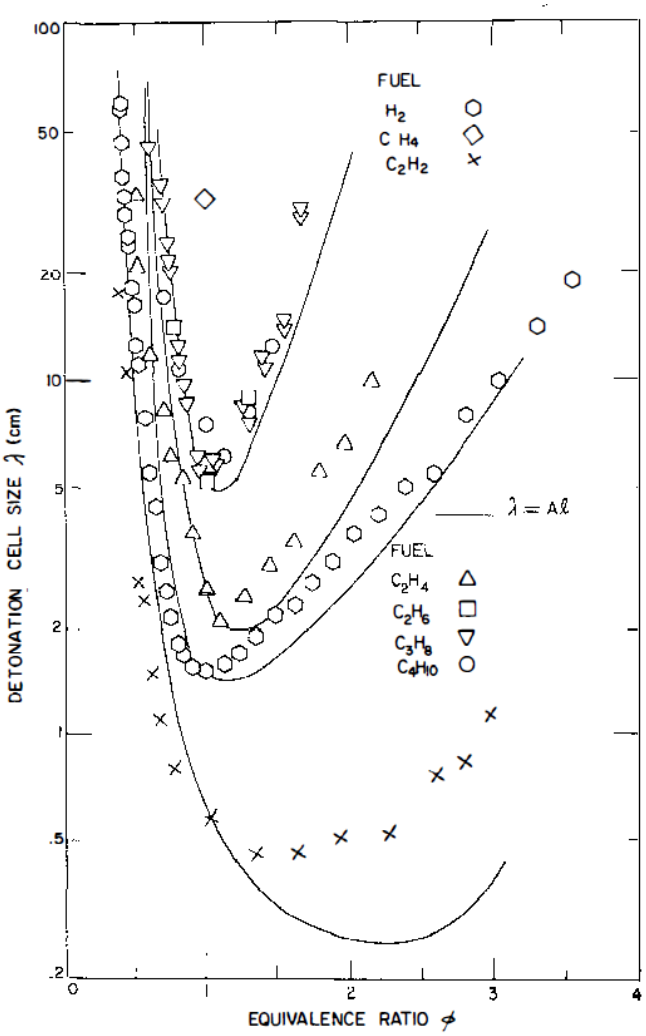

Figure 3.1: Cell size of fuel-air mixtures at atmospheric pressure. [35]

Detonation cell size is still used extensively as a parameter for characterizing the relative hazard a fuel represents. However, issues arise with the high level of uncertainty associated with the detonation cell size measurement for industrial hazard prevention applications. Through the entire cell size data record reported in literature there is a noticeable variation between sources all using the soot-foil method [35]. The soot-foil method is relatively straight forward to apply but

there is a large amount of subjectivity in interpreting the soot-foil traces. It is common to have substructure and cell irregularity in the traces due to the unstable nature of the detonation phenomenon. This variation in cell-size found in literature can be attributed to the difficulty in choosing the dominant triple point traces on the foil. This introduces a large amount of personal judgement and subjectivity resulting in the ± 50% uncertainty in the measured value [19]. This error can be reduced significantly by increasing the quantity of data collected and determining an average cell size based on a larger number of measurements. This has been done over time for only the most researched mixtures such as hydrogen-air, but data for less common fuel mixtures has been less established. For safety applications where the potential risk is measured in lives lost, this type of uncertainty is unacceptable. The complexity of the detonation wave makes the numerical simulation of this phenomenon not practical at this time for predicting cell size.

3.1.2 Critical Tube Diameter, d_c

The critical tube diameter d_c is defined as the minimum diameter tube in which a detonation can propagate and successfully transmit into an unconfined space filled with the same gas mixture. As the detonation emerges into the unconfined space the detonation wave diffracts around the corner. This diffraction proceeds by the propagation of expansion waves from the tube exit diameter towards the tube centerline. This expansion weakens the lead shock wave, reducing the post shock temperature and slowing the chemical reaction rate. This causes the reaction zone to increase and eventually decouple. The larger the tube diameter the longer it takes for the expansion to reach the tube centerline and thus more opportunity for the detonation to re-establish itself. A successful transmission produces a propagating spherical CJ detonation; conversely, a failed transmission produces a decoupled shock wave and flame where the distance between the two increases with time. This dynamic parameter is useful in the design of detonation prevention systems for industry where the spacing between pipes and the size of openings to

chambers/rooms can be specified to quench detonations and avoid transmission. A schematic of a critical tube diameter apparatus used by Knystautas et al. is shown in Figure 3.2.

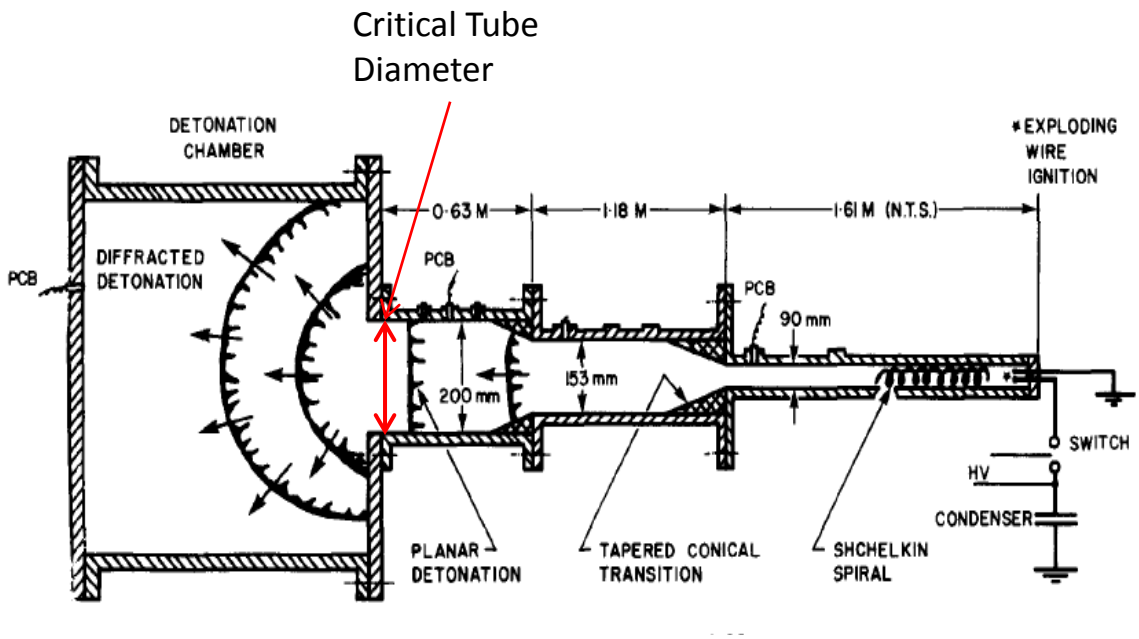

Figure 3.2: Schematic of experimental apparatus used by Knystautas et al. (1982) for critical tube diameter measurements. [31]

Zeldovich et al., 1956 first investigated the detonation transmission phenomenon using different diameter smooth tubes over a range of gas mixtures. They were able to specify a critical diameter for which a specific mixture would transmit from the smooth tube to an unconfined space [36]. From this they deduced that the critical tube diameter was determined by the chemical reaction induction zone length. This is along the line of reasoning used by Schelkin and Troshin, 1963 who proposed a linear correlation between the induction zone length and the detonation cell size [37]. With this commonality of both dynamic parameters, cell size and critical tube diameter, the two parameters could be used together to better define a method to characterize the hazard a gas mixture presents. Mitrofanov & Soloukhin were the first to recognize this correlation and proposed that $d_c = 13\lambda$ for a mixture of stoichiometric acetylene-oxygen [38]. This correlation was later confirmed to be universal to other detonation systems and gas mixtures by several

sources including Knystautas et al. 1982 [31]. A summary of these studies and their findings are shown in Figure 3.3, demonstrating a strong correlation between d_c and λ.

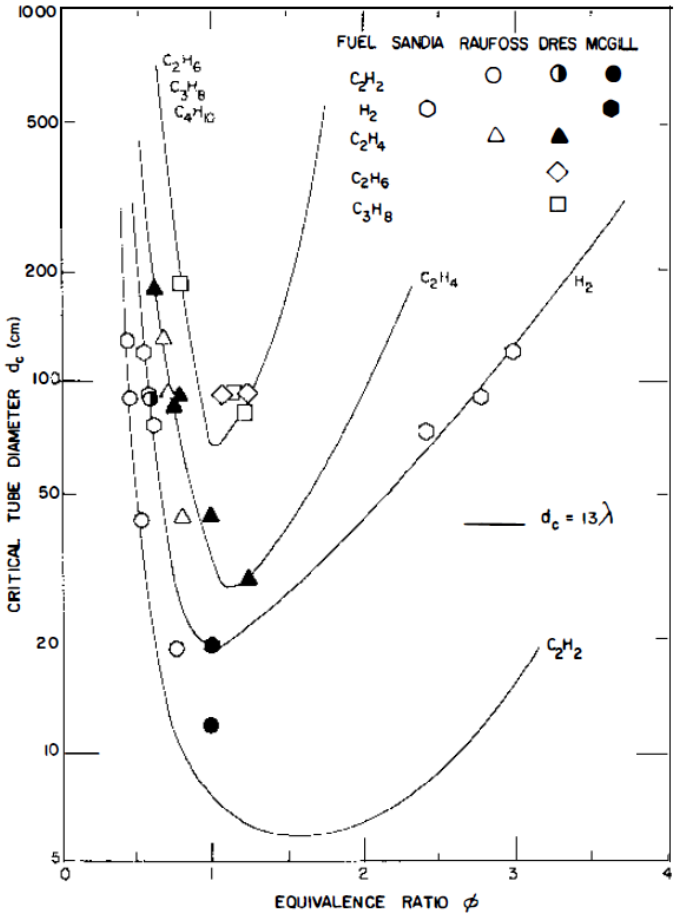

Figure 3.3: Comparison of experimental data for the critical tube diameter in fuel-air mixtures with the 13λ correlation, collected from various sources, as presented by Lee 1984. [7]

In a traditional experiment the size of the tube is increased until the detonation successfully transmits into the unconfined space. In order to make these experiments more practical Liu et al., 1984 [39] changed the size of an orifice plate placed at the end of a fixed diameter tube. The critical orifice diameter was determined in a similar fashion as in the critical tube diameter experiment. It was determined that the critical tube diameter for successful transmission from smooth tube is equivalent to the critical orifice diameter. This was explained

by hypothesizing that the attenuated core detonation wave (along the tube axis) is dominate in the development of the spherical detonation [7].The critical orifice diameter was applied to different geometries by defining an effective diameter, d_{eff} to be used in place of the critical orifice diameter. The effective diameter is defined differently based on the aspect ratio of the orifice plate [7]. For small aspect ratios, the effective diameter is specified as the mean of the largest and smallest characteristic dimensions of the orifice opening. For larger aspect ratios, the effective diameter is defined by the smallest characteristic length of the orifice opening. The distinction between aspect ratios is defined by $L/W > 7$, where L is the length of the slot and W is the width of the slot [39]. The effect of aspect ratio on the critical orifice diameter is best described by Lee, where he attributes the effect to a critical wave curvature criterion [7]. To avoid straying from topic, this effect will not be discussed in this thesis.

Compared to detonation cell size, the critical tube diameter is a much less subjective dynamic parameter. The detonation is either transmitted successfully to the unconfined space or fails upon diffraction. Therefore, the critical tube and orifice diameter are excellent parameters for determining the explosion hazard of a gas mixture but the cost associated with running these types of experiments for a range of fuels is extremely large. These costs arise from design of the test apparatus. Critical tube diameter experiments require the diameter of the entire tube be changed for each fuel and mixture composition. Additionally, the size of test apparatus necessary for less sensitive mixtures that have a critical diameter in the range of meters rather than centimeters makes these tests difficult to do in a laboratory environment. The combination of design and build costs with the scale of these tests make them an economically ineffective method of quantifying explosion hazards of large numbers of gas mixtures in industry.

3.1.3 Critical Initiation Energy, E_c

Critical Initiation Energy is another parameter used in characterizing the detonation sensitivity of a gas mixture at known initial conditions. The critical initiation energy is defined as the minimum energy required for direct or prompt initiation of a spherical detonation. This is typically done using a powerful ignition source such as a high explosive or a high voltage arc. This ignition source deposits a large amount of energy into the mixture generating a blast wave which decays asymptotically to a propagating CJ detonation wave. In the case of insufficient energy deposition, the shock reaction zone system will decouple and the wave will fail to propagate.

Critical initiation energy was extensively studied by Bull et al. [40] where he initiated several hydrocarbon-air mixtures using high explosive Tetryl charges [40]. It was determined that for mixtures close to the detonability limits the propagating wave pressure and velocity became very irregular. It was hypothesized that this irregularity occurred after initiation due to the decoupling of the shock and trailing reaction zone indicating a failed detonation initiation. Bull et al. confirmed the universality of this observation with five common hydrocarbon fuels where the critical initiation energy was recorded for a large range of equivalence ratios, see Figure 3.4.

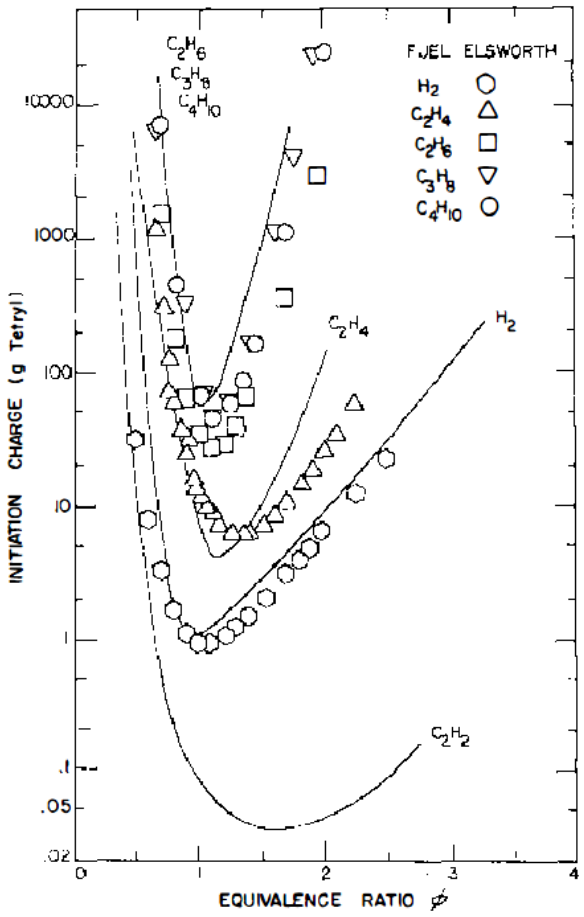

Figure 3.4: Summary of critical initiation energy data for fuel-air mixtures over a range of equivalence ratios. A comparison of these experimentally determined initiation energies with the surface-energy theory developed by Lee et al. are shown. [7, 40]

The surface-energy theory was developed by Lee et al. to provide a connection between the critical initiation energy and the detonation cell size through the application of the critical tube diameter [20]. The proposed connection is based on a minimum surface energy before a planar wave can successfully progress into a spherical wave. The result is Equation (3.1) based on strong blast theory that accurately relates the critical initiation energy to detonation cell size [7].

$$E_0 = (2197/16)\,\pi\rho_0 I D^2 \lambda^3 \qquad \textbf{(3.1)}$$

Figure 3.4 shows a comparison of the predicted critical initiation energies based on this theory with the experimentally determined energies from Bull & Elsworth [40]. The energies for both are measured in grams of Tetryl for a direct comparison based on Bull & Elsworth's data. The correlation between the two is strong enough to be used to approximate critical initiation energies. The shape of the curve produced is very similar to that of detonation cell-size and critical tube diameter, Figure 3.1 and Figure 3.3 respectively. This U-shaped curve is typical of all detonation properties [3].

Critical initiation energy is not without its issues for practical use as a method of quantifying an explosion hazard. The use of high explosives to experimentally determine this dynamic parameter introduces a hazard on its own working with a highly regulated and controlled material. This type of experiment requires a secure environment with the appropriate procedures in place to store high explosives, making them less than ideal to run repeatedly in order to gather the amount of data necessary to be used industry wide. The application of the surface-energy theory to obtain critical initiation energies eliminates the hazard associated with experiments but retains the issues associated with cell size measurement. As previously discussed, the lack of availability of cell size data for less common fuels and the large uncertainty associated with its measurement make it unreliable for explosion prevention applications.

3.2 Criteria for onset of detonation in tubes

3.2.1 DDT Limits

It is of interest to know what the minimum tube diameter is that can support the propagation of a detonation wave. Similarly, it is of interest to know composition range of a fuel-air mixture that can support a detonation wave in a tube of given diameter. These limits were measured in experiments where a flame accelerated and transitioned into a stable detonation wave [4]. For this reason they are often called DDT limits. There was some controversy concerning the DDT limit criterion for smooth tubes. One argument was that at the limit a single-head spin exists

(detonation where on a single triple exists that rotates along the wall as the detonation moves forward). A single-head spin detonation wave has an effective cell size of πd and therefore the corresponding limit criterion is $d/\lambda \geq 1/\pi$ [Moen et al., [25]]. Knystautas et al [31]performed experiments where a quasi-detonation was transmitted from a rough-tube into a smooth-tube of the same diameter and found that at the limit where the detonation could not be re-established in the smooth tube, $d/\lambda=1$.

The flame acceleration process in a smooth tube relies on the enhanced burning in the tube wall boundary layer and for fuel-air mixtures results in run-up distances (distance from ignition to the point of DDT) that are very long. To simulate more closely the obstructed tube geometries found in industry experiments were also carried out in tubes filled with obstacles. A series of DDT experiments were carried out by Peraldi et al. in a tube filled with orifice plates, spaced nominally at the tube diameter, with Hydrogen, Acetylene, Ethylene, Propane and Methane [4]. The results indicated that there are two necessary conditions for the onset of detonation in an obstacle filled tube. The first of these conditions is that the flame must accelerate up to a speed on the order of the speed of sound of the products. The second condition is that the minimum transverse dimension of the orifice plate must be equal to or larger than the characteristic cell size of the gas mixture. These findings are consistent with the findings in the smooth tube discussed above. These conditions are necessary but do not guarantee the transition to detonation will take place. The criterion specified by this minimum transverse dimension is commonly referred to as the minimum tube diameter criterion defined as, $d > \lambda$.

Additional studies have demonstrated this criterion and discovered a dependency on the obstacle configuration including the spacing between obstacles and the obstacle blockage ratio (BR) [41, 27, 42, 43]. These studies showed that the critical d/λ increases with a decrease in obstacle spacing (4.28d to 1.07d) [3, 27] or an increase in BR (0.1 to 0.75) [3, 42]. This tells us

that there is more than just the minimum transverse distance that is controlling the onset of detonation initiation. The minimum scale requirement criterion recognizes these findings.

3.2.2 Minimum Scale Requirement Criterion (L > 7λ)

A second DDT criterion was proposed by Dorofeev et al. [43, 5] termed the minimum scale requirement criterion. Similar in principle to the minimum tube diameter criterion, d > λ, proposed by Peraldi et al. but recognizes the dependence of the spacing between obstacles and the tube diameter as key parameters in the onset of detonation [44, 5]. This approach suggested that a minimum distance, L, characteristic of the obstacle configuration was necessary for a detonation to form. Dorofeev defined this length as the minimum length-scale of "sensitized" mixture in which a detonation could originate and specified that if L > 7λ detonation initiation is possible [5]. For practical applications the length L was defined using the concept of a channel containing repeated obstacles representative of a chain of connected rooms. L_1 was defined as the characteristic size of a single "room". This is shown in Figure 3.5 and Equation (3.2) as the average of the two largest dimensions of the room, where *S* is the obstacle spacing and *H* is the channel height.

$$L_1 = (S + H)/2 \qquad \textbf{(3.2)}$$

This definition can be applied to a system of connected rooms or repeated obstacles where an empirical factor, α is used to describe the opening between rooms/obstacles.

$$L = L_1 + \alpha L_n \qquad \textbf{(3.3)}$$

This value of α was found to be most accurately defined by d/D where d is the size of the unobstructed passage, and D is the tube diameter (or channel height, H) [5]. This was determined based on a comparison of L defined by Equation (3.3) and DDT data from studies of the

minimum tube diameter criterion. The definition of α was varied to provide the best correlation between the data sets and the two DDT criterion [5]. The result is a definition of L for repeated obstacles that can be applied to practical applications of similar geometry shown by Equation (3.4).

$$L = \frac{(S + H)/2}{1 - d/H} \tag{3.4}$$

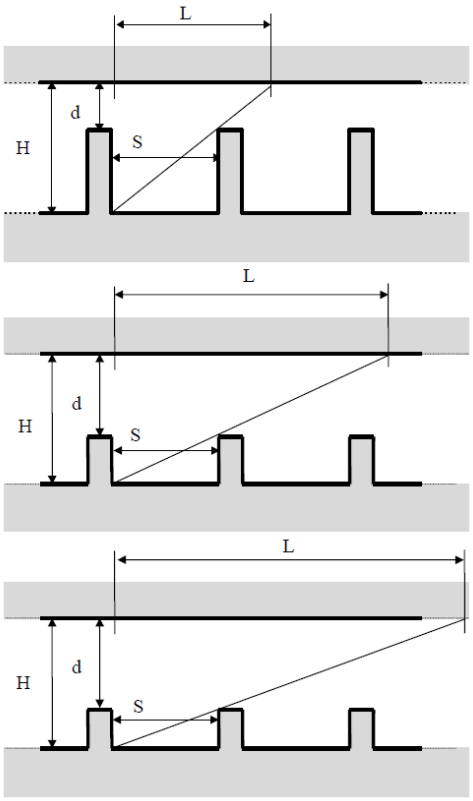

Figure 3.5: Illustration of characteristic size L for channels with obstacles. The effect of varying blockage ratio on the size L is shown [5].

For the specific case of a tube filled with repeated obstacles this equation takes the form of Equation (3.5).

$$L = \frac{(S + D)/2}{1 - d/D} \tag{3.5}$$

Where the channel height, H, is replaced by the tube diameter, D.

The L/λ correlation for the onset of detonations is based on a collection of DDT studies outlined by Dorofeev et al. [5]. Dorofeev et al. collected a large database of DDT studies done measuring the onset of detonation in similar geometries based on a simplistic “go and no-go” criteria. The characteristic size L, defined by Equations (3.4), (3.5) was used to describe each experimental configuration and cell size data was taken from each corresponding study, where available. By plotting the data from these studies with respect to the characteristic size, L, Dorofeev et al. were able to define a critical value of L/λ= 7, shown in Figure 3.6, where detonation initiation began universally.

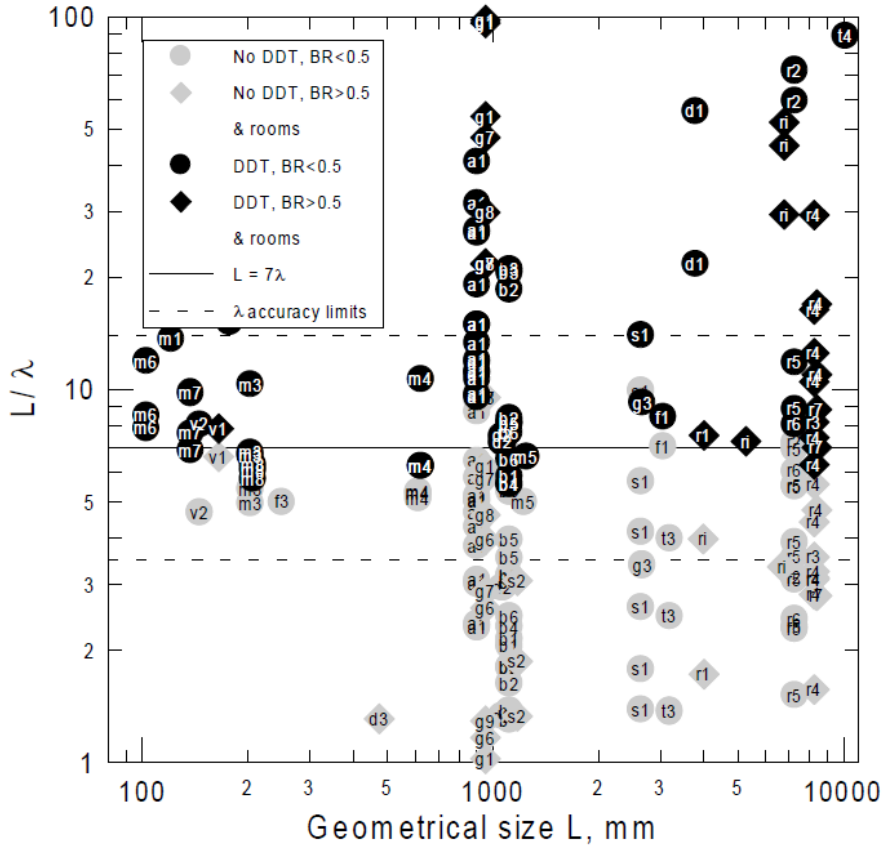

Figure 3.6: Summary of detonation onset conditions based on the proposed L/λ correlation by Dorofeev et al. [5] where black filled circles are DDT and gray filled circles are no DDT

The criteria, $L/\lambda > 7$ was fitted to the data based on the distinction between cases where DDT was observed and those where only a fast deflagration were observed. This criterion is indicated graphically as a solid horizontal line located at $L/\lambda = 7$. The deviation from this line was found to be approximately ±30% [5], indicated by the dashed horizontal lines above and below the $L/\lambda = 7$ line in Figure 3.6. The uncertainty is ultimately governed by the ±50% uncertainty of the measured cell size value [19].

Chapter 4

Experimental Apparatus and Procedure

4.1 Overview

In this study, the detonation hazard of several fuel-air mixtures was investigated based on the critical orifice plate diameter for detonation propagation. Equally spaced orifice plate obstacles were placed in the second half of the combustion tube. Ignition was via a weak automotive capacitive discharge spark positioned centrally at the tube endplate. A CJ detonation wave, initiated promptly using an oxygen-acetylene gas driver in the smooth tube, propagates into the obstacle section. The average combustion front velocity was obtained from flame time-of-arrival measurements deduced from flame ionization probes, spaced equally along the length of the tube. Six different orifice plate diameters between 38.1 mm (1.5”) and 76.2 mm (3”), in increments of 6.4 mm (1/4”) were used in the study. Soot foils were added between obstacles for select tests to gain insight into the propagation mechanism of a quasi-detonation. Mixtures investigated included hydrogen, ethylene, acetylene, propane, and DME -air mixtures. A series of tests was done for each orifice plate size where the lean and rich detonation propagation limits were obtained by varying the mixture composition.

4.2 Combustion Tube

Experiments were carried out in an apparatus consisting of a 6.1 m long, 10 cm inner-diameter tube (5” XXH), shown in Figure 4.1. The tube is constructed from two equal length 316 stainless steel tubes connected at the middle by 5” 1500 class ANSI flanges sealed with a metal spiral gasket [45]. This configuration allows for easy access to the middle of the tube for changing the obstacle configuration and placement of soot foils. Instrument ports are located along the top of the tube, spaced evenly at 0.305 m (12”), allowing for a total of 18 different measurement locations. As shown in Figure 1 a gas driver section is located at one end of the tube

where a small amount of reactive mixture can be added to the combustion tube in order to obtain a prompt detonation initiation in the less reactive test mixture.

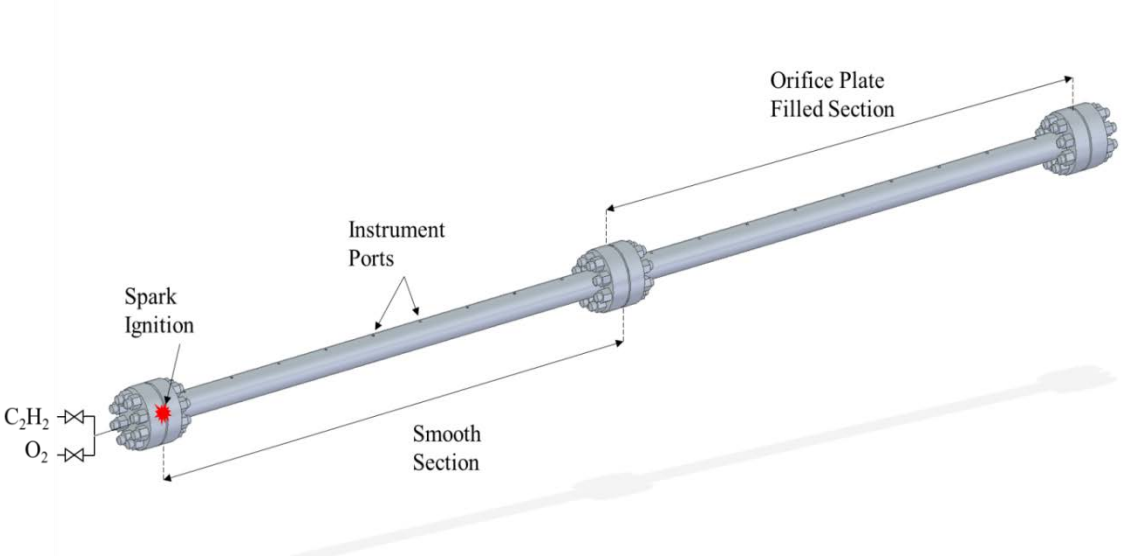

Figure 4.1: Combustion Tube Apparatus

4.2.1 Obstacles

Orifice plate obstacles of varying inner diameter were machined out of a 0.5” cold rolled steel plate, see Figure 4.2. The outer diameter of the orifice plates was approximately equal to the inner diameter of the combustion tube. The three holes along the outer edge of the orifice plate shown in Figure 4.3 allow for alignment and spacing of multiple plates using threaded rod. The orifice plate inner-diameter is defined as, *d*. and the spacing between obstacles, *S*. The spacing between obstacles was kept constant at a value equal to the tube diameter. This value was specified based on previous findings that obstacle spacing equivalent to the tube diameter provided the optimal distance for acceleration in the obstacle section [3].

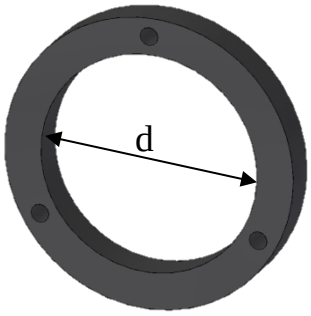

Figure 4.2: Orifice plate obstacle geometry

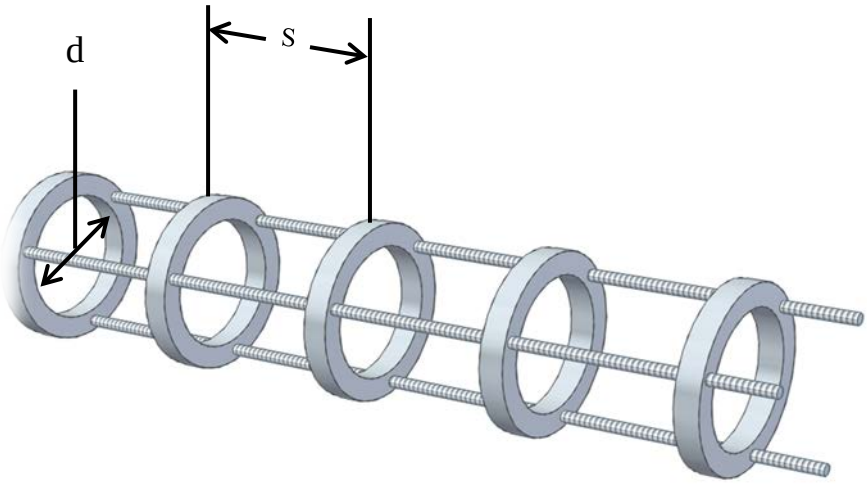

Figure 4.3: Series of equally spaced obstacles separated using threaded rod to maintain configuration.

A full set (enough to fill half the combustion tube) of thirty orifice plates were originally cut using a water jet cutting machine. These obstacles were cut to the smallest specified orifice diameter of 38.1 mm (1.5”) and after a complete set of experiments the diameter was opened up by an increment of 6.4 mm (1/4”). This was done manually using a TRAK lathe and a boring tool bar.

4.2.2 Obstacle Configuration

Two distinct obstacle configurations were used in this study. As shown in Figure 4.4 for "detonation propagation" experiments the second half of the tube contained orifice plates equally spaced at the tube diameter. For "DDT experiments" (see Figure 4.4) ignition was via a weak automotive capacitive discharge spark positioned centrally at the right-endplate, such that flame acceleration occurred from right-to-left in the obstacle field. For the detonation propagation limit experiments, a CJ detonation wave was initiated at the left-end of the tube using an oxygen-acetylene gas driver using the same spark ignition system. The CJ detonation wave is transmitted into the obstacle section. By using a gas driver to obtain a prompt detonation initiation the effects of flame acceleration and transition to detonation can be eliminated, allowing for the isolation of the detonation propagation mechanism conditions.

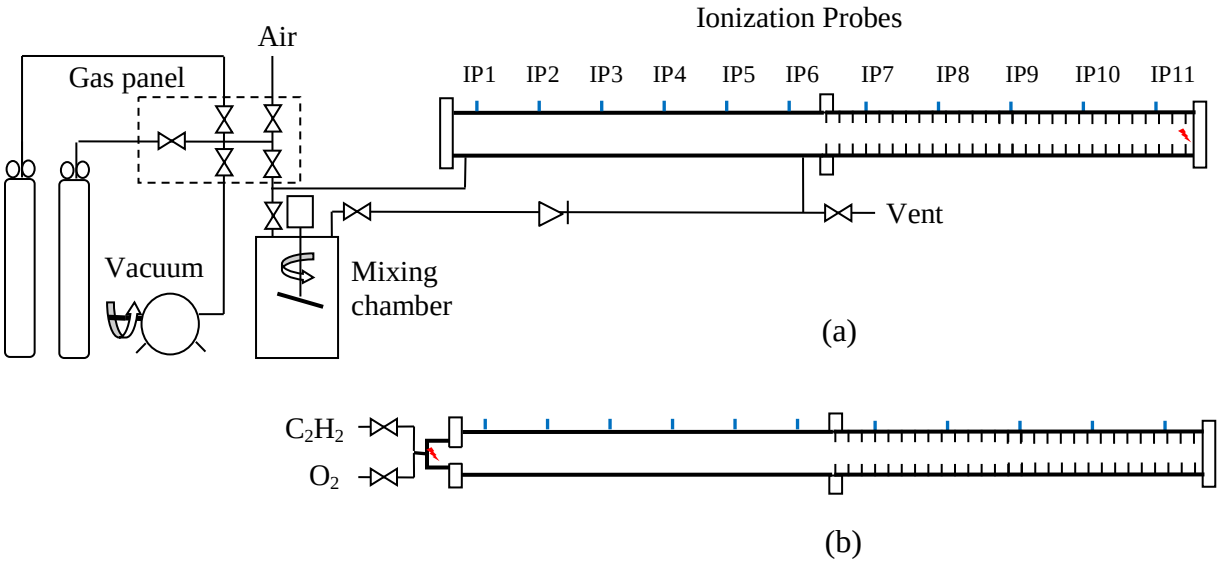

Figure 4.4: Experimental apparatus showing the gas handling system and obstacle filled tube. a) The DDT limits setup - flame propagation right to left, b) The detonation propagation limits setup - detonation propagation from left to right.

The average wave velocity was obtained from flame time-of-arrival measurements deduced from ionization probe (IP) signals. The IPs were distributed evenly, 305 mm apart (spanning roughly three orifice plates), down the length of the tube.

4.2.1 Driver Gas Setup

A gas driver system is used to deliver a small amount of reactive gas mixture to the combustion tube in order to obtain a prompt detonation initiation which transfers into the less reactive test mixture. A combination of acetylene and oxygen were chosen as driver gases based on extensive experiments performed previously by Diakow et al. [45] Diakow analyzed the gas driver gas dynamics using pressure transducers located in the driver section and combustion tube. The amount of driver gas added to the test section was set by pneumatic actuated valves controlled using LabVIEW. This allowed the acetylene and oxygen valves to be opened for a chosen amount of time with acceptable repeatability. Based on the findings of Diakow et al. an acetylene regulator pressure of 15 psig and oxygen regulator pressure of 60 psig was used and a valve open times between 0.2 and 0.5 seconds was specified to provide optimal detonation initiation without interfering with the gas characteristics of the test mixture. A schematic of the gas driver system is shown in Figure 4.5.

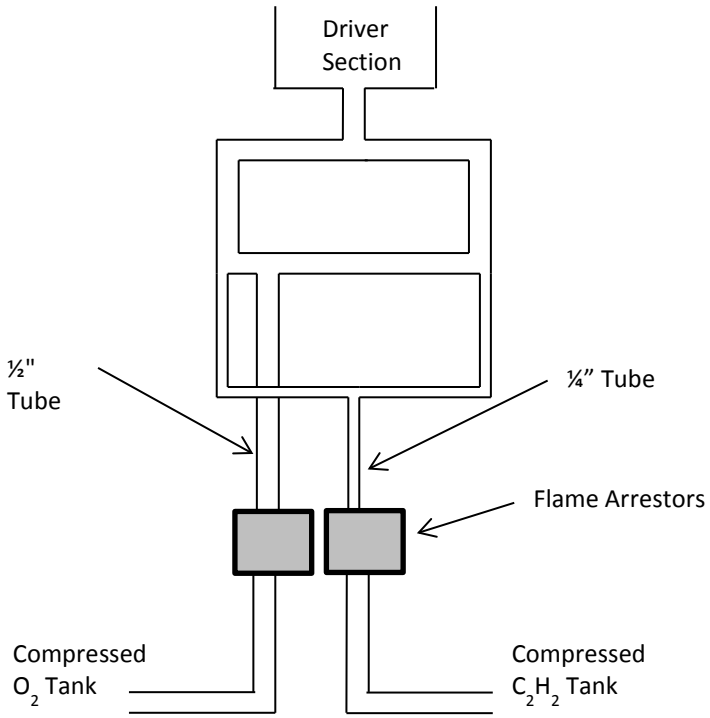

Figure 4.5: Schematic of gas driver setup used to produce the driver gas slug for prompt detonation initiation.

Acetylene was injected through ¼" tube and oxygen was injected using ½" in order to provide a suitable mixture concentration. The gas mixture system used to mix the two driver gases as they are injected is outlined in Figure 4.5. This piping system allows for both gases to be injected and mixed simultaneously. The flow generated by the injecting the high pressure gases allowed for adequate mixing of the gases at the T-fittings before being introduced to the driver section. Initial experiments were performed to determine the total pressure of the driver gas introduced to the combustion tube. This pressure is important as it contributes to the overall pressure of the test mixture in the combustion tube. A summary of these tests is shown in Table 4.1 for the various injection valve times used.

Table 4.1: Experimental driver gas pressure summarized as a function of valve injection time.

Driver Gas Injection Time (s)	Corresponding Driver Gas Pressure (kPa)
0.2	3.36
0.3	5.63
0.4	7.36
0.5	8.57
0.6	9.9
0.7	11.77

4.2.2 Mixing Chamber

The test mixture was prepared by the method of partial pressures in a separate mixing chamber equipped with an air driven impeller stirrer. The mixture constituents were added to the chamber and mixed for 20 minutes. Gases were supplied from standard compressed gas cylinders. The mixing chamber is an ASME certified 30 L pressure vessel equipped with a piezoelectric pressure transducer, Omega digital display and air driven belt stirrer which allow for the formation of accurate uniform gaseous test mixtures. The mixing chamber is certified to 3.4 MPa at 425 K with a failsafe rupture disk rated at 3.74 MPa at 425 K. A Parr Instruments magnetic sealing drive was used to provide a leak free linkage between the pneumatic motor and the internal propeller. The magnetic sealing drive solved issues encountered with a traditional packed gland assembly originally used. The mixing chamber is wrapped with conductive heating wire supplied by a voltage controller and insulated using fiberglass insulation. This setup allows for the heating of the mixing chamber to above room temperature which is favorable for fuels with low vapor pressures at standard temperature and pressure. A check valve was placed in-line between the mixing chamber and the combustion tube to ensure that there is no backflow to the mixing chamber when loading the test fuel.

4.2.3 Gas Panel

A gas panel was used to organize the majority of the valves and gauges for the operation of the combustion tube. The gas panel is plumbed with surface mounted ¼" (6.4 mm) stainless steel tubing. Mounting the plumbing on the surface of the panel allows for an easy understanding and visualization of the flow of gases involved in the operating procedure. All gases are supplied to the gas panel from standard compressed gas cylinders equipped with regulators for fine control over the flow of test gases. All fittings, valves and hoses used are supplied by Swagelok. The gas panel uses pneumatically actuated ball valves triggered with three-way solenoid valves. These solenoid valves are controlled using a computer equipped with two National Instruments USB-6525 data acquisition cards which are interfaced with LabVIEW software. Two data acquisition cards (8 digital outputs each) are necessary to remotely control a total of 12 valves. Power is supplied to the solenoid valves by a compatible National Instruments PS-16 24VDC power supply.

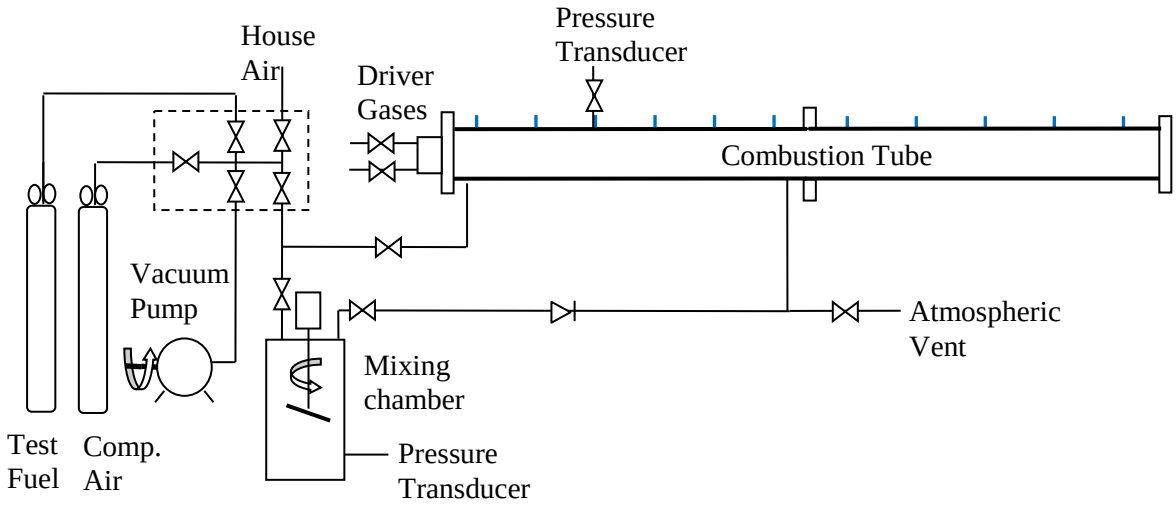

Figure 4.6: Detailed control panel and piping schematic

4.2.4 Test Gases

In order to validate the method chosen to characterize the detonation hazard several different test gases were used. These test gases ranged in detonation sensitivity from Acetylene to Methane, Table 4.2.

Table 4.2: Summary of test gases used and initial conditions

Fuel	Oxidizer	Temperature (K)	Pressure (atm)
Acetylene	Air	298	1
Hydrogen	Air	298	1
Ethylene	Air	298	1
DME	Air	298	1
Propane	Air	298	1
Methane	Air	298	1

All test gases were commercial grade and supplied from standard compressed gas cylinders equipped with regulators to maintain adequate control while introducing the gases to the mixing chamber. The initial temperature and pressure of the test mixture were maintained at approximately 298 K and 1atm over the entire range of experiments. The mixture equivalence ratio was varied in order to determine the detonation propagation limits of each fuel-air mixture at a given orifice plate diameter.

4.2.5 Instrumentation & Data Acquisition

Data acquisition was addressed using National Instruments LabVIEW, a NI PCI-6133 DAQ card and an external NI BNC-2110 terminal block. A LabVIEW program was created to sample inputs from ion probes at a rate of 2 MHz for an excessive total of 900,000 samples. A large number of samples were taken to ensure that data was not missed due to occasional spark ignition delay. A total of 8 ion probes were used along the length of the tube to record flame

velocity profile following ignition. The ignition system was triggered by a 5 V pulse provided by the NI card digital output, simultaneously starting the data acquisition system.

4.2.5.1 Ionization Probes (IP)

Ionization probes are ideal for measuring the average flame velocity along the length of the combustion tube. Chemical ionization in the hydrocarbon flame between two electrodes closes a simple circuit which provides a signal to the data acquisition system that can be interpreted to get the flame time-of-arrival. Ionization probes were made out of 1/2" Swagelok O-ring sealed male connectors. An electrically insulating Delrin core was inserted in the fitting and two conductive rods were drilled through the insulating material to provide an ionization gap. The rods were sealed using epoxy at the top and bottom of the fitting, see Figure 4.7. When the probes were fitted along the length of the tube the electrodes penetrated approximately 2.54 cm into the combustion tube.

Figure 4.7: Ionization Probe constructed from ½" Swagelok O-ring fitting

Two independent circuit boards were used, each with 4 ion probe circuits shown in Figure 4.8. A Systron RS320-2C DC power supply provided a voltage potential of approximately

260 V to each ion probe. As the flame propagates between the protruding electrodes in the tube the electrical circuit is temporarily closed. This results in a distinct voltage drop across the output resistor that is recorded by LabVIEW. The time associated with these voltage drops and the known distance between probes allows for a simple calculation of average flame velocity.

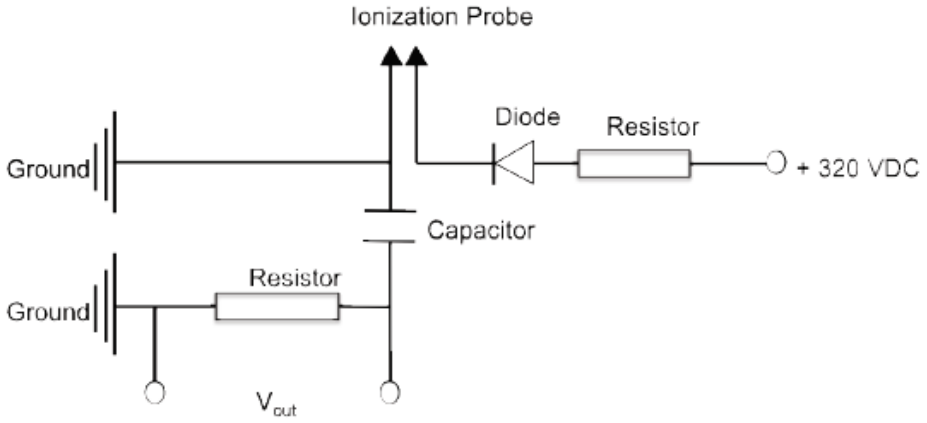

Figure 4.8: Ionization probe circuit schematic. The output voltage from the circuit, V_{out}, is relayed to the data acquisition system. [45]

A typical signal obtained for the passage of a detonation wave passed 8 ion probes is shown in Figure 4.9. A 5 V voltage drop is evident as the detonation wave passes each ionization probe. The red and green signals shown in Figure 4.9 are supplied by the two independent circuit boards supplying alternating ion probes along the length of the tube. This is done to make the analysis of successive ion probe signals obvious when the signal is not as clear as the one shown in Figure 4.9. The analysis of this signal will be discussed in the uncertainty section of this report.

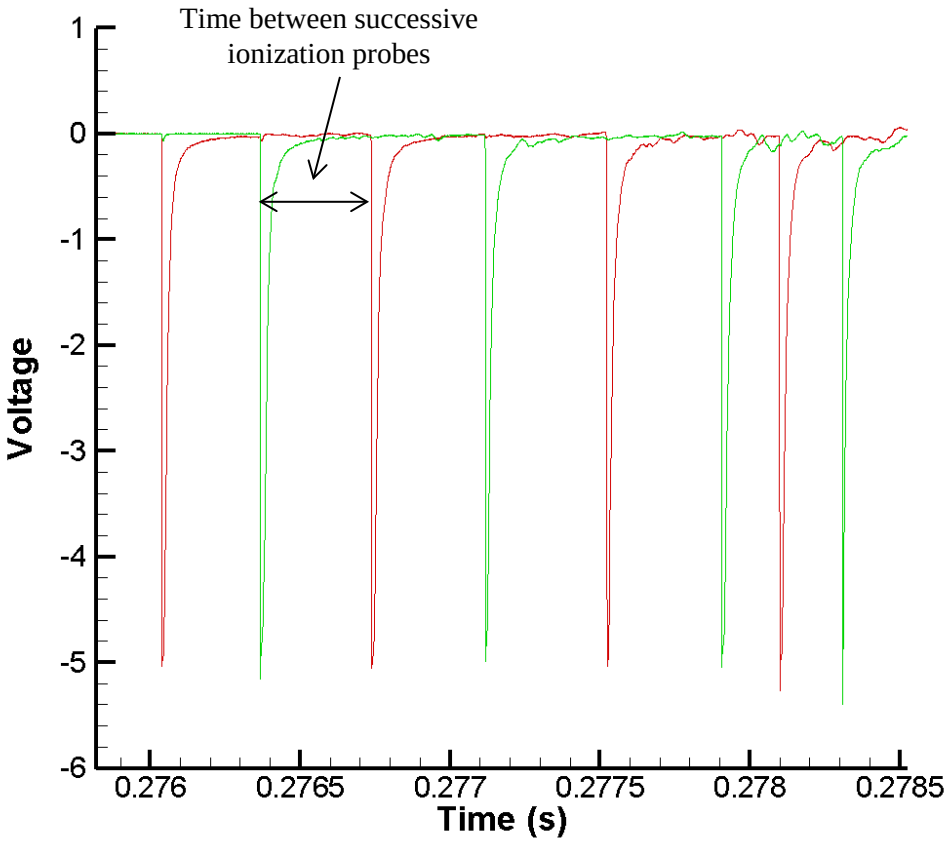

Figure 4.9: Ionization probe signal for stoichiometric Acetylene-Air mixture plotted using Tecplot 360. Each drop in voltage represents an individual ionization probe as the flame passes. The red and green signals are from independent alternating circuit boards.

4.2.6 Operating Procedure

The operating procedure for the combustion tube was dependent on the type of experiment. However, the method of preparing mixtures and introducing them to the combustion tube remained the same. This section will focus on the methods involved in this part of the experiment. The first step was to turn on the vacuum pump in order to evacuate the gas panel lines as well as the mixing chamber of all atmospheric and residual gas. While the gas panel and mixing chamber are being evacuated the compressed gas cylinders are opened. If a cylinder had been recently attached to the system the line connecting it to the control panel is also evacuated to ensure that only the desired gas is in the line. The mixing chamber is typically evacuated to a

pressure of 0.1 kPa but can vary marginally. The test gases were introduced to the mixing chamber individually using the method of partial pressures to create the desired mixture composition. The gas panel lines were evacuated between introducing gases to removed residual gas from the line. Once the mixture was formed the mixing chamber was isolated and the mixture was stirred using a pneumatic driven impeller stirrer for 20 minutes. This amount of time was previously determined to be sufficient for complete mixing based on a comparison of test data to data in literature. While the mixture is being mixed, the gas panel lines and the combustion tube were evacuated in preparation to load the test mixture. The combustion tube was typically evacuated to 0.5 kPa. A perfect vacuum was often not achievable due to the large volume of the tube and the potential for small leaks at fittings and instrument ports. When the mixture was finished, the stirrer was turned off and the mixture was loaded into the combustion tube to desired preset pressure. This pressure was 1 atm for tests where a driver gas was not used. If a driver gas was used the pressure of the introduced driver gas was considered in addition to the test mixture, resulting in a total test pressure of 1 atm. Immediately after the mixture was loaded into the combustion tube the mixture was ignited via a LabVIEW ignition program. The ignition program automatically records and saves the ion probe signals in a data file to the computer where it can be analyzed. Following the combustion of the test gas the remaining combustion products are purged using compressor supplied air to vent before creating the next test mixture and repeating the process.

Chapter 5

Results and Discussion

Experimental results are presented for each of the experiments involved in this project (DDT vs. Propagation Limits & Detonation Hazard Classification). To be concise not all of the experimental data is presented in this section due to the number of different fuels and blockage ratios tested. The trends presented in this section will focus on Hydrogen and Ethylene as test fuels; however other fuels were tested in addition. This additional experimental data is organized graphically in Appendix A for reference.

Theoretical CJ detonation velocity and speed of sound have been added to graphics where appropriate for comparison to experimental values. The theoretical velocities are calculated using the thermodynamic equilibrium program STANJAN. STANJAN was given its name based on its implementation of the JANNAF thermochemical data tables and Stanford University origin and solves for the chemical equilibrium state using the method of element potentials. This program and method is comprehensively described by Reynolds et al. in a report from Stanford University [46].

5.1 Influence of Blockage Ratio on the DDT and Detonation Propagation Limits

5.1.1 DDT experiments (BR= 44%)

DDT experiments were originally carried out in an apparatus consisting of a 6.1 m long, 0.10 m inner-diameter tube as described in the experimental section of the report. The tube contained 76.2 mm diameter orifice plates (44% area blockage) equally spaced at the tube diameter (L= 0.417 m) arranged in different configurations, as shown in Figure 5.1. In the first series of experiments a length of obstacles was positioned at the right-end of the tube and the left-end of the tube empty, as shown in Figure 5.1a. Tests were first carried out with 4.11 m of obstacles (with 1.07 m of obstacles to the left of mid-span of the tube), followed up with a few

tests with an extended 5.18 m of obstacles. Ignition was via a weak automotive capacitive discharge spark positioned centrally at the right-endplate, such that flame acceleration occurred in the left direction. In a second series of tests, a CJ detonation wave, initiated promptly using an oxygen-acetylene gas driver on the left-end of the tube, propagates into the obstacle section. These tests are done in two configurations (see Figure 5.1b). In configuration 1, the orifice plates filled the entire right-half of the tube. In configuration 2, the orifice plates were located in the first

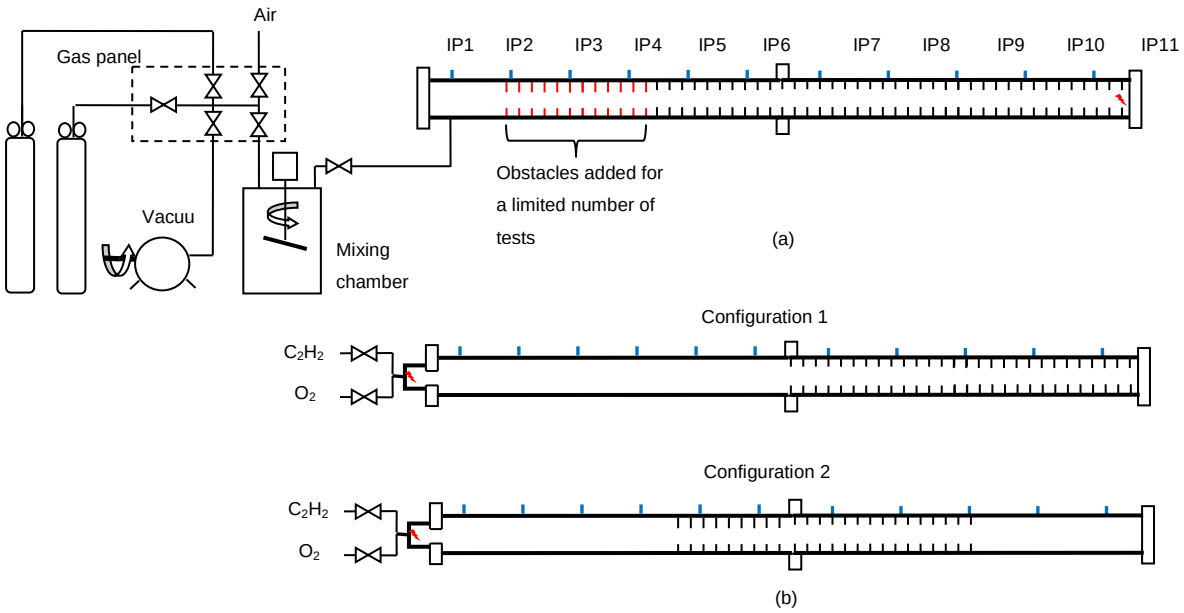

half of the second-half of the tube, i.e., 1.52 m long section of the tube starting at 3.04 m from the ignition endplate.

Figure 5.1: Experimental apparatus showing gas handling system and different obstacle configurations: a) flame acceleration and DDT in 4.11m/5.18 m obstacle section- flame propagation right-to-left, b) gas driver obstacle configuration 1 (3.05 m obstacle section) and 2 (2.44 m obstacle section) - propagation left-to-right.

Experiments were performed with hydrogen-air and ethylene-air mixtures at an initial pressure of approximately101 kPa (1 atm) and room temperature. Experiments were carried out using the traditional flame acceleration setup shown in Figure 5.1a with 4.11 m of obstacles. The

orifice plate configuration and blockage ratio used in this experiment is very similar to that used by Knystautas et al. [47] where they performed experiments in 0.05 m and 0.15 m diameter tubes. The measured flame velocity down the tube is shown in Figure 5.1a for three lean mixtures and stoichiometric hydrogen-air mixtures. The velocity data points in the obstacle section (open symbols) are based on the flame time-of-arrival for two ionization probes 0.61 m apart, whereas the flame velocity in the smooth part of the tube (closed symbols) is averaged over 1.22 m after the last obstacle. The lines represent a fourth order polynomial fit of the velocity data in the obstacle section. The speed of sound in the combustion products and CJ velocity for a 19% hydrogen in air mixture (dotted line and solid line respectively) calculated using the equilibrium code STANJAN is included for reference in Figure 5.2a. The test performed with 30% hydrogen resulted in relatively quick flame acceleration leading to DDT and quasi-detonation propagation in the obstacles. A detonation wave was successfully transmitted into the smooth part of the tube that propagated at close to the CJ value. For the other three fuel-lean mixtures the flame accelerates reaching a maximum velocity above the products speed of sound at 2.5 m. For the 19% mixture the flame velocity remains above the products speed of sound but for the 17% and 18% mixture the flame velocity dips below in the last part of the obstacles. For all three of these mixtures the flame decelerates in the smooth part of the tube to a velocity below the products speed of sound typical of a decoupled shock wave and flame. The velocity data for three rich mixtures is provided in Figure 5.2b. Also shown in this figure is the reference speed of sound of the combustion products. Quasi-detonation is achieved in the obstacle section for a 57% hydrogen mixture in air, but the detonation wave fails to transmit into the smooth tube. For a slightly richer mixture of 57.5% a choked flame propagates in the obstacle section that decouples into a decelerating flame and shock wave upon exiting the obstacles.

The quasi-steady combustion wave velocity in the obstacles, following flame acceleration and DDT, can be obtained from the velocity versus distance data. The term “quasi-steady” in this

context refers to an *average* velocity (note, large velocity fluctuations exist between obstacles). The measured average combustion wave velocity at the end of the obstacle section (measured between IP7 and IP5, i.e., between 2.74 m and 3.96 m) is shown in Figure 5.3 as a function of hydrogen mole fraction. The error bars represent the low and high average velocity between IP7 and IP6 and between IP6 and IP5. Also shown for reference, is the calculated CJ detonation velocity and isobaric speed of sound in the combustion products (represents the maximum steady deflagration velocity) calculated using STANJAN. The bulk of the data is concentrated at the detonation limits, in order to resolve the limit composition.

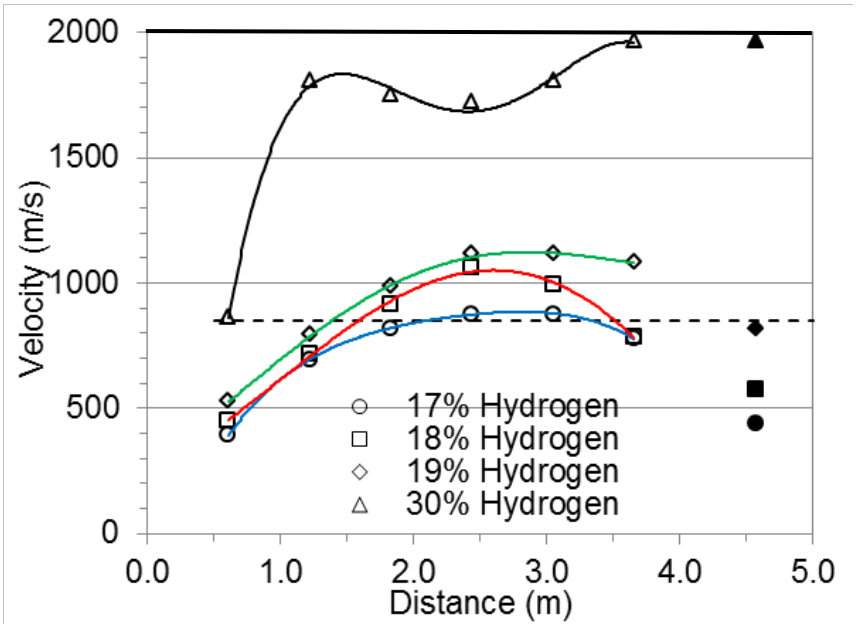

(a)

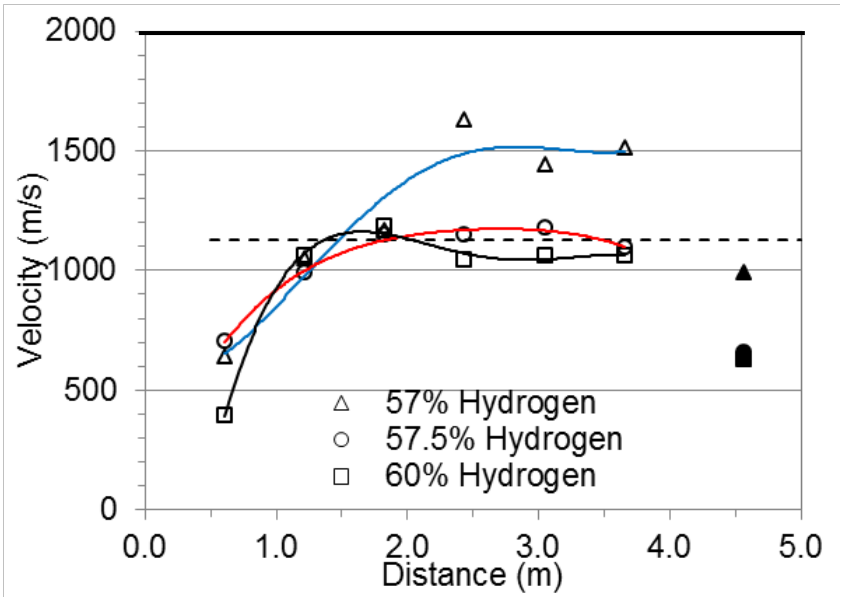

(b)

Figure 5.2: Flame acceleration in 4.11 m obstacles, setup shown in Figure 5.1a. Empty symbols are for inside obstacles, solid symbol is for in smooth tube after obstacles. Colored lines through the data are fourth order polynomial fits. A solid line represents CJ velocity and a dotted line represents the speed of sound in combustion products for a) 19% hydrogen and b) 60% hydrogen in air mixture.

There is a step-change in the quasi-steady velocity across the speed of sound in the products at the fuel-rich limit, similar to that observed by Knystautas et al. and Peraldi et al. [47, 4]. However, on the fuel-lean side the average velocity continuously decreases from stoichiometric (30% hydrogen) to 15% hydrogen, with a small jump at 18% hydrogen. Based on the traditional definition of the DDT limit (leanest and richest mixture where the quasi-steady velocity is above the isobaric speed of sound in the products), the limits are 16% and 57% hydrogen, corresponding to the vertical dotted lines in Figure 5.3.

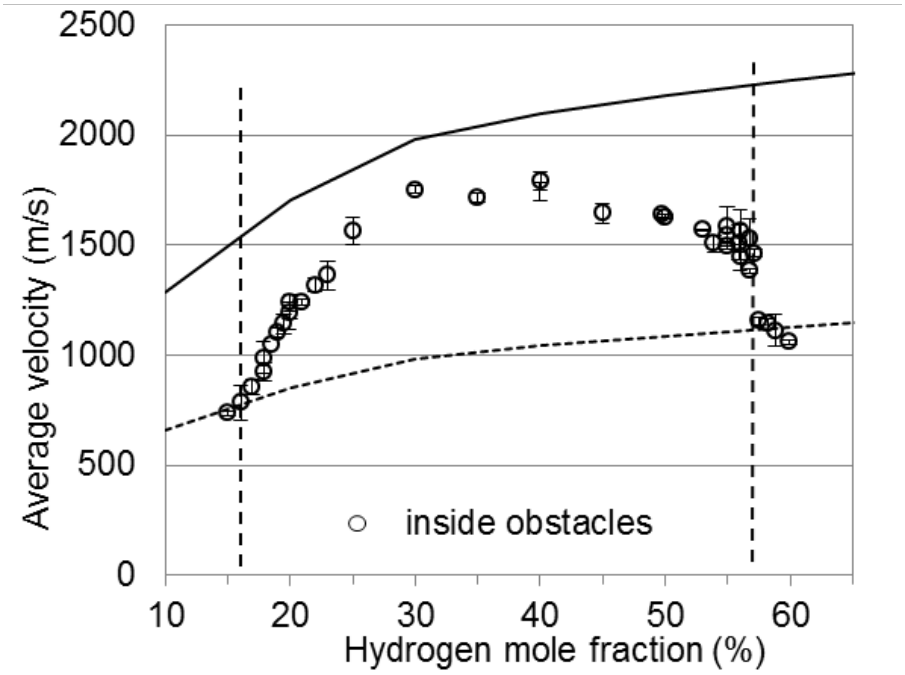

Figure 5.3: Average combustion wave velocity at the end of the 4.11 m obstacle section (setup in Figure 5.1a). Solid line is for CJ detonation velocity and dotted is for isobaric products speed of sound.

New detonation cell size data obtained in the smooth tube using a gas driver for prompt detonation initiation is provided in Figure 5.4 (average value plotted and the vertical error-bars represent the standard deviation). Also shown in the Figure 5.4 is detonation cell size data previously reported by Ciccarelli et al. [6] obtained in a 27 cm diameter tube. The cell size data on the lean and rich sides of the curve are fit with straight lines (lean-side data fit: λ=-

19.7%H2+431.1*; rich-side data fit: λ= *5.6*%H2-257.4*). Based on the detonation cell size data, the lean and rich DDT limits correspond to d/λ=0.6 and d/λ=1.1, respectively. The rich-limit is consistent with the d/λ>1 DDT criterion proposed by Peraldi et al. [4], but the lean-limit (even taking into account the uncertainty in cell size measurements) does not agree with the d/λ>1 criterion. A similar disagreement exists between the L/λ values at the lean limit (L/λ=3.5 and L/λ=6.0) and the L/λ>7 DDT correlation (Dorofeev et al., [5]).

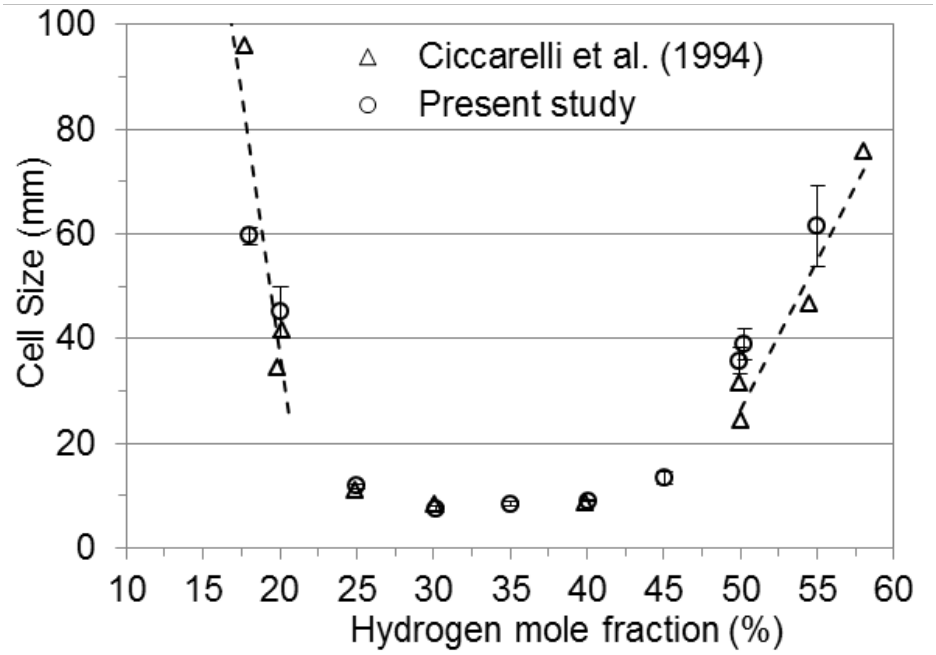

Figure 5.4: Detonation cell size for hydrogen-air at atmospheric pressure. Dotted lines are linear fits of data.

As seen from the results given in Figure 5.2 after the combustion wave exits the obstacle section into the smooth part of the tube, it either propagates as a CJ detonation wave, or continues as a decaying, decoupled shock wave and flame. The velocity of the detonation wave, or flame, in the smooth section (measured between IP2 and IP3) is overlaid with the quasi-steady velocity measured within the obstacle section in Figure 5.5. It is well known that in this effectively "one-dimensional" geometry the decoupled flame decelerates at a faster rate than the shock wave (shock velocity not measured in the experiment). For mixtures just outside the detonation limits

the reflection of the decoupled shock wave at the endplate initiated an explosion (most likely a detonation). This finding is based on the final ionization probe (IP1) signal that showed a weak pulse, associated with the passage of the flame, followed by a large amplitude pulse associated with ionization of the combustion products behind the reflected shock/detonation. This explosion at the endplate does not affect the transmission phenomenon at the end of the obstacle section, and thus is not discussed further.

The study by Knystautas et al. [47], performed in a similar geometry, found that for mixtures just outside the detonation limits, the decoupled-flame could re-accelerate and transition to detonation. This transition to detonation typically occurred over a very long distance (roughly 80 tube diameters). Due to the limited length of the smooth part of the tube in this study, this re-acceleration phenomenon did not occur. Knystautas et al. [47] used the re-acceleration and DDT in these near limit mixtures to define the DDT limit in the smooth tube. Based on this data they proposed the $D/\lambda>1$ correlation for the detonability limits in a smooth tube.

The data shown in Figure 5.5 shows a sharp transition for the transmission of the detonation wave into the smooth tube on both the lean and rich sides. For mixtures between 20% and 55% (vertical dotted lines in Figure 5.5) the quasi-detonation wave transmission into the smooth tube results in a CJ detonation wave. Outside these limits the quasi-detonation wave fails after exiting the obstacles, decoupling into a decaying shock wave and quickly decelerating flame (note: in this case the data point represents a single velocity measurement between IP2 and IP3). The limits are narrower than the DDT limits based on a propagation velocity greater than the isobaric speed of sound in the products in the obstacles shown in Figure 5.3. Specifically the lean limit for transmission to detonation after the obstacles is 20% hydrogen versus 16% for the lean DDT limit.

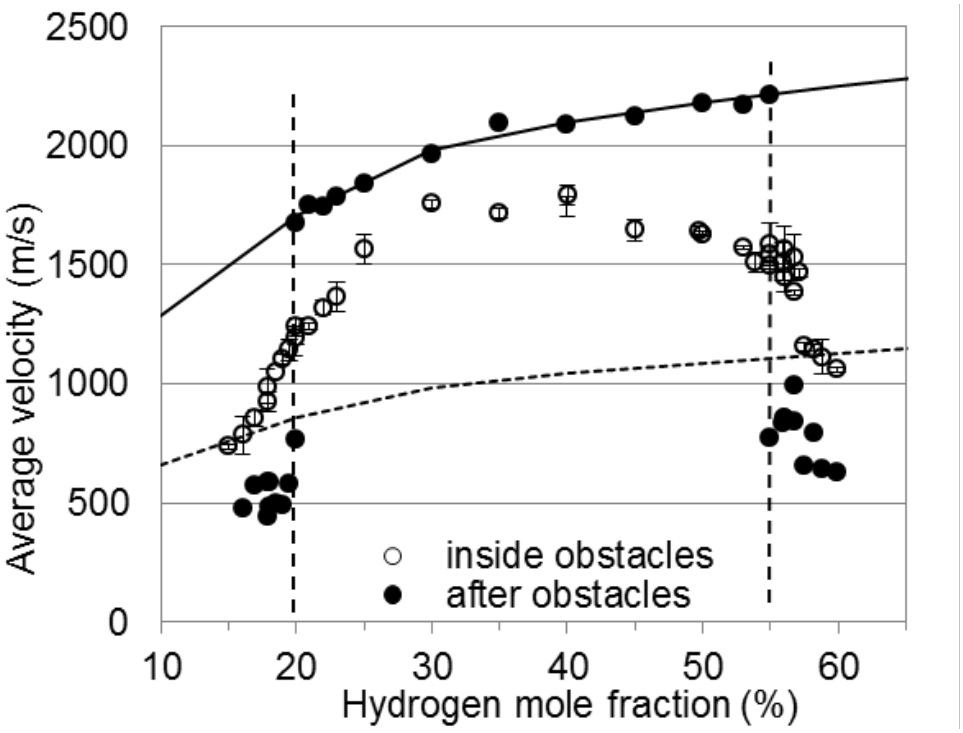

Figure 5.5: Average combustion wave velocity at the end of the 4.11 m obstacle section (see Figure 5.3), and in the smooth tube after the obstacles (setup in Figure 5.1a). Solid line is for CJ detonation velocity and dotted is for isobaric products speed of sound.

The large difference in the measured lean DDT and lean transmission limit, and the continuous decrease in the quasi-detonation velocity to the products speed of sound puts into question the measured lean DDT limit. In order to confirm that the DDT limits were not affected by the length of the obstacle section, a few tests were performed with the obstacle section lengthened to 5.1 m (obstacles shown in red up to IP2 in Figure 5.1a) for mixtures near the lean and rich DDT limits. The measured steady-velocities from these tests are shown in Figure 5.6. With this longer obstacle section the rich limit was unchanged at 57% hydrogen but the fuel lean side data was strongly affected. The data on the lean side shows a step-change at 19% hydrogen, the true lean DDT limit. Based on the detonation cell size data, the lean and rich DDT limits obtained using the longer obstacle section correspond to d/λ=1.3 and d/λ=1.1, respectively. These limits are consistent with the d/λ>1 DDT criterion proposed by Peraldi et al. [4]. A similar agreement exists between the L/λ values at the limits (L/λ=7.3 and L/λ=6.3) and the L/λ>7 DDT

correlation (Dorofeev et al., [5]). The d/λ and L/λ values at the limits for the different experiment configurations are summarized in Table 5.1. A closer look at the flame acceleration data for 18% hydrogen in Figure 5.2a shows an overshoot in the flame velocity between 2 and 3 m. This raises the average velocity to a value greater than the products speed of sound but the wave is not steady, resulting in a false lean DDT limit. This gradual increase in flame velocity past the speed of sound of the products in the lean hydrogen mixtures is very different from the sudden change in velocity at the time of DDT observed in the 30% and 57% hydrogen tests in Figure 5.2 that more closely resembles what happens with DDT in a smooth tube.

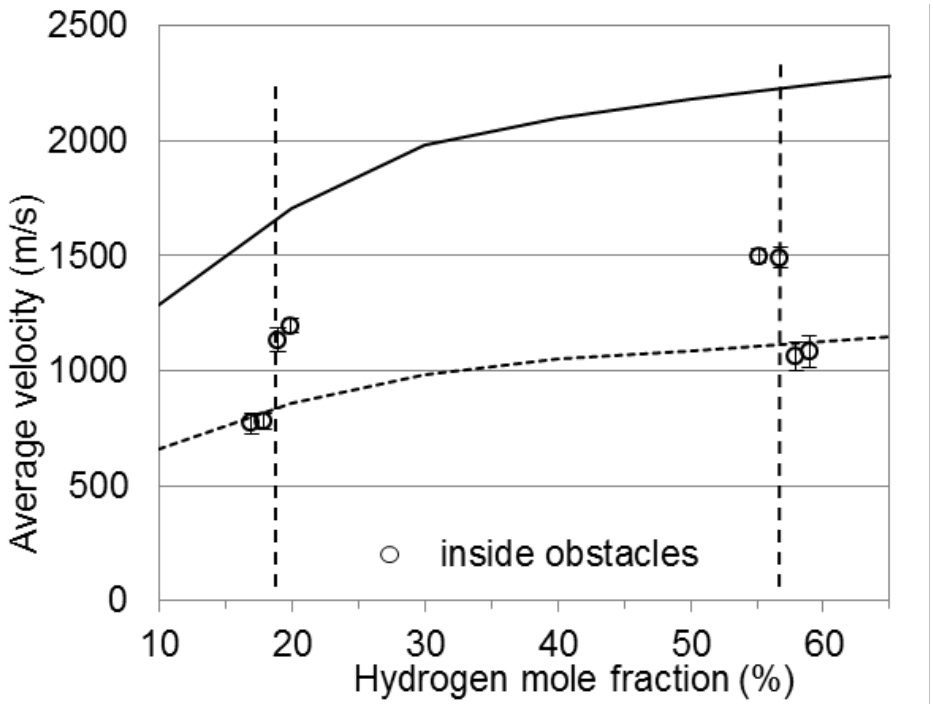

Figure 5.6: Average combustion wave velocity at the end of the 5.18 m obstacles (setup in Figure 5.1a). Solid line is for CJ detonation velocity and dotted is for isobaric products speed of sound.

Similar DDT experiments were performed with ethylene-air. The quasi-steady velocity values obtained in the shorter obstacle section is shown in Figure 5.7 and in the longer obstacle section in Figure 5.8. The DDT limits obtained from the short and long obstacle section are both

4.8% and 11.4% ethylene, respectively. However, the velocity data obtained in the long obstacle section shows a well-defined jump in velocity at the limits. For mixtures near the limits the flame velocity measured in the shorter obstacle section does not reach steady state, as evidenced by the larger error bars in Figure 5.7, similar to that observed in the lean hydrogen data. Based on the cell size data obtained from Knystautas et al. [19] the corresponding d/λ is 0.9 and 1.9. Taking into account the inherent uncertainty in cell size measurements, the lean DDT limit is in agreement with the $d/\lambda>1$ DDT limit but the rich limit is not. The values of L/λ at the lean and rich limits are 4.8 and 10.5, respectively, and are summarized in Table 5.2. The limits for detonation transmission into the smooth tube were measured to be 5.3% and 11.5% ethylene, very close to the DDT limits.

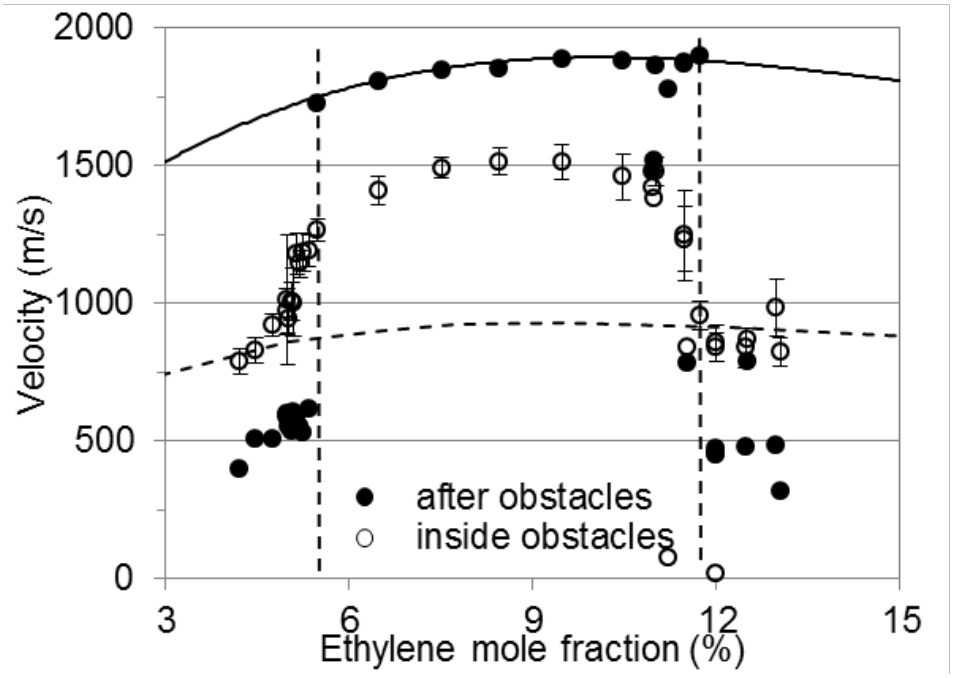

Figure 5.7: Average combustion wave velocity at the end of the 4.11 m obstacle section, and in the smooth tube after the obstacles (setup shown in Figure 5.1a). Solid line is for CJ detonation velocity

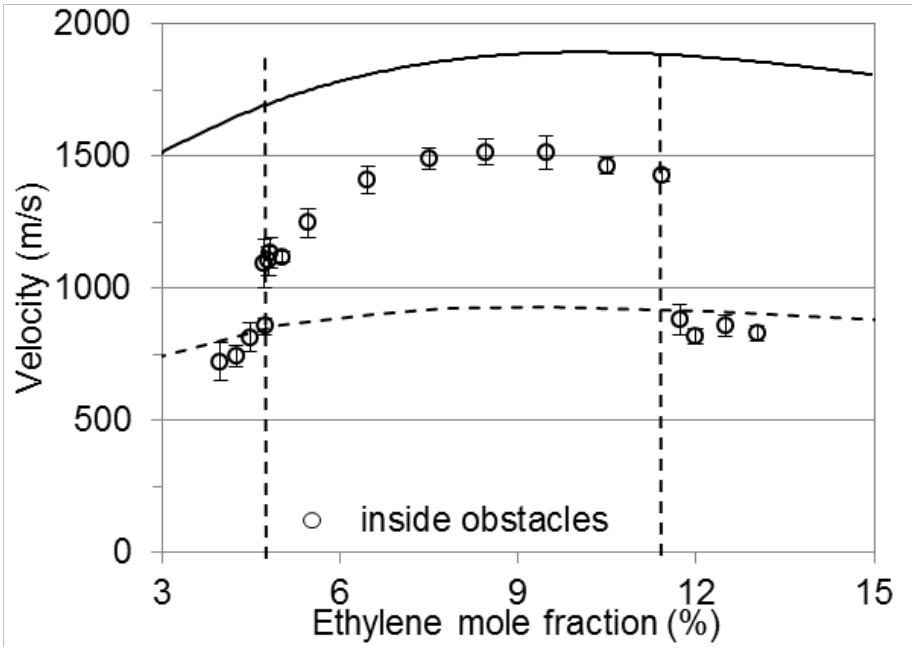

Figure 5.8: Average combustion wave velocity at the end of the 5.18 m obstacles (setup in Figure 5.1a). Solid line is for CJ detonation velocity and dotted is for isobaric products speed of sound.

5.1.2 Detonation propagation experiments (BR= 44%)

The detonation limits for an obstacle filled tube are governed by detonation propagation and DDT requirements, e.g., a detonation cannot propagate if the geometry cannot accommodate the propagation mechanism or conditions are not met for initiation. The detonation propagation limits in the obstacle-section obtained in the experiments performed in the traditional setup (see Figure 5.1a) include effects associated with the flame acceleration and local DDT event. In order to obtain the quasi-detonation propagation limits (independent of the DDT process) experiments were performed where a CJ detonation wave was transmitted into the obstacle-section. For these experiments the orifice plates were set up in configuration 1 (see Figure 5.1b), with the second half of the tube filled with obstacles and where the gas driver was used to achieve prompt detonation initiation. The detonation velocity measured just before the obstacles (between IP5 and IP6) for hydrogen-air mixtures is provided in Figure 5.9, along with the calculated CJ

detonation velocity and the speed of sound of the combustion products. Detonation waves were successfully initiated by the gas driver for mixtures between 17% and 60% hydrogen. The measured detonation velocity is in agreement with the theoretical CJ detonation value, indicating that the gas driver successfully generates a self-sustained detonation entering the obstacle section. Based on the cell size linear fits shown in Figure 5.4 (the plot includes data from a larger 27 cm tube from Ciccarelli et al [6]), the corresponding cell size for these mixtures are 96 mm and 84 mm, respectively. This is in agreement with the $D/\lambda>1$ (where D=100 mm is the inner-diameter of the tube) smooth tube detonation propagation correlation proposed by Knystautas et al. [47].

The average velocity recorded at the end of the obstacle-section of the tube (between IP9 and IP11) is shown in Figure 5.9. The error bars represent the low and high average velocity between IP9 and IP10 and between IP10 and IP11. The small size of the error bars indicates that the combustion wave achieves steady-state propagation by the end of the tube. Transmission of the CJ detonation wave leading to quasi-detonation propagation in the long obstacle field (average velocity above the speed of sound in the products) was observed for mixtures between 18% and 58% hydrogen. These limits are identical to the DDT limits obtained in the traditional setup (refer to Table 5.1).

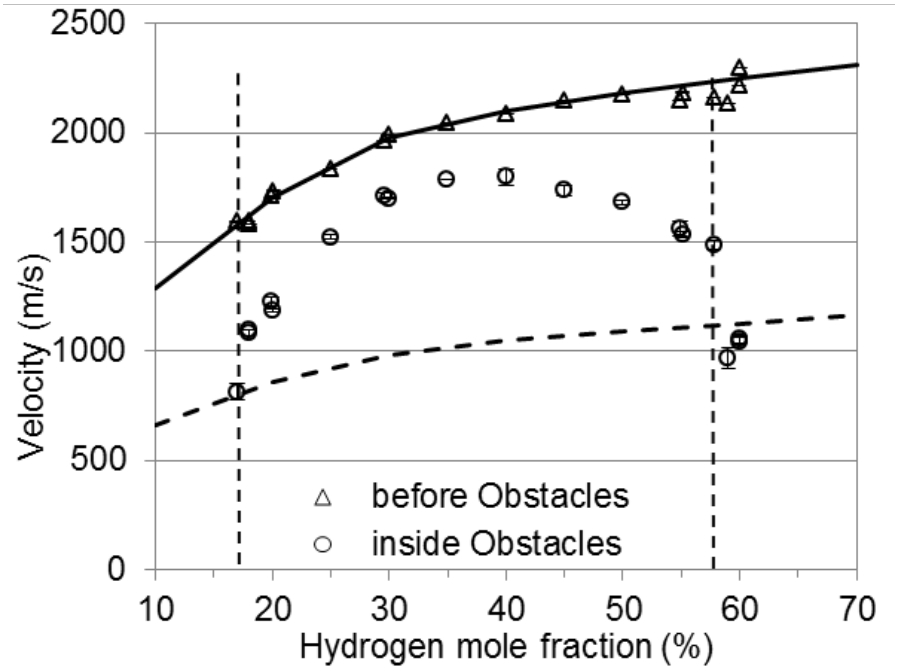

Figure 5.9: Detonation velocity before and at the end of 3.05 m obstacle section (setup shown in Figure 5.1b config 1). Solid line is for CJ detonation velocity and dotted is for isobaric products speed of sound.

In order to measure the detonation transmission limits (obstacle to smooth tube) experiments were carried with configuration 2, shown in Figure 5.1b, with the gas driver. The velocities measured at the end of the obstacle section and in the smooth-tube section after the obstacles are shown in Figure 5.10. The detonation velocity just before the obstacle section (not shown in Figure 5.10 in order to avoid data clutter) was close to the CJ detonation velocity, similar to the values obtained in the configuration 1 tests, shown in Figure 5.9. Detonation transmission to quasi-detonation propagation in the obstacle section was observed for mixtures between 19% and 57% hydrogen. These limits are exactly the same as the DDT results obtained with the longer obstacle section in configuration 1 (see Table 5.1). Transmission of a quasi-detonation to a CJ detonation in the smooth tube was observed in the range of 20% and 57% hydrogen. The corresponding d/λ and L/λ for the transmission tests (see Table 5.1) agrees very well with the with the $d/\lambda > 1$ and $L/\lambda > 7$ limit correlations. The rich limit is slightly wider than the transmission results obtained in the DDT tests performed in the setup shown in Figure 5.1a

(20% and 55% hydrogen, see Table 5.1). The difference in these limits could be attributed to insufficient obstacle length for the quasi-detonation to achieve steady-state in the DDT tests.

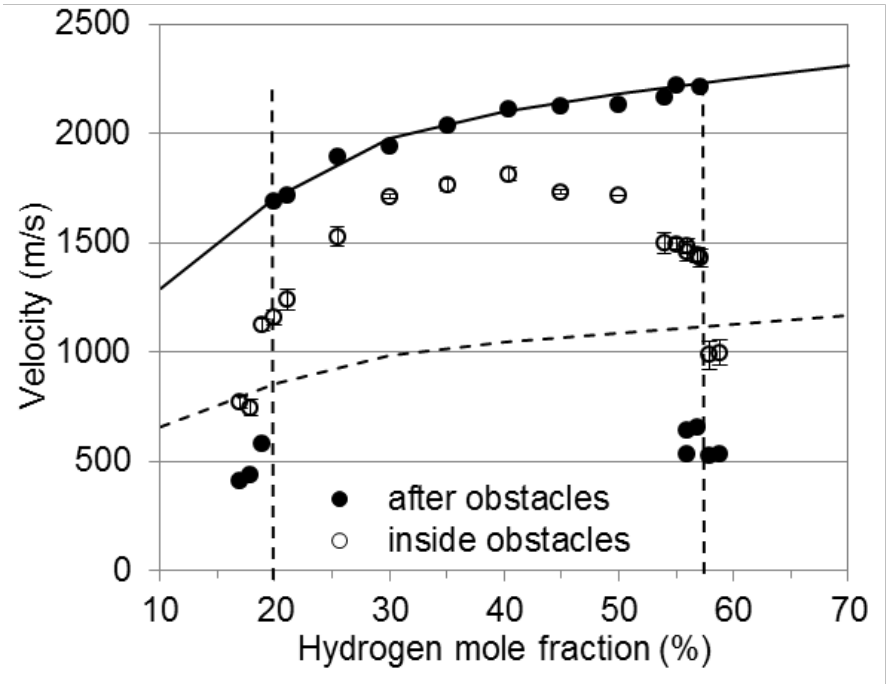

Figure 5.10: Detonation velocity inside and after the 2.44 m obstacle section (setup shown in Figure 5.1b config 2). Solid line is for CJ detonation velocity and dotted is for isobaric products speed of sound.

The detonation transmission limit experiments with the gas driver were also carried with ethylene-air mixtures. The velocities measured at the end of the obstacle section and in the smooth-tube section after the obstacles are shown in Figure 5.11. For all tests the detonation velocity measured just before the obstacle section was very close to the CJ detonation velocity (not shown in Figure 5.11). Detonation transmission to quasi-detonation propagation in the obstacle section was observed for mixtures between 4.8% and 13% ethylene. The lean limit is the same as the DDT result obtained with the obstacle section in configuration 1 (see Table 5.2). However, the rich limit is slightly larger than the 11.4% ethylene value measured in the DDT tests. The 13% ethylene rich limit was confirmed by experiments with the obstacle section extended all the way to the end of the tube (similar geometry to configuration 1 in Figure 5.1b but

with 3.96 m of obstacles). The corresponding d/λ values are 0.9 and 1.2 for the lean and rich limits, in good agreement with the d/λ >1 criterion. For the transmission into the smooth tube the limits were 5.3% and 13% again in good agreement with the limit correlations (see Table 5.2).

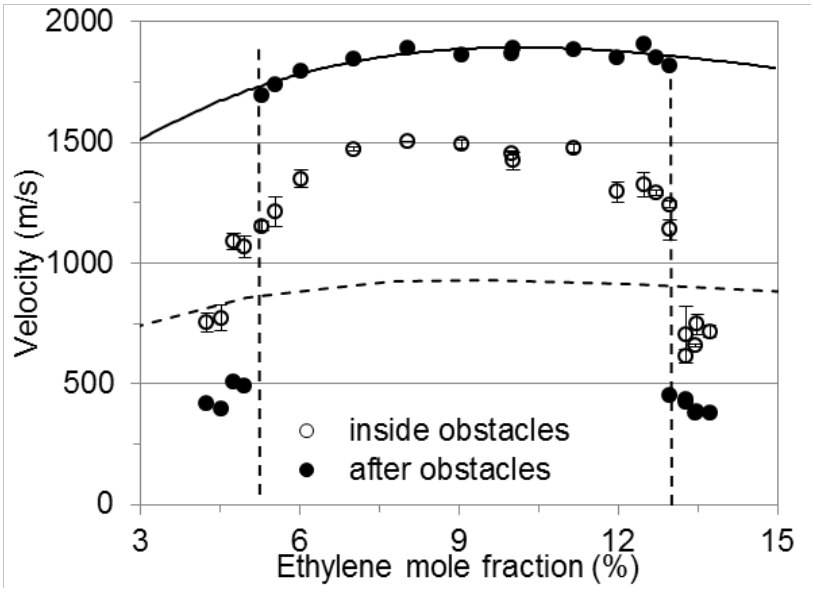

Figure 5.11: Detonation velocity inside and after the 2.44 m obstacle section (setup shown in Figure 5.1b config 2). Solid line is for CJ detonation velocity and dotted is for isobaric products speed of sound.

Table 5.1: Measured limits for hydrogen-air in the three different configurations in Figure 5.1.

Experiment	**Limits (%)**		**d/λ**		**L/λ**	
Flame acceleration and DDT						
DDT (V_D>c_b) in 5.12 m long obstacles	19	57	1.3	1.1	7.3	6.3
Gas driver						
Config. 1- velocity greater than speed of sound	18	58	1.0	1.1	5.5	5.8
Config. 2 - velocity greater than speed of sound	19	57	1.3	1.1	7.3	6.3
Config. 2 - detonation transmission	20	57	2.1	1.1	11.3	6.3

Table 5.2: Measured limits for ethylene-air in the three different configurations in Figure 5.1.

Experiment	Limits (%)		d/λ		L/λ	
Flame acceleration and DDT						
DDT (V_D>c_b) in 5.12 m long obstacles	4.8	11.4	0.9	1.9	4.8	10.5
Gas driver						
Config. 2 - velocity greater than speed of sound	4.8	13	0.9	1.2	4.8	6.5
Config. 2 - detonation transmission	5.3	13	1.1	1.2	6.2	6.5

5.1.3 DDT & Detonation Propagation Limits with Increasing Blockage Ratio

An additional series of tests was performed where the lean and rich DDT and detonation propagation limits were obtained for higher BR (0.44, 0.53, 0.61, 0.75, and 0.81) orifice plates. The DDT experiments were performed using the setup shown in Figure 5.1a. The flame velocity measured down the obstacle filled first-half of the tube equipped with higher BR (0.53), 69.9 mm, orifice plates is shown in Figure 5.12a. For most of the tests the flame accelerates reaching a quasi-steady velocity before the end of the obstacles at 3.05 m. For example, for the 30% hydrogen test the flame accelerates quickly with a sudden jump in velocity establishing a steady-state velocity before the end of the obstacle section. Whereas for 22% and 52% hydrogen the flame acceleration is slower and there is no sharp rise in velocity associated with a DDT event, resulting in a shorter velocity plateau. For the other two tests the terminal velocity is lower and thus a longer velocity plateau is established.

The detonation propagation experiments were performed for the higher BR (0.53) orifice plates using the typical setup in configuration (a) of Figure 5.1b. The explosion front velocity measured in the obstacle section filled with 69.9 mm orifice plates is shown in Figure 5.12a. The detonation velocity measured in the smooth tube just before the obstacles corresponds to the data

point at 2.6 m. In all the tests the velocity measured at the end of the smooth part of the tube was within 2% of the theoretical CJ detonation wave velocity. The velocity data point at 3.05 m in Figure 5.12b represents the average velocity measured between ion probes located 305 mm before and after the first orifice plate (located at the mid-span of the tube). For all the mixtures tested, the detonation velocity drops rapidly upon entering the obstacle section and stabilizes within the first 0.5 m of the start of the obstacle section.

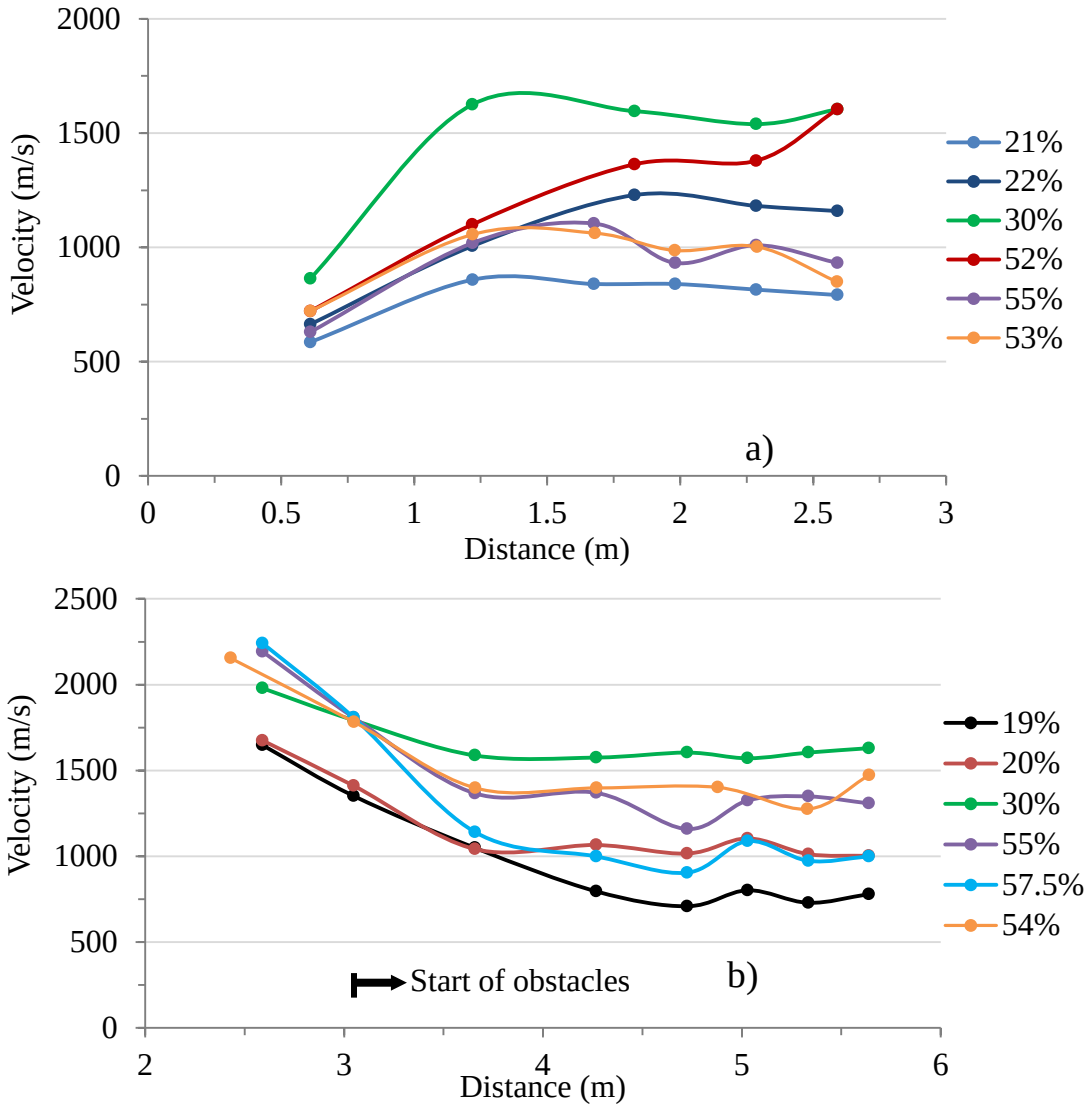

Figure 5.12: Explosion front velocity versus distance for hydrogen-air mixtures with 69.9 mm orifice plates.

For both the DDT and detonation propagation experiments the average velocity measured at the end of the obstacle section (69.9 mm orifice plate diameter) for hydrogen-air mixtures is plotted in Figure 5.13. The error bars represent the maximum and minimum velocity measured over the steady part of the velocity profile. For points with no error bars a velocity plateau was not achieved and the velocity based on the last two ionization probes was used. Also shown in Figure 5.13 for reference are the theoretical CJ detonation velocity and the speed of sound of the products (isobaric process). The velocity data shows that two propagation regimes exist. In the quasi-detonation mode, as defined by the lean and rich limits (shown as vertical dotted lines), the velocity is between the isobaric speed of sound of the products and the CJ detonation velocity. In general, the magnitude of final average velocity for each mixture is similar for both the DDT and the detonation propagation experiments. This is an indication that the propagation mode is independent of the initiation process. However, the initiation process does influence the quasi-detonation regime limits. Specifically, the propagation limits are wider than the DDT limits. Similar experiments were carried out with ethylene-air mixtures, the average velocity data is provided in Figure 5.14. The DDT limits are narrower than the detonation propagation limits, similar to that observed for hydrogen-air, with a significant difference on the rich side, also reported in [17].

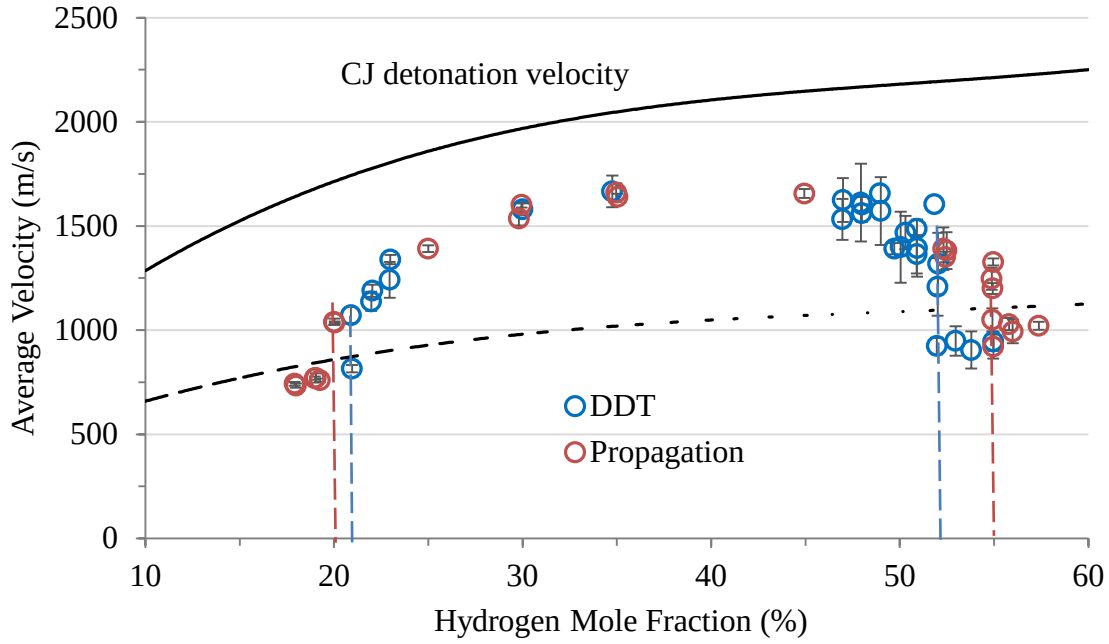

Figure 5.13: Average explosion front velocity for hydrogen-air mixtures with 69.9 mm orifice plates. The CJ detonation velocity and isobaric speed of sound in products (dashed) are shown for reference.

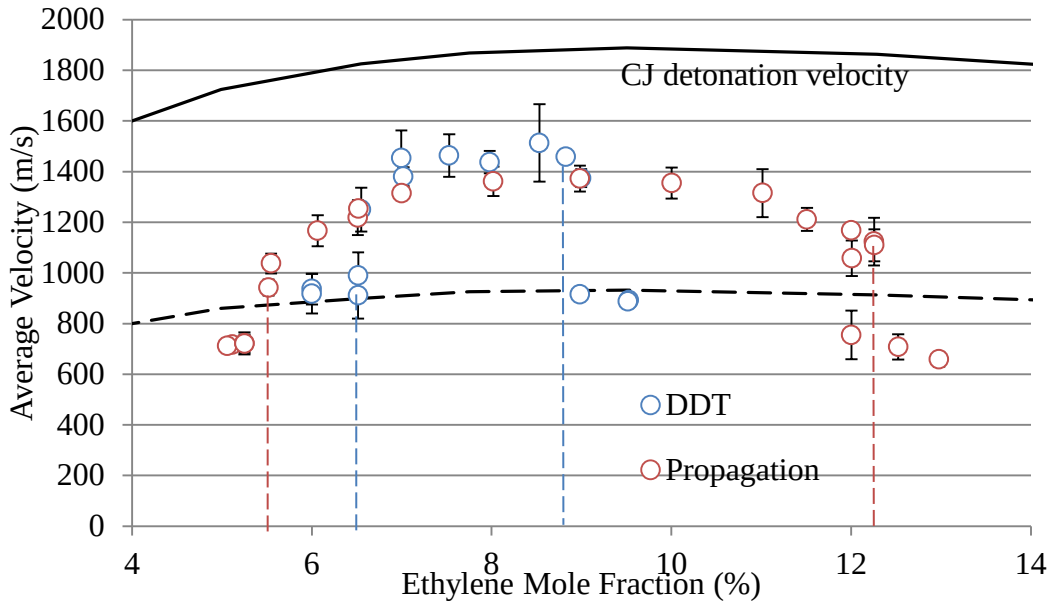

Figure 5.14: Average explosion front velocity for ethylene-air mixtures with 69.9 mm orifice plate. The CJ detonation velocity and isobaric speed of sound in products (dashed) are shown for reference.

The distinction between the DDT and Propagation limits observed in Figure 5.13 and Figure 5.14 for hydrogen and ethylene respectively is not unique to these fuels. This trend of diverging limits is also observed for acetylene (only lean limit data provided), DME, and propane air mixtures. Graphs associated with these fuels are organized in Appendix A.

Similar experiments were carried out for 63.5, 57.2, 50.8 and 44.5 mm orifice plate diameters in order to further understand the relationship between the obstacle blockage ratio and the detonation limits. The quasi-detonation regime limits obtained for all the orifice plate diameters for the DDT experiments are summarized in Table 5.3. The limits represent the leanest and richest mixture that resulted in DDT before the end of the obstacle section. The data shows that the DDT limits widen with increase in orifice diameter for all test fuels. The value of d/λ corresponding to the DDT limits varies significantly with the orifice plate BR. For both hydrogen, ethylene, and acetylene fuels the value of d/λ (lean and rich) decreases with decreasing orifice plate BR to a value of roughly 1 for BR=0.44. This convergence to unity is also projected for DME and propane. However, due to limitations with the test apparatus, smaller blockage ratios than 0.44 could not be investigated to confirm this. The exception to this trend is rich ethylene-air for which $d/\lambda=1.9$. The breakdown of the $d/\lambda=1$ criterion for BR greater than 0.6 was also reported by Kuzntesov et al. [48]. A similar divergence from the L/l= 7 criterion is also observed with increasing BR.

Table 5.3: DDT limits for hydrogen-air, ethylene-air, acetylene-air, and DME-air

Orifice diameter (mm)	BR	Limit resolution (% fuel)	Lean limit (% fuel)	Equiv. ratio	Lean limit d/λ	Lean limit L/λ	Rich limit (% fuel)	Equiv. ratio	Rich limit d/λ	Rich limit L/λ
Hydrogen-air										
44.5	0.81	DDT not observed								
50.8	0.75	1	30	1	6.9	25.7	33	1.2	6.4	27.6
57.2	0.68	1	29	0.95	6.8	26.8	37	1.4	6.6	27.8
63.5	0.61	1	24	0.74	4.2	20.3	44	1.8	4.8	18.1
69.9	0.53	1	22	0.66	2.2	8.5	52	2.5	1.8	10.2
76.2	0.44	1	19	0.55	1.3	6.1	57	3.1	1.1	7.2
Ethylene-air										
63.5	0.61	DDT not observed								
69.9	0.53	0.25	6.5	0.99	2.1	9.9	9	1.41	2.7	12.6
76.2	0.44	0.25	4.75	0.71	0.9	4.7	11.4	1.84	1.9	10.2
Acetylene-air										
44.5	0.81	0.25	9	1.18	8.6	34.9				
50.8	0.75	0.25	8.75	1.14	9.8	39.2				
57.2	0.68	0.25	6.75	0.86	8.3	33.7				
63.5	0.61	0.25	6	0.76	7.9	33.9				
69.9	0.53	0.25	4.75	0.59	3.4	15.9				
76.2	0.44	0.25	4.25	0.53	2.8	14.9				
DME-air										
63.5	0.61	DDT not observed								
69.9	0.53	DDT not observed								
76.2	0.44	0.25	6.54	1	14.2	86.7	8.75	1.37	16.3	99.3

The quasi-detonation limits from the detonation propagation experiments using the configuration (a) setup shown in Figure 5.1b are provided in Table 5.4. Similar to that observed for the DDT limits, the propagation limits widen with decreasing BR, and the d/λ corresponding to the limits (lean and rich) decrease to a value of roughly unity for BR=0.44. The detonation propagation and DDT composition limits from Table 5.3 and Table 5.4 are plotted as a function of the orifice plate BR in Figure 5.15. The propagation and DDT limits for the largest orifice

plate diameter (BR=0.44) are in general very similar. The exception is rich ethylene that also has the DDT limit anomaly of $d/\lambda=1.9$. For both fuels the DDT limits are narrower than the detonation propagation limits, and the DDT limits are more strongly affected by the orifice plate BR.

Table 5.4: Detonation propagation limits for hydrogen-air, ethylene-air, acetylene-air, and DME-air

Orifice diameter (mm)	BR	Limit resolution (% fuel)	Lean limit (% fuel)	Equiv. ratio	Lean limit d/λ	Lean limit L/λ	Rich limit (% fuel)	Equiv. ratio	Rich limit d/λ	Rich limit L/λ
Hydrogen-air										
44.5	0.81	Detonation propagation not observed								
50.8	0.75	1	26	0.82	4.3	17.2	41	1.62	5.7	22.7
57.2	0.68	1	24	0.74	3.8	15.5	46	1.98	3.2	13.2
63.5	0.61	1	22	0.66	2	8.5	50	2.33	2.4	10.1
69.9	0.53	1	20	0.58	1.9	8.8	54	2.74	1.4	6.6
76.2	0.44	1	18	0.51	1	5.3	58	3.22	1.1	5.6
Ethylene-air										
54.5	0.81	Detonation propagation not observed								
50.8	0.75	Detonation propagation not observed								
57.2	0.68	Detonation propagation not observed								
63.5	0.61	0.25	6.25	0.95	1.7	7.3	10.5	1.68	1.9	8.2
69.9	0.53	0.25	5.5	0.83	1.2	5.4	12.25	1.99	1.3	6.2
76.2	0.44	0.25	4.75	0.71	0.9	4.7	13.5	2.23	1.1	5.7
Acetylene-air										
44.5	0.81	0.25	7.75	1	7.7	31.2				
50.8	0.75	0.25	6.75	0.86	7.4	29.5				
57.2	0.68	0.25	5.5	0.69	5.3	21.5				
63.5	0.61	0.25	4.75	0.59	3.1	13.2				
69.9	0.53	0.25	4.5	0.56	2.9	13.5				
76.2	0.44	0.25	4	0.5	2.7	14.5				
DME-air										
63.5	0.61	Detonation propagation not observed								
69.9	0.53	0.25	6.54	1	14.9	69.5	9.75	1.54	14.2	66.2
76.2	0.44	0.25	5.5	0.83	N/A	N/A	11.25	1.81	10.2	54.3

In a cylindrical tube at the limit a single head spin exists (an effective cell size of πd) and therefore the corresponding limit criterion is $d/\lambda \geq 1/\pi$. Knystautas et al [47] found when a quasi-detonation was transmitted from a rough-tube into a smooth-tube of the same diameter the limit where the detonation could not be re-established in the smooth tube corresponded to $d/\lambda=1$. The trend in the data in the present tests indicates that as the BR decreases, the critical orifice plate diameter, for both the DDT and propagation experiments, approaches the cell size (i.e., at the limit $d/\lambda \rightarrow 1$). This is consistent with the smooth-tube limit condition ($BR \rightarrow 1$) reported by Knystautas et al. [47]. For both the DDT and the propagation limits, for the highest BR the orifice plate diameter was at least five times greater than the detonation cell size for hydrogen-air, and two times larger for ethylene-air. The orifice plate plays a key role in the DDT process by providing a surface for the leading shock wave of the fast-flame to reflect and generate a hot spot. Concurrently the lead shock wave must diffract around the orifice plate, thereby weakening it before the interaction with the next orifice plate. Weakening of the shock wave makes it more difficult to generate the critical condition for a hot spot to form and transition to detonation. The beneficial effects of the orifice plate in providing a reflection surface diminishes with increased BR due to the increased effect of shock wave weakening by diffraction.

In the present study the DDT and propagation limits for a given orifice plate diameter are distinguished by the two experiments. For the larger BR orifice plates, the DDT composition limits were found to be significantly narrower than the detonation propagation limits. Kellenberger and Ciccarelli [28] showed using high-speed schlieren photography that the global propagation of a quasi-detonation wave near the limit is largely governed by local detonation initiation at the obstacle face following shock reflection. The present study shows that if this mechanism can artificially be engaged (in this case by transmitting a CJ detonation wave into the obstacle field) then a detonation wave can propagate beyond the restrictions of the DDT limits

that require flame acceleration to a fast-flame as well as the local DDT process itself that is not well understood.

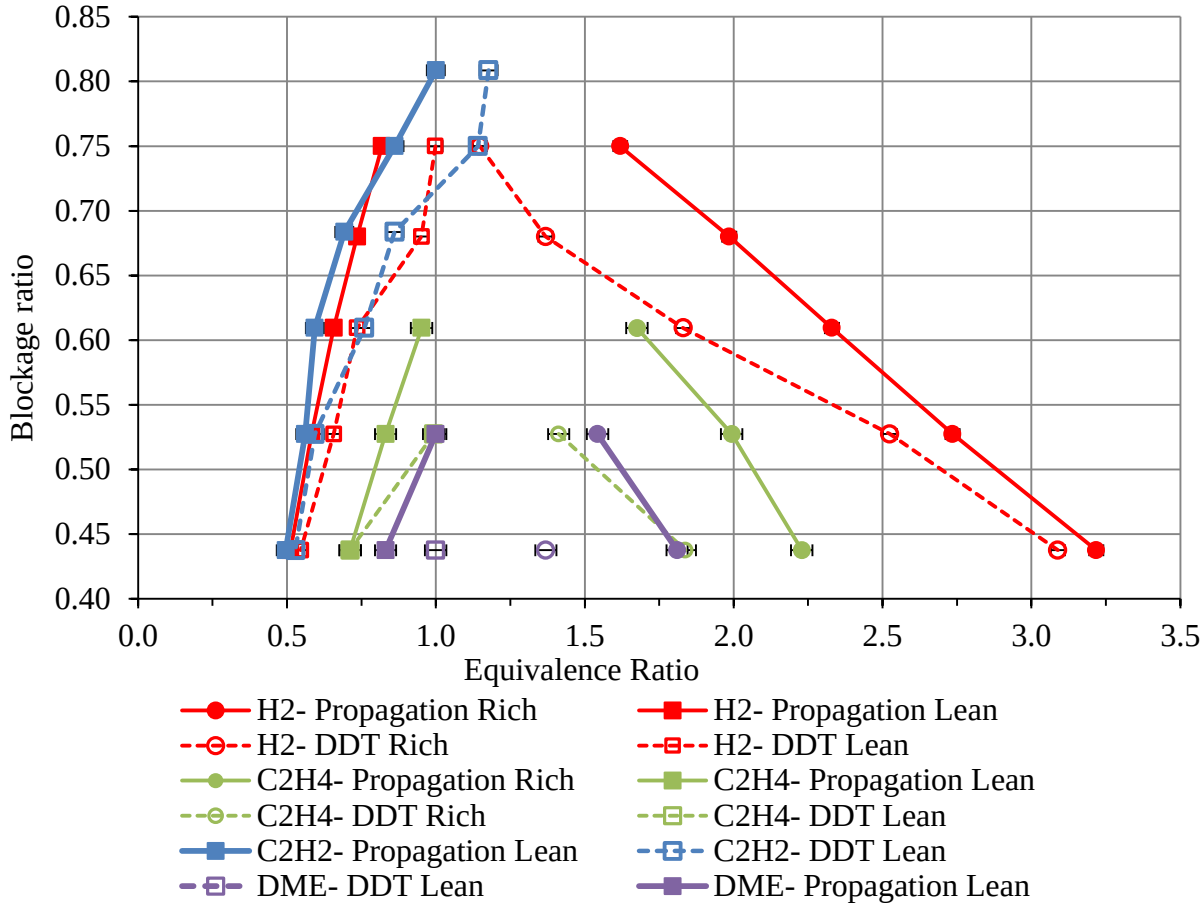

Figure 5.15: Detonation propagation and DDT limits as a function of orifice plate BR. A larger version of this figure can be found in Appendix A.

In conclusion, the experimental results demonstrated that the detonation propagation and the DDT limits are strongly affected by the orifice plate BR. For the 100 mm diameter tube used in the experiment, the propagation and DDT limits are similar for 0.44 BR orifice plates. Both the propagation and the DDT limits narrow with increasing BR, more significantly for the DDT limits. The narrowing of the limits with increasing BR is accompanied by a large deviation from the $d/\lambda=1$ detonation limit criterion. The beneficial effects of the orifice plate providing a

reflection surface for detonation initiation diminishes with increased BR due to the increased effect of shock wave weakening by the diffraction process.

5.2 Detonation Hazard Classification Based on the Critical Orifice Plate Diameter for Detonation Propagation

A sensitivity parameter (measured from a standardized experiment) is required to categorize the detonation hazard potential for fuels. Lee et al. [49] proposed that the minimum initiation energy be used as a parameter for the sensitivity of a fuel-air mixture to detonation. In a follow-up study Matsui and Lee [21] inferred the minimum initiation energy of a range of fuel-oxygen and fuel-air mixtures from critical tube experiments. The critical tube diameter represents the smallest diameter of an open-ended tube from which a detonation wave can emerge and continue to propagate in the surrounding explosive atmosphere. The scale of a critical tube diameter apparatus is very large because a "receiver vessel" is required. For less reactive fuels, tests are carried out in remote outdoor test sites using a large plastic bag to contain the fuel-air mixture at the exit of the tube. Due to the experiment scale requirement, critical tube diameter data is only available for a limited number of hydrocarbon fuel-air mixtures [31]. Correlations exist relating both the critical tube diameter and critical initiation energy with the detonation cell size [31, 19]. However, detonation cell size measurements are subject to a high level of s uncertainty that greatly reduce their reliability and usefulness for safety applications. The objective of this portion of the study is to establish a new parameter that can be used to categorize the relative detonation explosion hazard of a fuel that can be measured in a smaller, more practical apparatus. This new parameter is the minimum orifice plate diameter required for detonation propagation in a tube (of given diameter) equipped with orifice plates. For diameters below the critical orifice plate diameter a fast-flame (or choked flame) propagates [4]. As a

significant part of this study the critical orifice diameter was measured for stoichiometric acetylene, hydrogen, ethylene, propane and dimethyl ether (DME) air mixtures.

These experiments were carried out in parallel to the DDT/detonation propagation study using the apparatus shown in Figure 5.1b, configuration (a). A detonation was initiated in the first half of the tube using an acetylene-oxygen driver ignited by a weak spark. The second half of the tube contained orifice plates equally spaced at the tube diameter. Six different orifice plate diameters between 38.1 mm (1.5″) and 76.2 mm (3″), in increments of 6.4 mm (1/4″) were used in the study. These orifice plate diameters correspond to the BR's used in the DDT/detonation propagation study. The average combustion front velocity was obtained from ionization probe time-of-arrival measurements. The probes were distributed evenly, 305 mm apart (spanning roughly four orifice plates), down the length of the tube.

The measured explosion front velocity versus distance for stoichiometric hydrogen-air and ethylene-air for different size orifice plates is provided in Figure 5.16. In all the tests a CJ detonation wave (1979 m/s for hydrogen-air, 1825 m/s for ethylene-air) entered the obstacle section that starts at 3.05 m. The velocity data point at 3.05 m in Figure 5.16 represents the average velocity measured between ion probes located 105 mm before and after the first obstacle. In most cases, the front stabilizes to a sub-CJ detonation velocity within the first 0.5 m of the obstacle section. The data shows that the smaller the orifice plate diameter, the lower the steady-state wave velocity. For hydrogen a transition in the propagation regime occurs for an orifice plate diameter of 44.5 mm, see Figure 5.16a. For diameters smaller than 44.5 mm a significantly lower final velocity is achieved (roughly 650 m/s). For ethylene the change in propagation regime occurs for a 63.5 mm diameter.

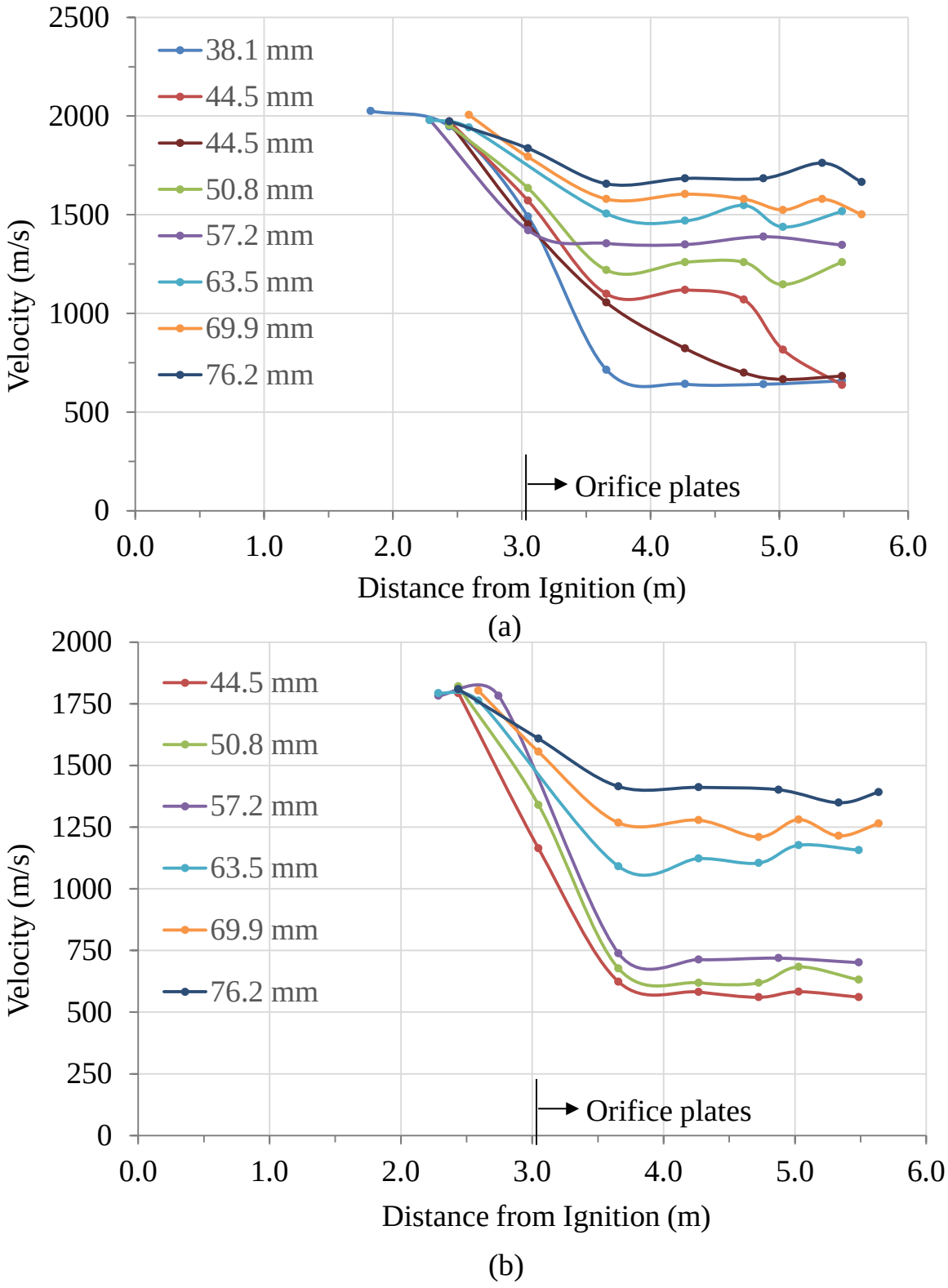

Figure 5.16: Explosion front velocity versus distance for stoichiometric a) hydrogen-air and b) ethylene-air.

The steady-state average wave velocity (normalized with the CJ detonation velocity) measured at the end of the obstacle section for stoichiometric hydrogen (30% by volume) is plotted in Figure 5.17a. The average velocity measurement was made over the last 1 m of the tube and the “error bars” correspond to the maximum and minimum velocity measured over this distance. Note the deviation in velocity is typically no greater than ±3% of the average value. Also shown in Figure 5.17a is the data for 35% hydrogen that corresponds to the hydrogen-air mixture with the smallest detonation cell size. The speed of sound of the combustion products for these two mixtures is roughly half the CJ detonation velocity (i.e., 984 m/s). The step change in average velocity for the 44.5 mm and 50.8 mm orifice plate diameters for 30% hydrogen (and between 38.1 mm and 44.5 mm for 35% hydrogen) represents a change in propagation mode from fast-flame to quasi-detonation. The smaller critical orifice plate diameter, and slightly smaller detonation velocity deficit, for 35% hydrogen suggests that the change in propagation mode is influenced by the detonation cell size. There is a linear drop in the CJ detonation velocity deficit with increasing orifice plate diameter. The average velocity measured for the two mixtures in the 38.1 mm diameter orifice plate, where fast flames were observed, are identical.

The average wave velocity measured at the end of the obstacle section for the different orifice plate diameters for stoichiometric ethylene (6.5% by volume) and 7% ethylene are plotted in Figure 5.17b. Again there is a linear drop in the detonation velocity deficit with increasing orifice plate diameter. The critical orifice plate diameter for both mixtures is 63.5 mm, which is larger than that observed in both the hydrogen-air mixtures, see Figure 5.17a. The average fast-flame velocity data (obtained for three orifice plate sizes) are identical for both mixtures (6.5% and 7% ethylene-air) and show a linear dependence with the orifice plate diameter, similar to the quasi-detonation velocity but with a different slope.

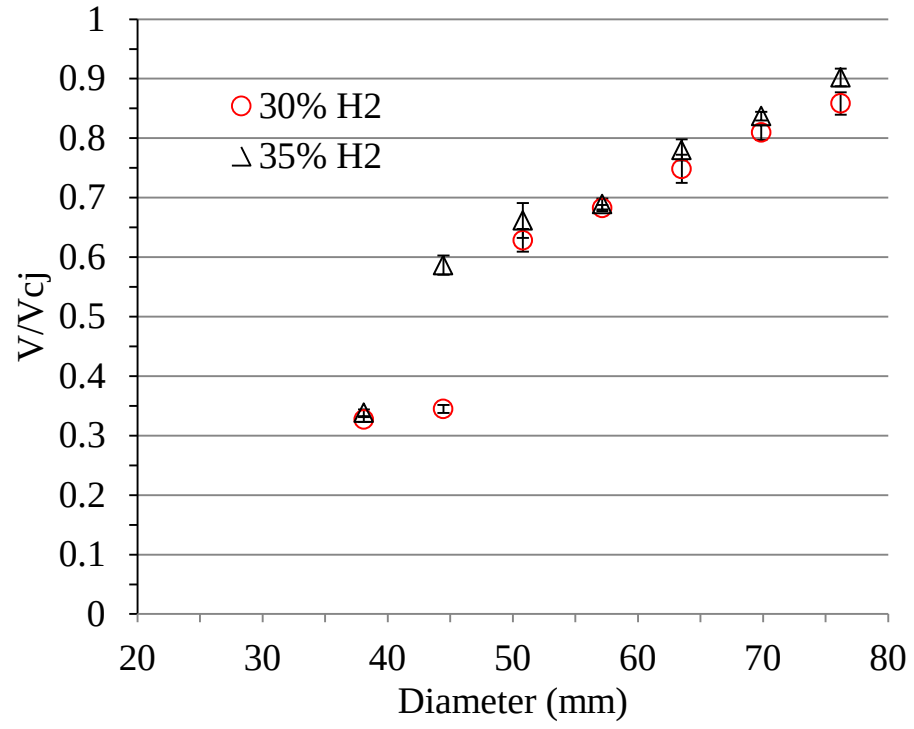

(a)

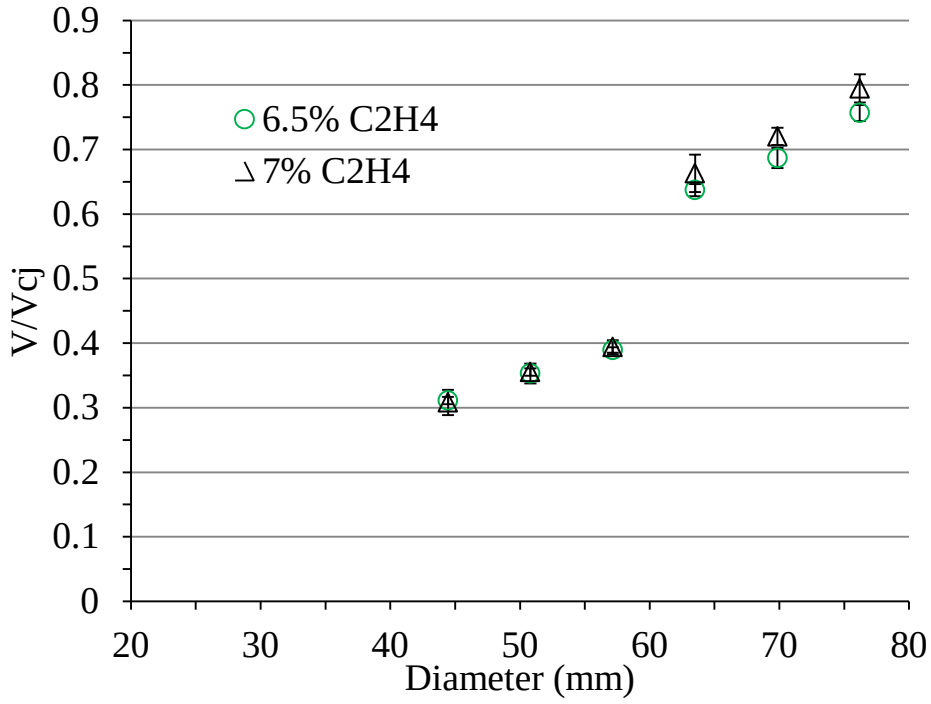

(b)

Figure 5.17: Normalized detonation velocity versus orifice plate diameter for (a) hydrogen-air, and (b) ethylene-air.

Additional experiments were performed with stoichiometric acetylene, propane and DME air mixtures. These results are summarized in Figure 5.18. Tests were carried out with stoichiometric methane-air but a stable detonation before the obstacle section could not be achieved. The critical orifice plate diameter data obtained from Figure 5.18 is summarized in Table 5.5, along with the detonation cell size data. Note, two cell sizes were reported for DME in [18]. In Figure 5.18 the critical orifice plate diameter (corresponding to an abrupt change in average velocity) for each fuel is highlighted by a dotted vertical line. The smallest to largest critical orifice plate diameter corresponds to: acetylene, hydrogen, ethylene, DME, propane. This ranking is slightly different from that of Matsui and Lee [21], as they categorized hydrogen as being less sensitive to detonation than propane.

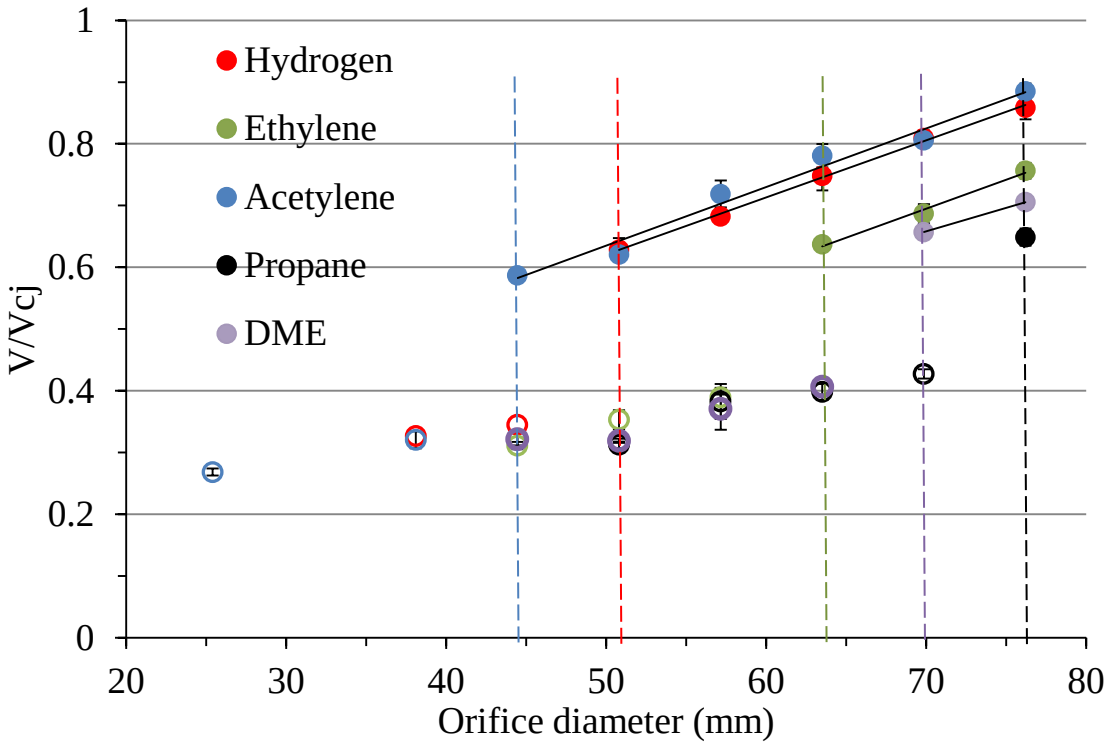

Figure 5.18: Flame front velocity as a function of orifice plate diameter for different stoichiometric fuel-air mixtures. A larger version of this is located in Appendix A.

The linear relationship between the wave front velocity (both for the fast-flame and quasi-detonation) and the orifice plate diameter appears to be universal for all the fuels tested. Figure 5.18 indicates that the velocity deficit itself could also be used as a detonation sensitivity parameter, e.g., the larger the deficit the less sensitive the fuel. In fact for each orifice plate the ranking of the fuels based on velocity deficit is the same as that for the critical orifice plate diameter. However, it is prudent to only use the velocity deficit to fine-tune data where two fuels have similar critical orifice plate diameters.

A similar linear relationship between CJ detonation velocity deficit and diameter is observed in smooth tubes [50]. In smooth tubes the linear drop in velocity deficit is due to the curvature of the detonation wave caused by the interaction of the detonation wave with the boundary layer. In a very-rough wall tube the boundary layer is severely disrupted by the orifice plates and thus cannot explain the linear velocity dependency with orifice diameter. Assuming detonation initiation occurs at the outer- edge of the upstream orifice plate face following shock reflection, as observed in [28], a decrease in the orifice diameter translates into a proportional increase in distance for the detonation to travel across the obstacle-face resulting in a slower axial velocity. A better understanding of the detonation propagation mechanism in a *round* tube with orifice pates is required to advance this postulation.

Table 5.5: Detonation propagation limits for stoichiometric fuel-air mixtures speed diagnostics

Fuel	Fuel % By volume	Critical orifice plate diameter (mm)	Blockage ratio	Cell size, λ (mm)	d/λ
Acetylene	7.8	45.5	0.83	5.7 [19]	7.9
Hydrogen	29.6	50.8	0.78	7.6 [17]	6.7
Ethylene	6.5	63.5	0.61	31.5 [17]	2.0
DME	6.5	69.9	0.53	34 [18]	2.1
				119 [18]	0.6
Propane	4.0	76.2	0.44	53 [19]	1.4

5.3 Quasi-detonation-wave structure

All the available data in the literature on quasi-detonation propagation comes in the form of velocity measurements and DDT limits, similar to that in Section 5.1. The results reported in Section 5.1 show that there is a strong dependence of the propagation of a quasi-detonation on the orifice plate BR. The objective of the study reported in this section is to gain some insight into the quasi-detonation propagation mechanism. The soot foil technique was used to record triple-point trajectories indicative of a detonation wave.

Soot foils were placed at the middle and end of the tube between adjacent orifice plates, see Figure 5.19 for the plate numbering scheme used here on in. The two types of soot foils used are shown in Figure 5.20. A curved foil is shown on the tube-wall between orifice plates #1 and #2 in Figure 5.19 with a 10 mm gap on the top of the tube for easy foil installation and retraction. A flat foil, sooted on both sides, is shown placed horizontally across the tube diameter between #2 and #3 in Figure 5.19. Three 6.4 mm diameter threaded rods fit through the holes in the orifice plate that maintain the angular alignment. Tube spacers (89 mm long, 12.7 mm outer-diameter), that are not shown in Figure 5.19, are slid over each threaded rod between the orifice plates, to maintain axial spacing. The flat foil was held in place by tabs (at the four corners) that permitted the foil to fit into the orifice-plate hole, as seen in Figure 5.19, resting on one of the spacer tubes.

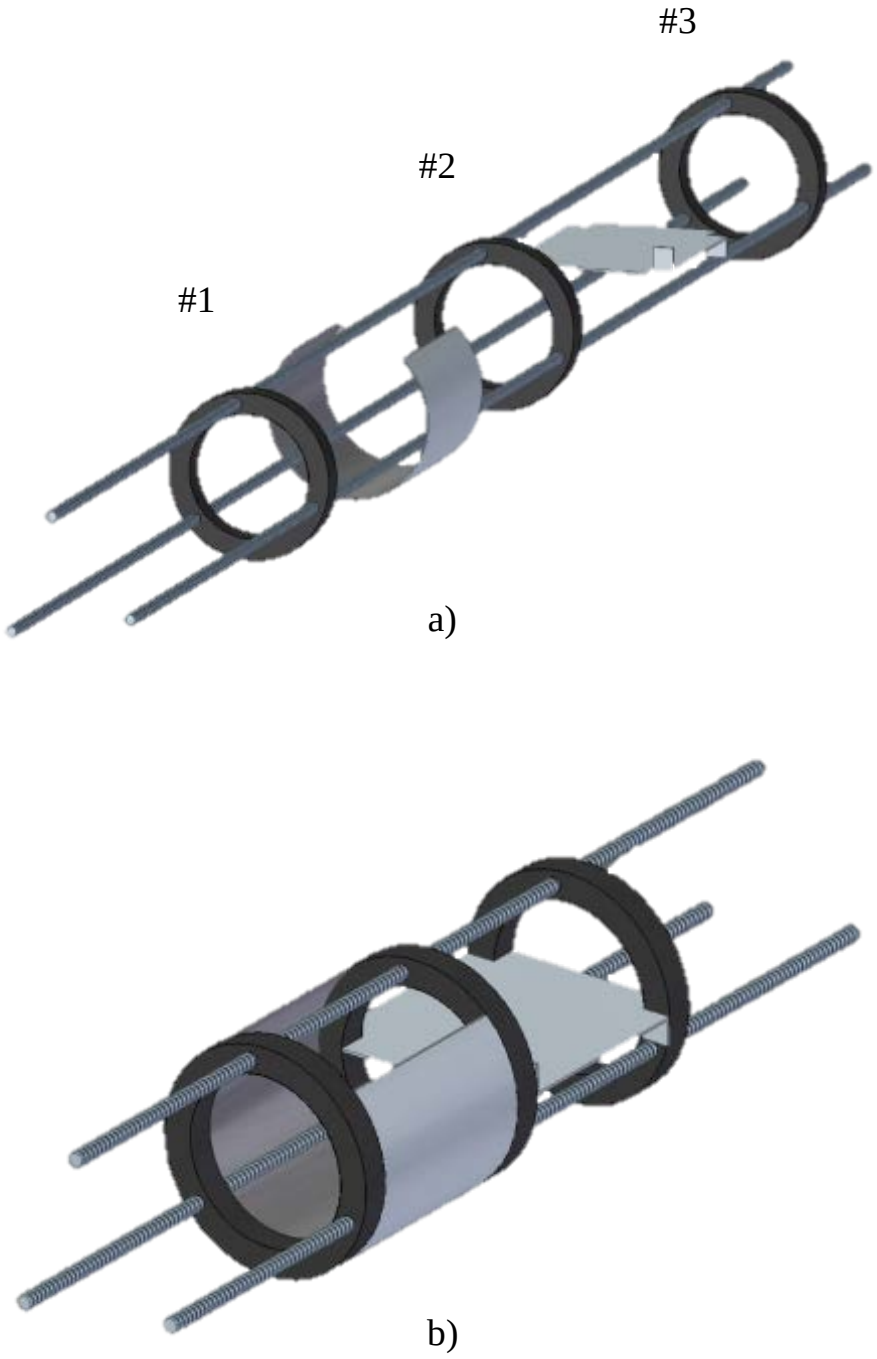

Figure 5.19: Soot foil installation between orifice plates. Both Flat and Wall style foils are shown.

Experiments were performed with horizontal and curved soot foils located at the beginning of the orifice plate section. These locations are shown in Figure 5.20 between orifice

plates 1, 2 and 3. These foil locations were chosen because a planar CJ detonation (propagating left – right in Figure 5.20) is known to exist just before orifice plate #1.

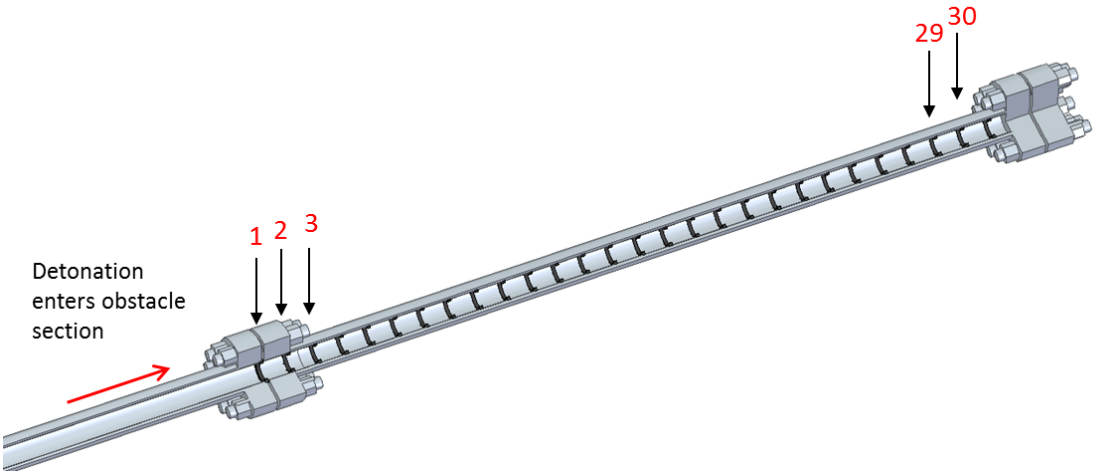

Figure 5.20: Soot Foil Locations to investigate the detonation structure between orifice plates at the start of the obstacle section. Detonation propagation is in the direction left – right.

A planar CJ detonation enters the obstacle section shown in Figure 5.20 where it subsequently diffracts passing through the first orifice plate. In order to confirm the CJ detonation wave structure prior to the first obstacle a 30.5 cm long soot foil was placed on the wall of the tube. This foil was placed such that the end of the foil butted up against the face of orifice plate #1 as indicated in Figure 5.21. The cellular pattern observed on the soot foil is consistent with a CJ detonation wave. A sample of triple-point trajectories is shown by dotted lines. The average cell size measured from this foil is 10 mm, which is consistent with values reported for stoichiometric hydrogen-air in the literature [19] .

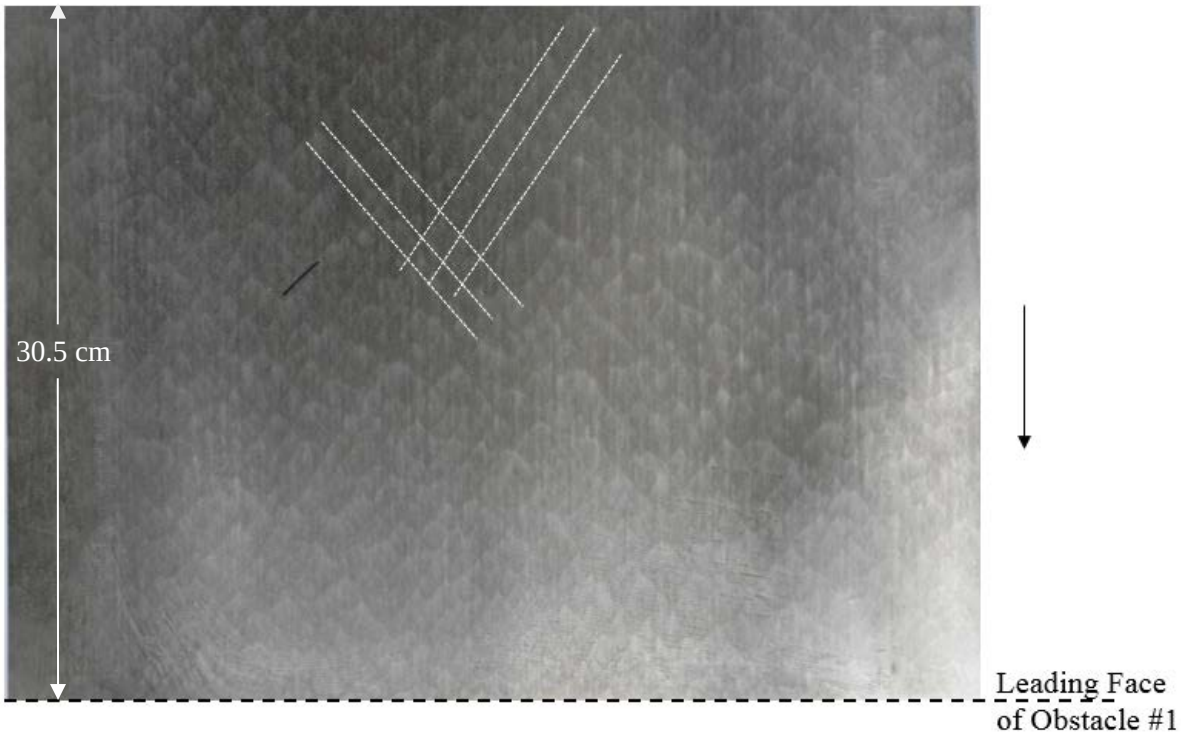

Figure 5.21: Stoichiometric Hydrogen – Air (44% BR) wall foil located prior to obstacle #1.

When the detonation wave reaches the first orifice plate the planar wave reflects off the orifice plate face and the core of the detonation wave remains planar producing a cellular pattern similar to that observed in Figure 5.21 as it propagates through the orifice plate. This core part of the detonation wave diffracts as it propagates around the inner-edge of the orifice plate. This diffraction produces expansion waves that propagate from the orifice plate inner-edge radially inward to the tube centreline. The expansion waves cool the gas behind the detonation shock wave resulting in an increase in the reaction time and decoupling of the detonation wave. This results in a progressive disappearance of the cellular pattern from the orifice plate inner-edge to the tube centreline. This can clearly be seen in both the top and bottom-sides of the flat foil placed after orifice plate #1, see white dashed triangular area with cells in Figure 5.22. The number of detonation cells across the unaffected core decreases linearly from 8 at the orifice plate to none after 71 mm of axial propagation. The radial symmetry of the core cellular imprint on

both the top and bottom of the flat foil indicates that the planar detonation wave crosses the foil orthogonally.

The flat foils shown in Figure 5.22 are cut out of 1100 aluminum sheet. Based on the buckling damage observed on the flat foil it is clear that this aluminum alloy is too soft to be used at the middle flange locations where the leading edge of the plate is exposed to the CJ detonation wave. Experiments conducted with steel flat foils located at the middle flange did not incur the same damage (see Figure 5.23), however, the steel foil produced a lower quality soot foil pattern.

Wall mounted foils after orifice plates #1 and #2 are also provided in Figure 5.22. The part of the foil at the bottom of the tube is indicted in the figure along with the position of the two rods onto which the flat foil rests. The third rod is located in the foil gap at the top of the tube. The wall foil located after orifice plate #1 shows a very complex pattern where immediately after the orifice plate there are no detonation cells. This is expected as the diffraction around the orifice plate causes the part of the detonation wave nearest to the back of the plate to fail (shock wave decouples from reaction zone). The diffracted shock wave reflects off the tube wall downstream from the orifice plate initiating a detonation wave.

The first indication of activity is the appearance of a few “wispy” tongues that are not characteristic of triple-point tracks and do not appear to contain any detonation cells. These tracks most likely form where the stronger surviving triple-points from the decoupled detonation wave collide with the wall. Note, the triple-points represent the locations on the shock wave with the highest pressure and temperature. Detonation initiation occurs at several “hot spots,” after the wispy tongues, where two triple-points collide. The cellular pattern then spreads laterally across the tube wall as it propagates forward such that the cells fill the full circumference of the tube by the end of the foil at orifice plate #2. The individual cells can be observed and are of similar scale to that observed on the foil obtained before the obstacle section, i.e., Figure 5.21. The wall foil after orifice plate #2 does not show any wispy tongues, but a similar detonation initiation pattern

is observed. The cells originate at several points with a larger spread angle and finer cells indicative of an overdriven detonation wave. The flat foil located after orifice plates #2 is not symmetric (top and bottom) like the one after orifice plate #1. This asymmetry is caused by the non-orthogonal approach of the detonation wave to the flat foil. Based on the pattern the wave is most likely inclined forward, reflecting off the top and diffracting downwards.

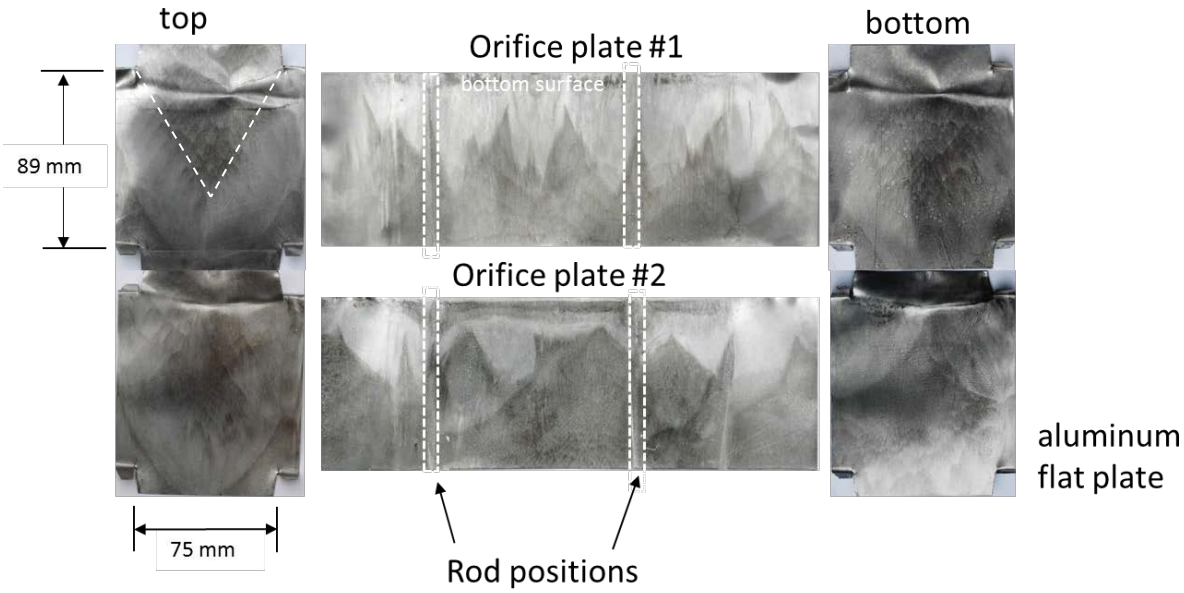

Figure 5.22: Stoichiometric Hydrogen – Air (44% BR) propagation between Obstacles #1 - #2 and Obstacles #2 - #3. Aluminum soot foils were used for this test.

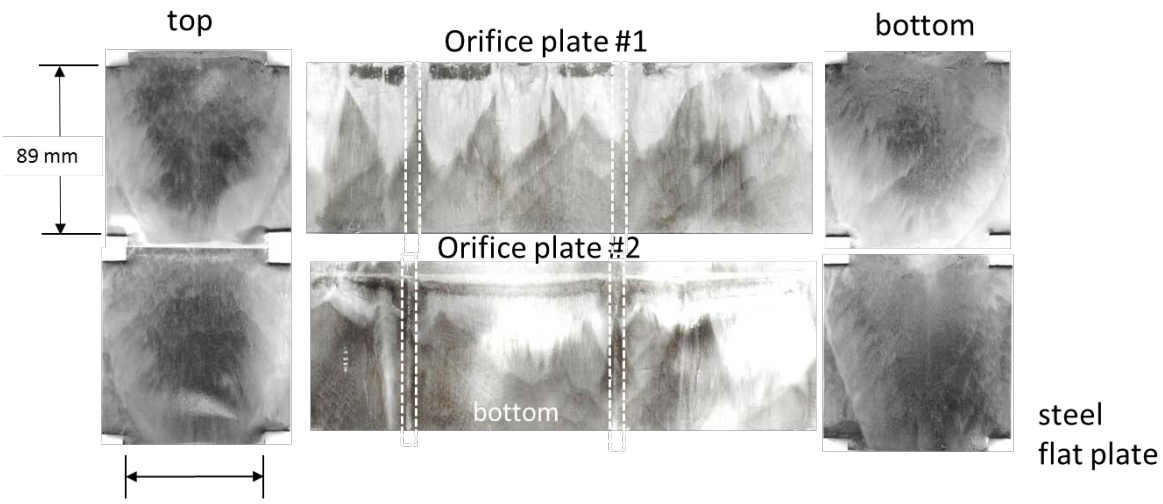

Figure 5.23: Stoichiometric Hydrogen – Air (44% BR) propagation between Obstacles #1 - #2 and Obstacles #2 - #3. Steel soot foils were used for this test.

Soot foils located at the end of the tube at orifice plates #29 and #30 (refer to Figure 5.20) obtained from a test with stoichiometric hydrogen-air propagating through 69.9 mm orifice plates (BR=0.53) are shown in Figure 5.24. From the wall foil in Figure 5.24a it is clear that the explosion front propagating between orifice plates is not uniform. A detonation wave is initiated at a single point on the top half of the tube. It appears that a detonation wave survives the diffraction process around the left-side of orifice plate #29. Based on the cascade of cells from a point (on the right hand side), a detonation wave was initiated when the diffracted shock wave reflected off the tube wall. Based on the wall foil it appears that a detonation waveforms across the entire tube entering orifice plate #30 before the horizontally oriented flat foil located after obstacle #30. However, a non-symmetric pattern appears on the bottom and top of the horizontal foil in Figure 5.24b and Figure 5.24c, respectively. On the bottom side of the foil (Figure 5.24b) transverse waves collide at the centerline forming a hot spot (see arrow) from which a detonation wave forms and then fails (evidenced by the increasing size of the cells). On the top side of the foil (Figure 5.24c) a detonation wave sweeps around the right side of the orifice plate (arrow points to a band of small cells) but fails by the time the front reaches the next orifice plate.

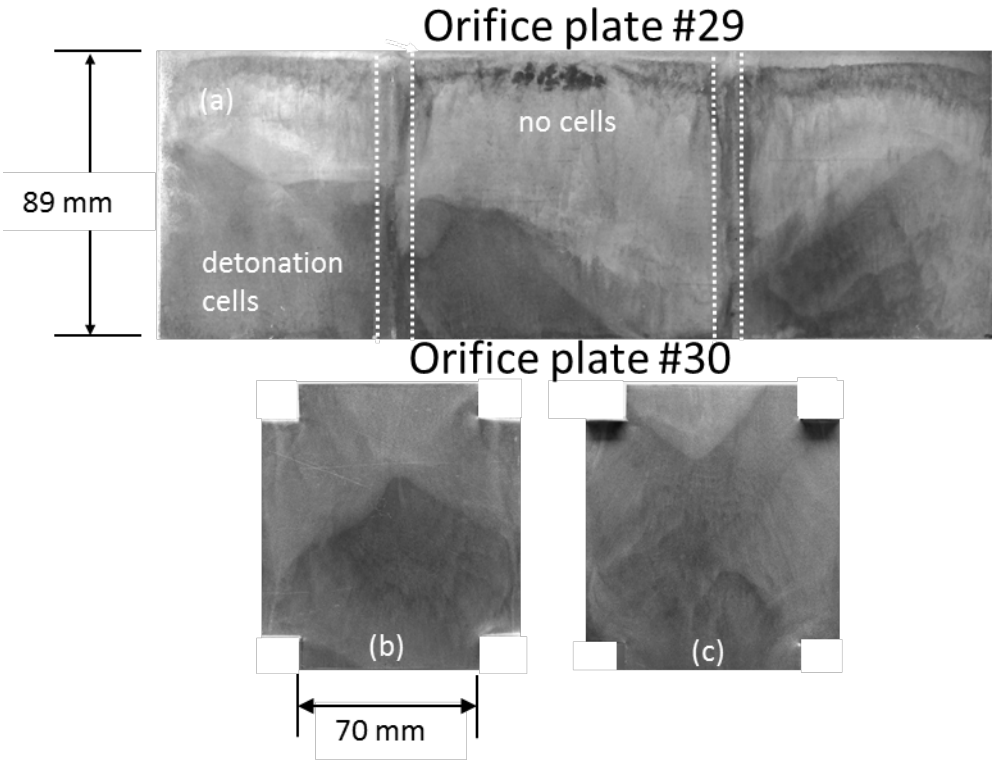

Figure 5.24: Soot foils for stoichiometric hydrogen-air with 69.9 mm orifice plates (test #296); a) wall foil b) bottom of horizontal foil, c) top of horizontal foil. Orifice plate numbers correspond to designation in Figure 5.19.

In the standard experimental setup, the detonation re-initiation process is interrupted by the following orifice plate. A set of experiments was carried out in order to study the unimpeded detonation wave initiation process following diffraction past an orifice plate. For this experiment the last two obstacles in the detonation tube were removed and a longer wall foil was set flush to the back face of the last obstacle. Tests were carried out in this configuration for both 70mm and 76mm orifice plates. The corresponding wall foils are shown in Figure 5.25 .

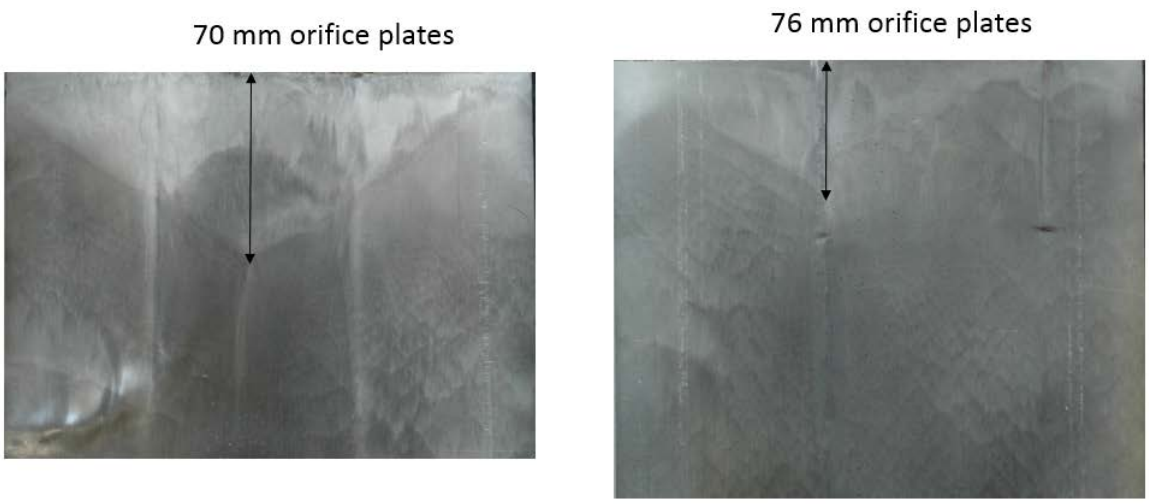

Figure 5.25: Extended wall foils located after orifice plate #29 for both 70 mm and 76 mm orifice plates. The images are shown on the same scale to clearly indicate the required distance for the diffracted shock to recover.

The re-initiation process depends largely on the size of the orifice or the associated blockage ratio. The two foils displayed in Figure 5.25 show similar cell patterns, specifically initiation occurs at two distinct points after the orifice plate. The detonation waves spread laterally that collide roughly at midspan of the foil producing an overdriven detonation wave with associated fine cells. The distance from the orifice plate required for re-initiation is noticeably shorter for the larger 76 mm orifice plates. This is consistent with the shorter distance required for the diffracted shock wave to reflect off the wall for the larger 76 mm orifice plate. For very small orifice plates (high BR) this interruption of the re-initiation process could prevent the propagation of the quasi-detonation wave.

Soot foils obtained after orifice plates #1 and #2 for a test with 50.8 mm orifice plates (BR= 0.75) are shown in Figure 5.26 . Unfortunately the steel flat foils are very poor quality but the pattern is similar to that observed in the lower BR tests shown in Figure 5.22. The core detonation region is shorter on the flat foil due to the smaller orifice diameter and thus shorter distance for the expasion to reach the centreline. The main conclusion that can be drawn from the

wall foils is that the detonation re-initiation occurs further downstream and as such the propagation detonation wave is strongly influenced.

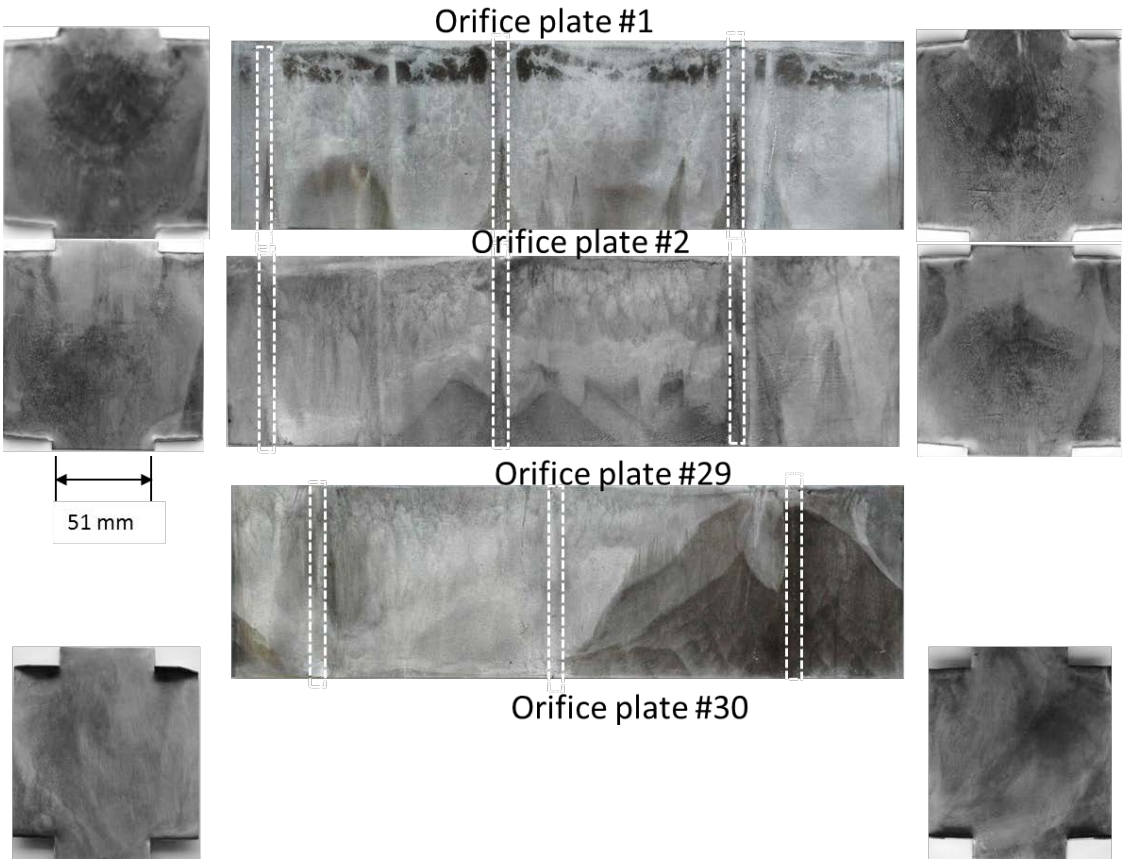

Figure 5.26: Stoichiometric Hydrogen – Air (75% BR)

Soot foils obtained from a test with stoichiometric hydrogen-air and a 50.8 mm the orifice plate (BR=0.75), corresponding to the minimum orifice plate diameter for a quasi-detonation, are provided in Figure 5.27. A single hot spot that develops into a detonation wave is observed on the wall foil, see arrow in Figure 5.27a. The top of the horizontal flat foil shows no detonation cells and the bottom of the foil shows a patch of fine detonation cells (see arrow) but the detonation fails before the next obstacle.

In general, it is very difficult to interpret the flat foils because the structure and orientation of the front incident on the foil leading-edge is not known. What is clear is that the front is not uniform entering the orifice plate, e.g., in no test did cells cover the leading edge of

the flat foil, and re-initiation between the orifice plates occurs at a point despite the axisymmetric geometry.

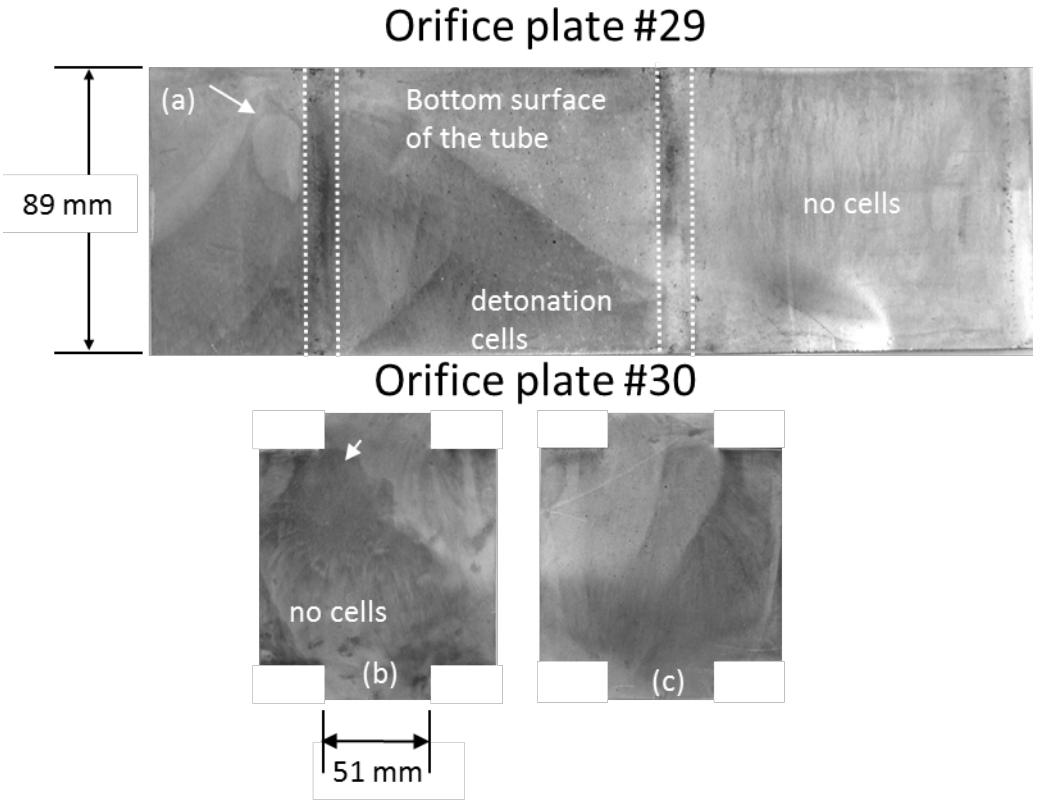

Figure 5.27: Soot foils for stoichiometric hydrogen-air with 50.8 mm orifice plates (test #309); a) wall foil b) bottom of horizontal foil, c) top of horizontal foil. Orifice plate numbers correspond to designation in Figure 5.19.

Chapter 6: Conclusions

In the present study the influence of the orifice plate blockage ratio (BR) on the DDT and detonation propagation limits is investigated for hydrogen, ethylene, DME, propane and acetylene air mixtures. The experimental results demonstrated that the detonation propagation and the DDT limits are strongly affected by the orifice plate BR. For the 100 mm diameter tube used in the experiment, the propagation and DDT limits are similar for 0.44 BR orifice plates. Both the propagation and the DDT limits narrow with increasing BR, more significantly for the DDT limits. The narrowing of the limits with increasing BR is accompanied by a large deviation from the $d/\lambda=1$ detonation limit criterion for both the DDT and propagation limits. The beneficial effects of the orifice plate providing a reflection surface for detonation initiation diminishes with increased BR due to the increased effect of shock wave weakening by the diffraction process.

The critical (minimum) orifice plate diameter required for successful transmission of a detonation from a smooth tube was measured for hydrogen, ethylene, acetylene, and DME stoichiometric fuel-air mixtures. Again the ratio of the critical orifice diameter and the detonation cell size was found to vary strongly with the orifice plate blockage ratio, with a value approaching unity ($d/\lambda \rightarrow 1$) with decreasing blockage ratio. It is proposed that the critical orifice plate diameter (and velocity deficit) be used to categorize a fuel's detonation hazard potential. This characterization parameter is advantageous because of its independence from cell size as well as the requirement for a large scale apparatus.

The placement of soot foils has previously been limited to smooth tube or channel applications. Novel use of both wall and suspended flat soot foils between adjacent obstacles, at the beginning and end of the obstacle section, confirmed that the detonation wave structure of sustained quasi-detonation propagation is not inherently uniform which is contradictory to results universally reported for a smooth tube. This instability suggests that a detonation requires a length of unobstructed tube to regain uniformity which is not always provided in the obstacle

spacing used in this project. It was consistently observed that the propagation mechanism involves detonation failure and re-initiation on the tube wall. This re-initiation occurs at hot spots generated by shock compression, most likely associated with a triple point collision with the wall. It is recommended that the use of soot foils between obstacles be continued to further understand the quasi-detonation propagation process.

Bibliography

[1] J. H. Lee and I. O. Moen, "The mechanism of transition from deflagration to detonation in vapour cloud explosions," *Prog. Energy Combust. Sci.,* vol. 6, no. 4, pp. 359-389, 1980.

[2] OECD Nuclear Energy Agency, "Flame Acceleration and Deflagration-to-Detonation Transition in Nuclear Safety," Nuclear Energy Agency, Issy-les-Moulineaux, France, 2000.

[3] G. Ciccarelli and S. Dorofeev, "Flame acceleration and transition to detonationin ducts," *Progress in Energy and Combustion Science,* vol. 34, pp. 499-550, 2008.

[4] O. Peraldi, R. Knystaustas and J. H. Lee, "Criteria for transition to detonation in tubes," *Symposium (International) on Combustion,* vol. 21, no. 1, pp. 1629-1637, 1988.

[5] S. B. Dorofeev, V. P. Sidorov, M. S. Kuznetsov, I. D. Matsukov and V. I. Alekseev, "Effect of scale on the onset of detonations," *Shock Waves,* vol. 10, pp. 137-149, 2000.

[6] G. Ciccarelli, T. Ginsberg, J. Boccio, C. Economos, K. Sato and M. Kinoshita, "Detonation cell size measurements and predictions in hydrogen-air-steam mixtures at elevated temperatures," *Combustion and Flame,* vol. 99, no. 2, pp. 212-220, 1994.

[7] J. H. S. Lee, "Dyanmic Parameters of Gaseous Detonations," *Annual Review Fluid Mechanics,* vol. 16, pp. 311-336, 1984.

[8] E. Mallard and H. Le Chatelier, "Recherches Experimentales et Theoriques sur la Combustion des Melanges Gaseoux Explosifs," *Ann Mines,* vol. 8, no. 4, pp. 274-568, 1883.

[9] D. Chapman, "On the rate of explosions in gases," *Philisophical Magazine Series 5,* vol. 47, no. 284, pp. 90-104, 1899.

[10] J. Jouguet, "On the propagation of chemical reactions in gases," *Journal des Mathematiques Pures et Appliquees,* vol. 6, no. 1, pp. 347-425, 1905.

[11] G. Ciccarelli, *Mech832: Combustion Dynamics Class Notes,* Kingston: Queen's University, 2013.

[12] Y. B. Zeldovich, "On the theory of the propagation of detonation in gaseous systems," *Journal Experimental Theoretical Physics,* vol. 10, pp. 542-568, 1940.

[13] D. Stamps and S. Tieszen, "The influence of Initial Pressure and Temperature on Hydrogen-Air-Diuluent Detonations," *Combustion and Flame,* vol. 83, pp. 353-364, 1991.

[14] J. M. Austin, F. Pintgen and J. E. Shepherd, "Reaction zones in highly unstable detonations,"

Proceedings of the Combustion Institute, vol. 30, pp. 1849-1857, 2005.

[15] G. Ciccarelli, T. Ginsberg, J. Boccio, C. Finfrock, L. Gerlach, H. Tagawa and A. Malliakos, "Detonation cell size measurements in high-temperature hydrogen-air-steam mixtures at he BNL High-Temperature Combustion Facility," Brookhaven National Laboratory, Upton, NY, 1997.

[16] R. A. Strehlow and A. J. Crooker, "The structure of marginal detonation waves," *Acta Astronautica,* vol. 1, pp. 303-315, 1974.

[17] M. Cross and G. Ciccarelli, "Detonation Propagation Limits in an Obstacle Filled Tube," *Journal of Loss Prevention in the Process Industries,* vol. In Press Corrected Proof, 2014.

[18] P. Diakow, M. Cross and G. Ciccarelli, "Detonation characteristics of dimethyl ether and ethanol–air mixtures," *Shock Waves,* vol. 25, no. 3, pp. 231-238, 2015.

[19] R. Knystautas and J. H. Lee, "Measurements of cell size in hydrocarbon-air mixtures and predictions of critical tube diameter, critical initiation energy and detonability limits," in *9th International Colloquium on Dynamics of Explosions and Reactive Systems,* Poitiers, France, 1983.

[20] J. H. Lee, R. Knystautas and C. M. Guirao, "The link between cell size, critical tube diameter, initiation energy and detonability limits," *Fuel-Air Explosions, University of Waterloo Press,* pp. 157-187, 1982.

[21] H. Matsui and J. H. Lee, "On the measure of the relative detonation hazard of gaseous fuel-oxygen and air mixtures," *Proceedings of the Combustion Institute,* no. 17, pp. 1269-1280, 1979.

[22] G. Ciccarelli, *Personal Correspondance,* Kingston, 2015.

[23] F. Pintgen, J. M. Austin and J. E. Shepherd, "Detonation Front Structure: Variety and Characterization," in *Confined detonations and pulse detonation engines,* Moscow, Torus-Press, 2003, pp. 105-116.

[24] R. A. Strehlow, "Gas phase detonations: Recent Developments," *Combustion and Flame,* vol. 12, no. 2, pp. 81-101, 1968.

[25] I. Moen, S. Murray, D. Bjerketvedt, A. Rinnan, R. Knystautas and J. H. Lee, "Diffraction of detonation from tubes into a large fuel-air explosive cloud," *Symposium (International) on Combustion,* vol. 19, no. 1, pp. 635-644, 1982.

[26] W. R. Chapman and R. V. Wheeler, "The propagation of flame in mixtures of methane and

air," *Journal of the Chemical Society,* vol. 129, pp. 2139-2147, 1926.

[27] A. Teodorczyk, J. Lee and R. Knystautas, "Propagation mechanism of quasi-detonations," *Proceedings of the Combustion Institute,* vol. 22, pp. 1723-1731, 1988.

[28] M. Kellenberger and G. Ciccarelli, "Propagation mechanisms of supersonic combustion waves," *Proceedings of the Combustion Institute,* vol. 35, no. 2, pp. 2109-2116, 2015.

[29] J. Li, Z. Zhao, A. Kazakov and F. L. Dryer, "An Updated Comprehensive Kinetic Model of Hydrogen Combustion," *International Journal of Chemical Kinetics,* vol. 36, pp. 566-575, 2004.

[30] S. Taki and T. Fujiwara, "Numerical simulation of triple point shock behavior of gaseous detonation," *Symposium (International) on Combustion,* vol. 18, no. 1, pp. 1671-1681, 1981.

[31] R. Knystautas, J. Lee and C. Guirao, "The critical tube diameter for detonation failure in hydrocarbon-air mixtures," *Combustion and Flame,* vol. 48, pp. 63-83, 1982.

[32] S. Tieszen, M. Sherman, W. Benedick, J. Shepherd , R. Knystautas and J. Lee, "Detonation cell size measurements in hydrogen-air-steam mixtures," *Progress in Astronautics and Aeronautics,* vol. 106, pp. 205-219, 1986.

[33] S. Tieszen, D. Stamps, C. Westbrook and W. Pitz, "Gaseous hydrocarbon-air detonations," *Combustion and Flame,* vol. 84, pp. 376-390, 1991.

[34] J. Shepherd and M. Kaneshige, "Detonation Database," GALCIT, July 1997. [Online]. Available: http://www.galcit.caltech.edu/detn_db/html/.

[35] H. D. Ng and J. H. Lee, "Comments on explosion problems for hydrogen safety," *Journal of Loss Prevention in the Process Industries,* vol. 21, pp. 136-146, 2008.

[36] I. B. Zeldovich, S. M. Kogarko and N. N. Simonov, "An experimental investigation of spherical detonation in gases," *Sov. Phys. Tech. Phys.,* vol. 1, pp. 1689-1713, 1956.

[37] K. I. Shchelkin and Y. K. Troshin, "Non-stationary phenomena in the gaseous detonation front," *Combustion and Flame,* vol. 7, pp. 143-151, 1963.

[38] V. V. Mitrofanov and R. I. Soloukhin, "The diffraction of multifront detonation waves," *Sov Phys Dokl,* vol. 9, p. 1055, 1964.

[39] Y. K. Liu, J. H. Lee and R. Knystautas, "Effect of geometry on the transmission of detonation through an orifice," *Combustion and Flame,* vol. 56, no. 2, pp. 215-225, 1984.

[40] D. C. Bull and J. E. Elsworth, "Initiation of spherical detonation in hydrocarbon/air mixtures," *Acta Astronautica,* vol. 5, no. 11-12, pp. 997-1008, 1978.

[41] J. H. Lee, R. Knystautas and C. K. Chan, "Turbulent flame propagation in obstacle-filled tubes," *Symposium (International) on Combustion*, vol. 20, no. 1, pp. 1663-1672, 1985.

[42] M. Kuznetsov, V. Alekseev, A. Bezmelnitsyn, W. Breitung, S. Dorofeev, I. Matsukov, A. Veser and Y. Yankin, "Effect of obtacle geometry on behaviour of turbulent flames," Forschungszentrum Karlsruhe Technik und Umwelt, 1999.

[43] M. Kuznetsov, V. Alekseev and S. Dorofeev, "Comparison of critical conditions for DDT in regular and irregular cellular detonation systems," *Shock Waves,* vol. 10, pp. 217-223, 2000.

[44] S. Dorofeev, A. Kochurko, A. Efimenko and B. Chaivanov, "Evaluation of the hydrogen explosion hazard," *Nuclear Engineering and Design,* vol. 148, no. 2-3, pp. 305-316, 1994.

[45] P. Diakow, "DETONATION CHARACTERISTICS OF DIMETHYL ETHER AND ETHANOL AIR MIXTURES," Queen's University, Kingston, 2012.

[46] W. C. Reynolds, "The Element-Potential Method For Chemical Equilibrium Analysis: Implementation In The Interactive Program STANJAN," Stanford University, Stanford, CA, 1986.

[47] R. Knystaustas, J. H. Lee, O. Peraldi and C. K. Chan, "Transmission of a flame from a rough to a smooth-walled tube," *Prog. Astronaut. Aeronaut,* no. 106, pp. 37-52, 1986.

[48] M. Kuznetsov, G. Ciccarelli, S. Dorofeev, V. Alekseev, Y. Yankin and T. Kim, "DDT in Methane-Air Mixtures," *Shock Waves,* no. 12, pp. 215-220, 2012.

[49] J. H. Lee, ""Measure of chemical reactivity," Discussion on vapor explosions," in *Colloquium on Gasdynamics of Explosion and Rective Systems*, Sotckholm, 1977.

[50] J. Fay, "Two-dimensional gaseous detonations: Velocity deficit," *Physics Fluids,* no. 21, pp. 1629-1637, 1959.

[51] White, "Turbulent Structure of Gaseous Detonation," *The Physics of Fluids,* vol. 4, no. 4, pp. 1958-1988, 1961.

[52] E. Oran, J. Boris, T. Young, M. Flanigan, T. Burks and M. Picone, "Numerical simulations of detonations in hydrogen-air and methane-air mixtures," *Symposium (International) on Combustion,* vol. 18, no. 1, pp. 1641-1649, 1981.

[53] A. K. Oppenheim and R. I. Soloukhin, "Experiments in gasdynamics of explosions," *Annual Review Fluid Mechanics,* vol. 5, pp. 31-58, 1973.

[54] Y. N. Denisov and Y. K. Troshin, "On the mechanism of detonative combustion," *Symposium (International) on Combustion,* vol. 8, no. 1, pp. 600-610, 1961.

[55] H. F. Coward and G. W. Jones, "Limits of Flammability of Gases and Vapors," United States Government Printing Office, Washington, 1952.

Appendix A: Detonation Propagation and DDT Limits Graphs

This appendix serves to organize experimental results including results that were not directly referenced in the results section of this thesis. The CJ detonation velocity (─) and isobaric speed of sound in the products (- -) are shown for reference.

Table A. 1: Reference Table – Detonation Propagation and DDT Limit Graphs

Figure #	Orifice Plate Size [in/mm]	Blockage Ratio	Fuel-Air Mixture
Figure A. 1	3”/76.2mm	0.44	Hydrogen - Air
Figure A. 2	2.75”/69.9mm	0.53	Hydrogen - Air
Figure A. 3	2.5”/63.5mm	0.61	Hydrogen - Air
Figure A. 4	2.25”/57.2mm	0.68	Hydrogen - Air
Figure A. 5	2”/50.8mm	0.75	Hydrogen - Air
Figure A. 6	3”/76.2mm	0.44	Ethylene - Air
Figure A. 7	2.75”/69.9mm	0.53	Ethylene - Air
Figure A. 8	2.5”/63.5mm	0.61	Ethylene - Air
Figure A. 9	3”/76.2mm	0.44	Acetylene - Air
Figure A. 10	2.75”/69.9mm	0.53	Acetylene - Air
Figure A. 11	2.5”/63.5mm	0.61	Acetylene - Air
Figure A. 12	2.25”/57.2mm	0.68	Acetylene - Air
Figure A. 13	2”/50.8mm	0.75	Acetylene - Air
Figure A. 14	1.75”/44.5mm	0.81	Acetylene - Air
Figure A. 15	3”/76.2mm	0.44	DME - Air
Figure A. 16	2.75”/69.9mm	0.53	DME - Air
Figure A. 17	3”/76.2mm	0.44	Propane - Air

Hydrogen-Air

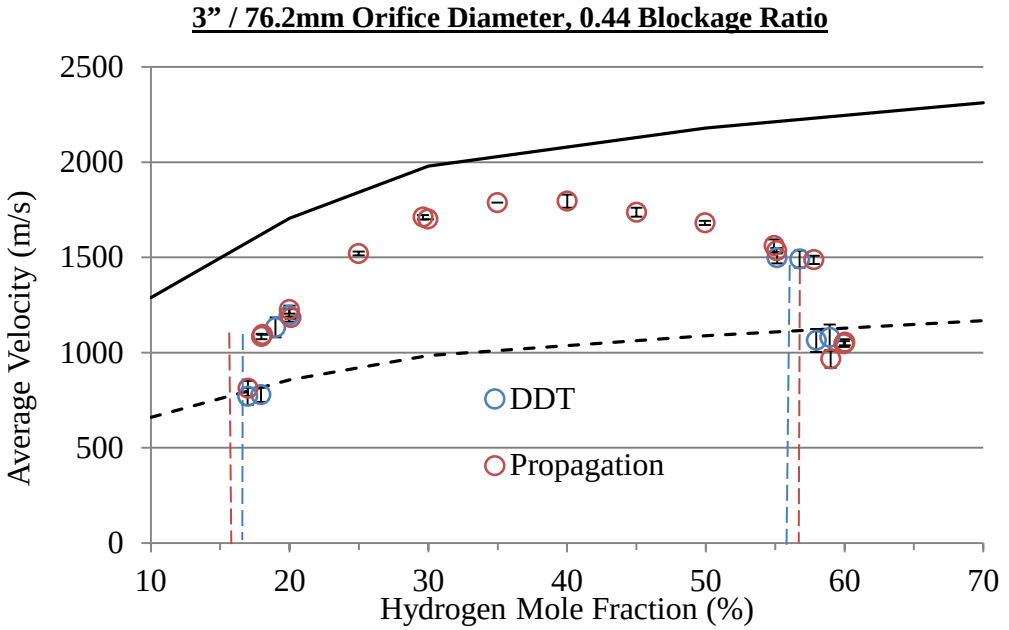

Figure A. 1: Average explosion front velocity for hydrogen-air mixtures with 76.2 mm orifice plate

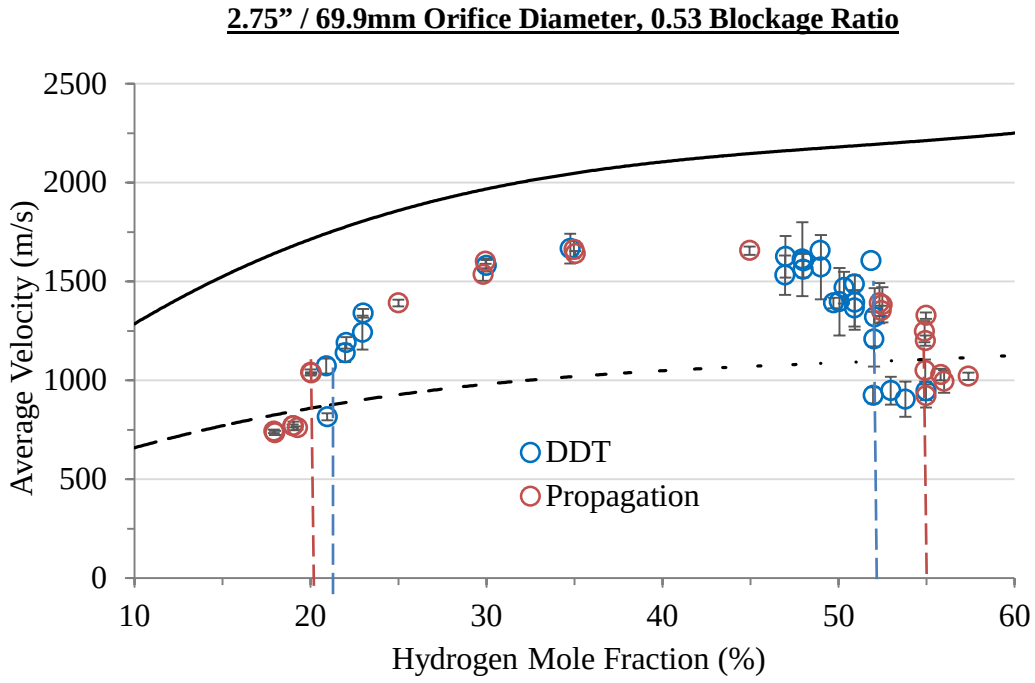

Figure A. 2: Average explosion front velocity for hydrogen-air mixtures with 69.9 mm orifice plate

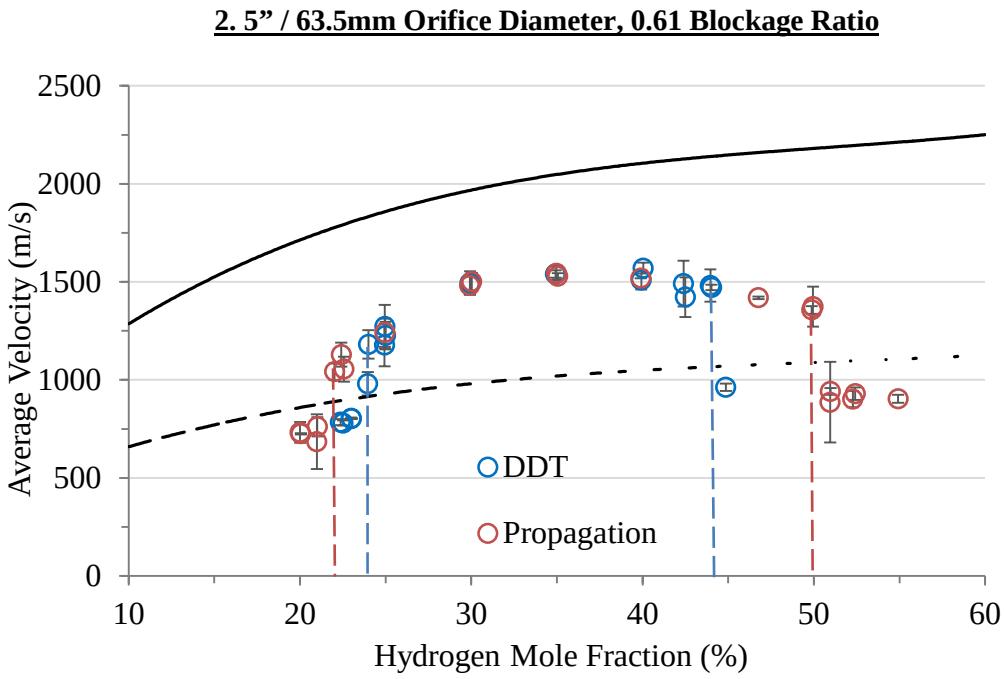

Figure A. 3: Average explosion front velocity for hydrogen-air mixtures with 63.5 mm orifice plate

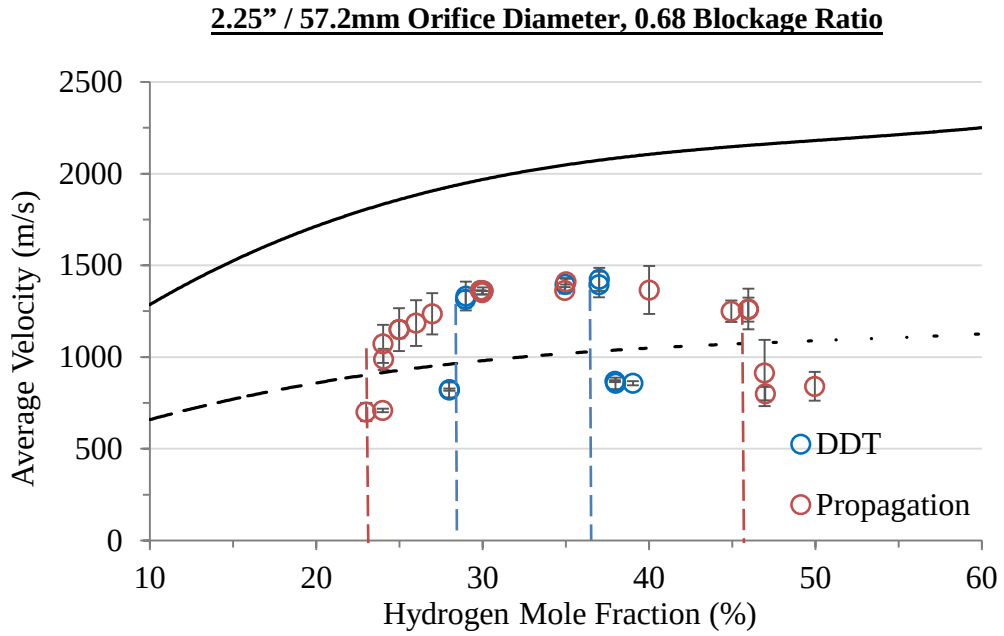

Figure A. 4: Average explosion front velocity for hydrogen-air mixtures with 57.2 mm orifice plate

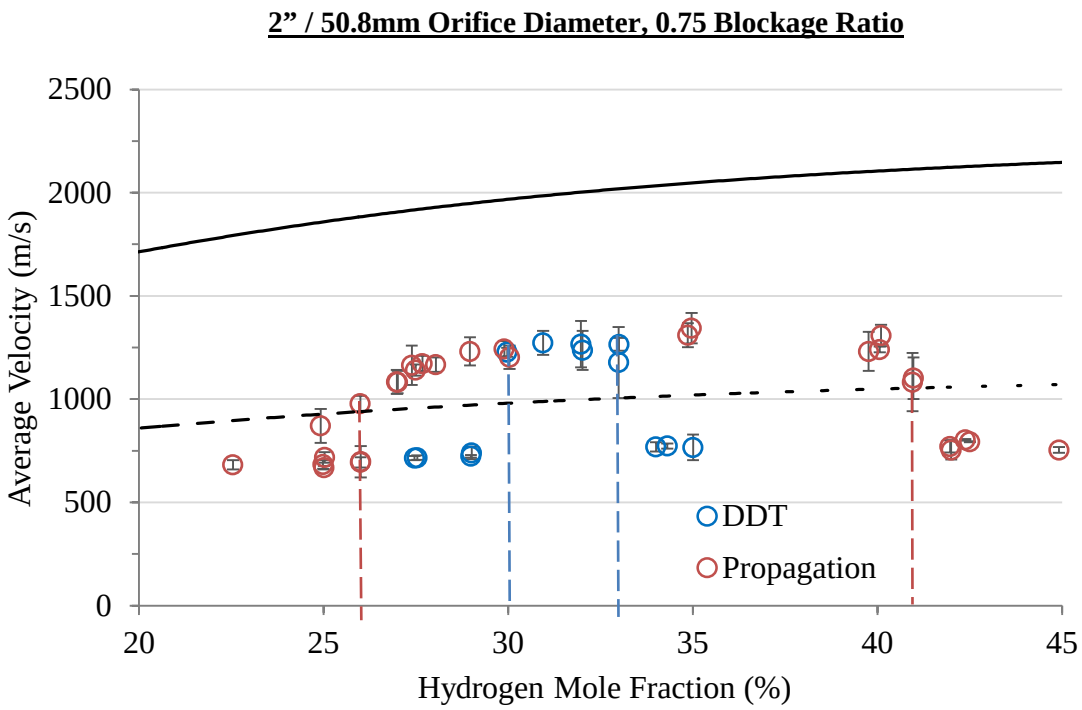

Figure A. 5: Average explosion front velocity for hydrogen-air mixtures with 50.8 mm orifice plate

Ethylene-Air

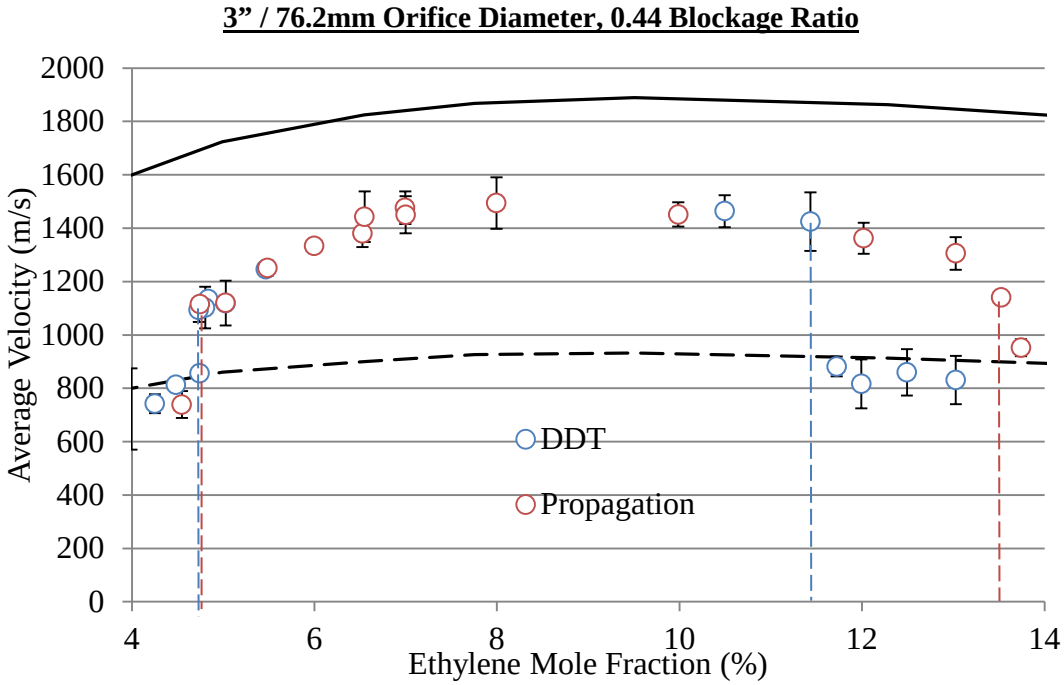

Figure A. 6: Average explosion front velocity for ethylene-air mixtures with 76.2 mm orifice plate

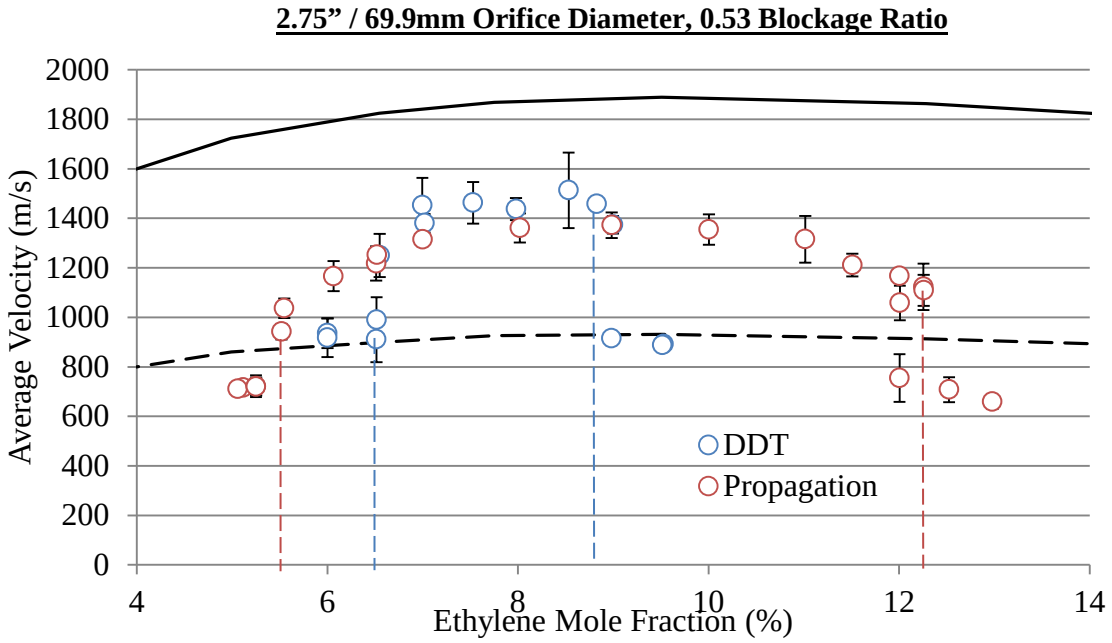

Figure A. 7: Average explosion front velocity for ethylene-air mixtures with 69.9 mm orifice plate

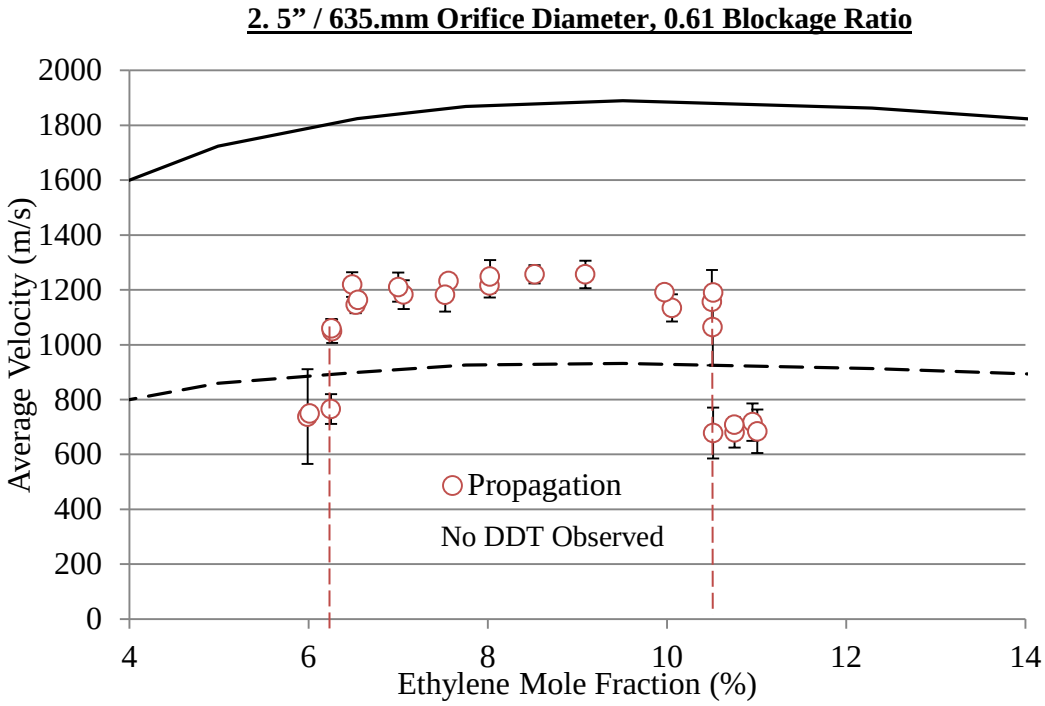

Figure A. 8: Average explosion front velocity for ethylene-air mixtures with 63.5 mm orifice plate

Acetylene-Air

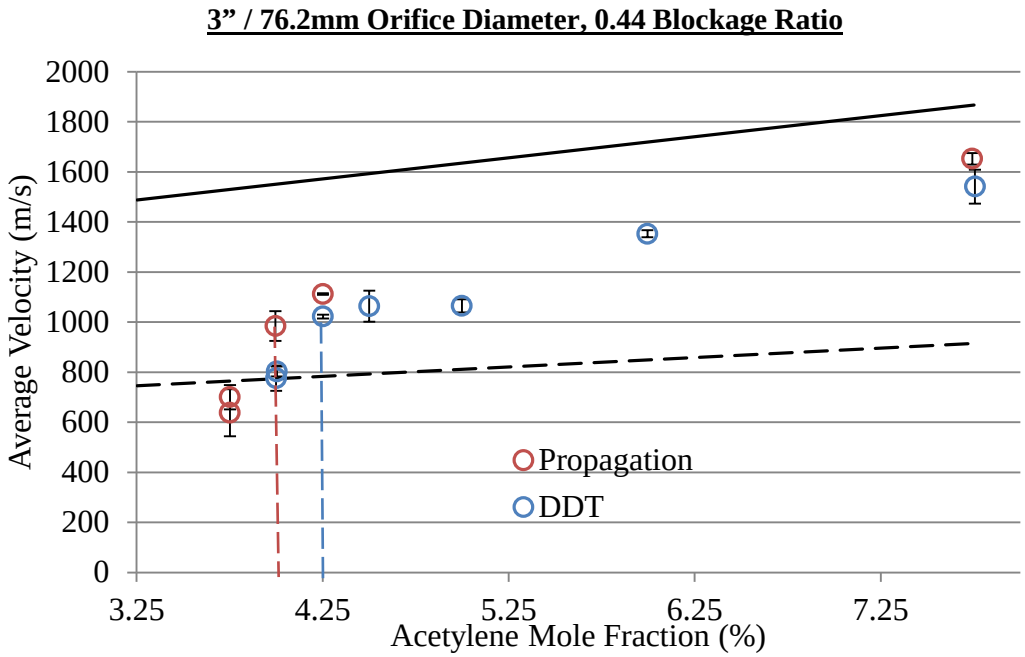

Figure A. 9: Average explosion front velocity for acetylene-air mixtures with 76.2 mm orifice plate

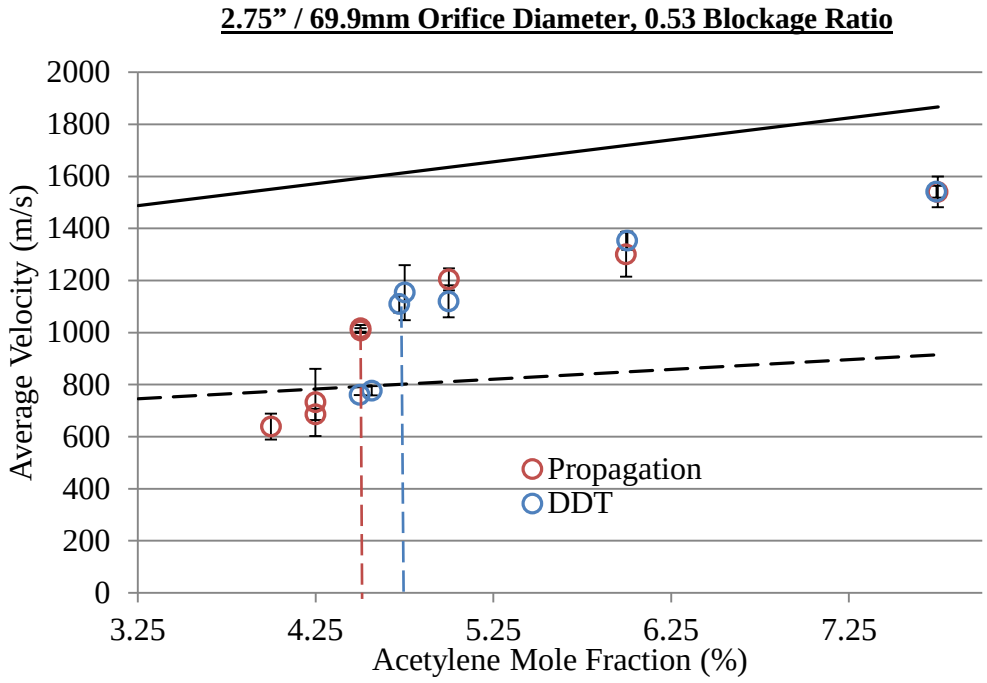

Figure A. 10: Average explosion front velocity for acetylene-air mixtures with 69.9 mm orifice plate

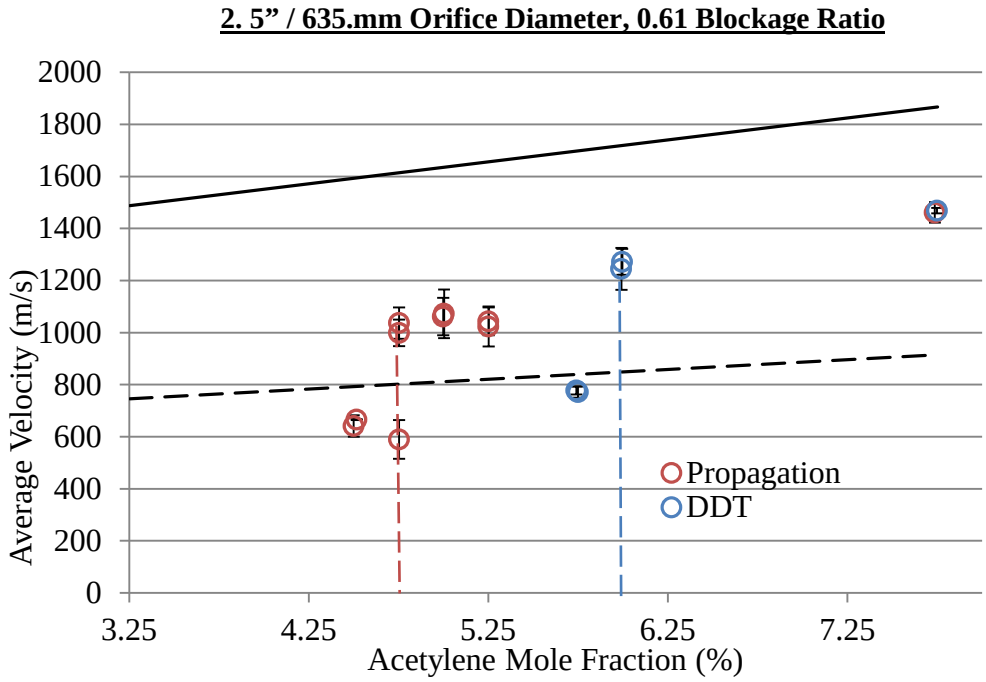

Figure A. 11: Average explosion front velocity for acetylene-air mixtures with 63.5 mm orifice plate

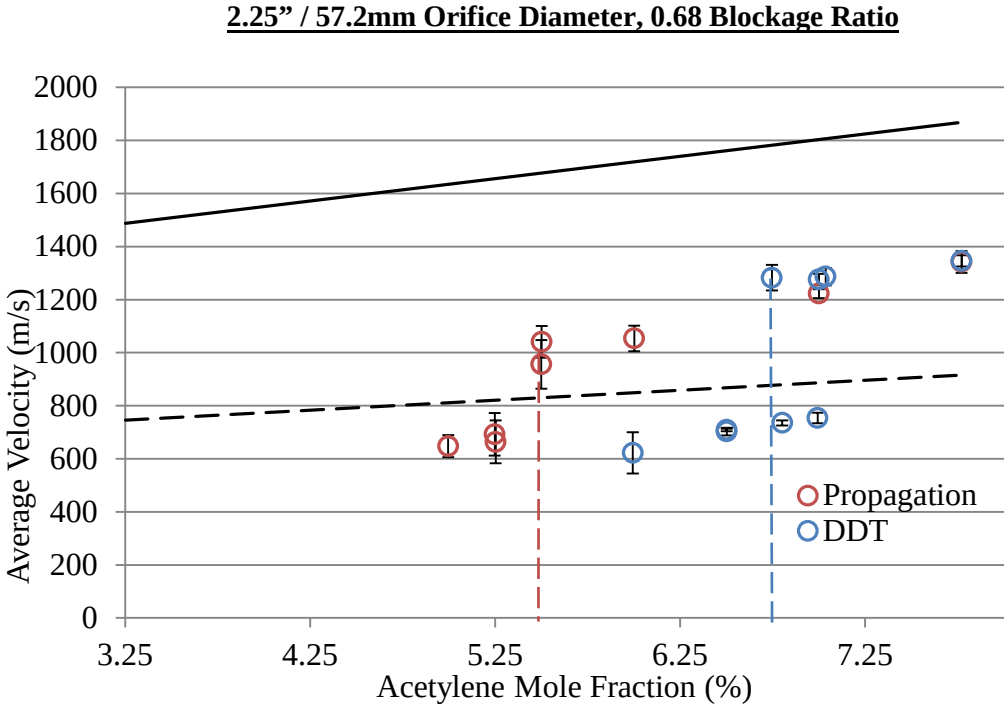

Figure A. 12: Average explosion front velocity for acetylene-air mixtures with 57.2 mm orifice plate

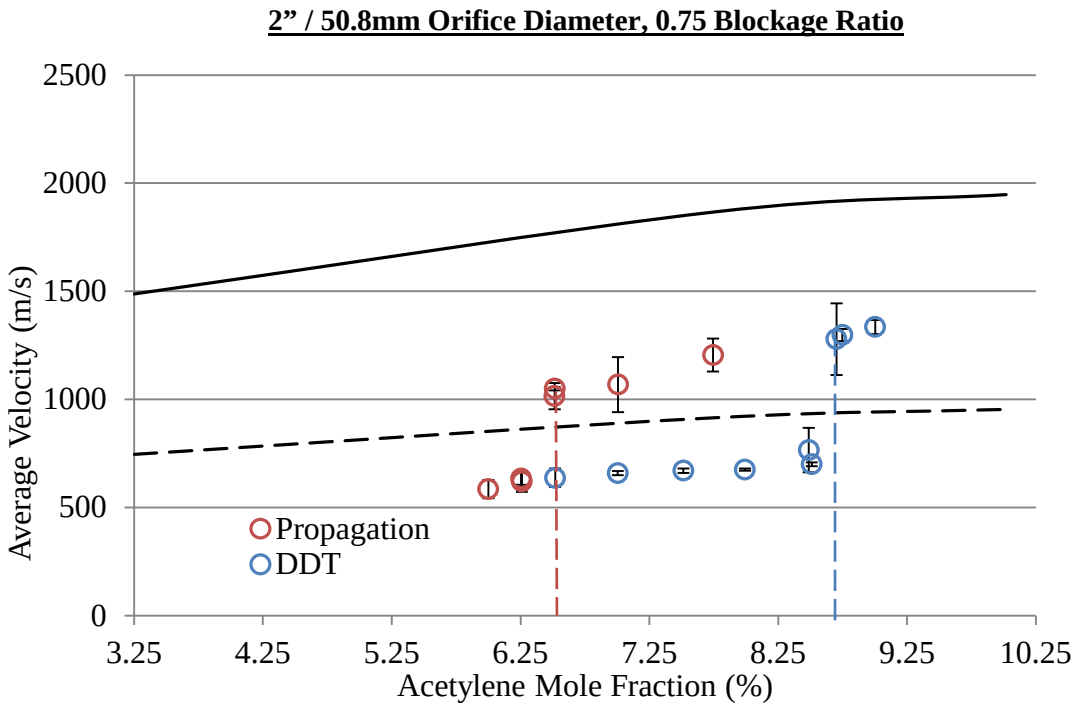

Figure A. 13: Average explosion front velocity for acetylene-air mixtures with 50.8 mm orifice plate

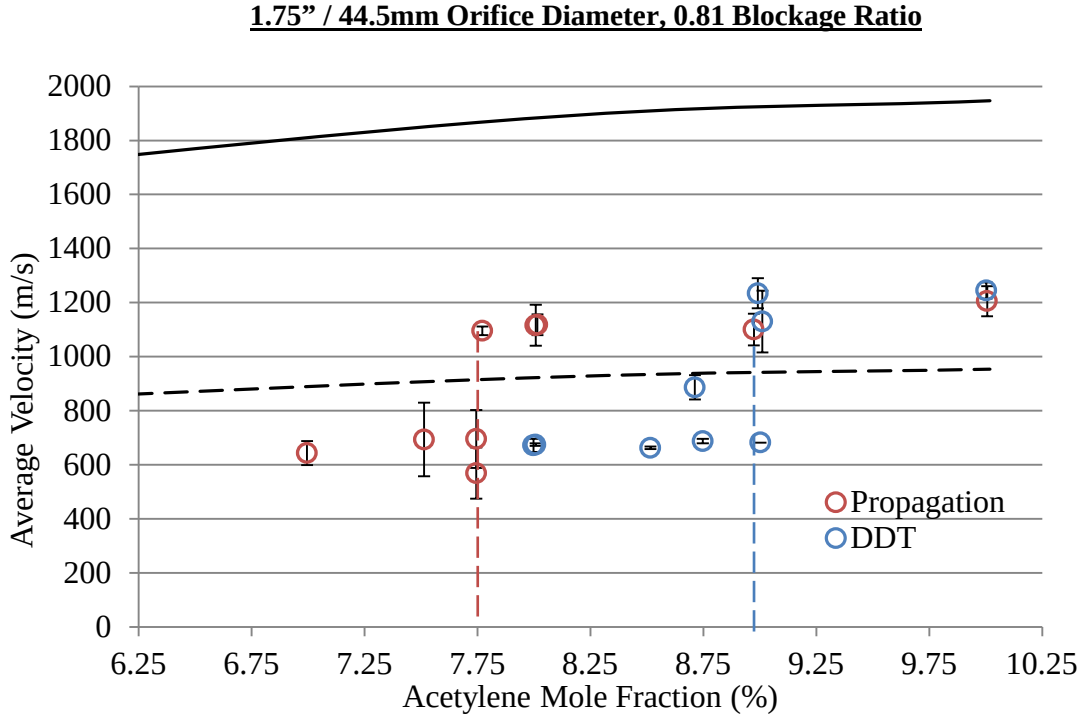

Figure A. 14: Average explosion front velocity for acetylene-air mixtures with 44.5 mm orifice plate

DME-Air

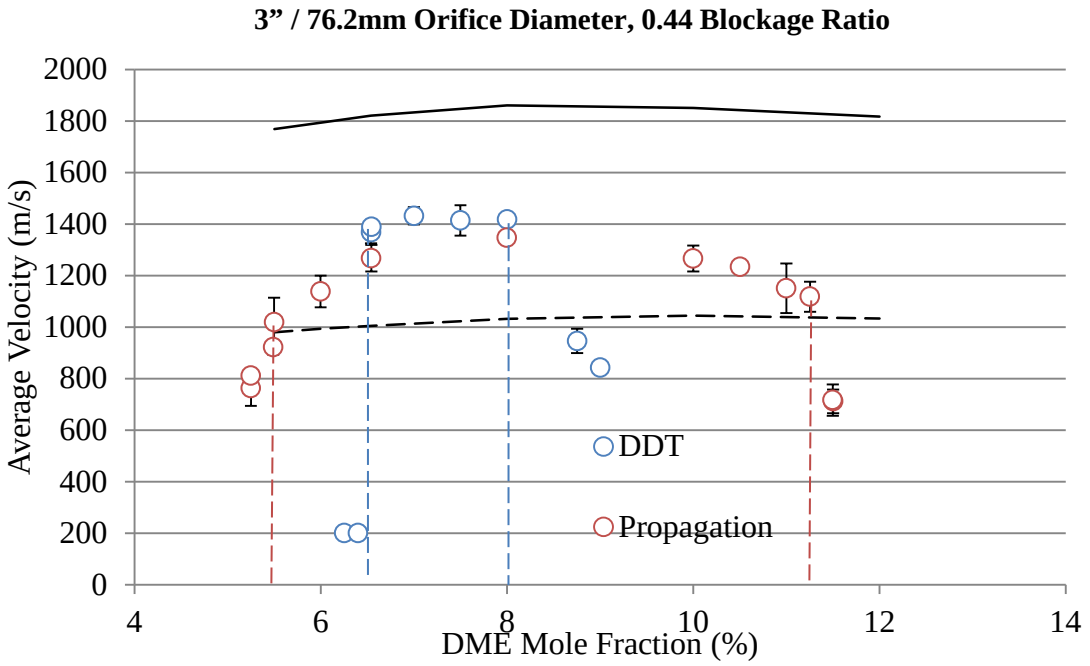

Figure A. 15: Average explosion front velocity for DME-air mixtures with 76.2 mm orifice plate

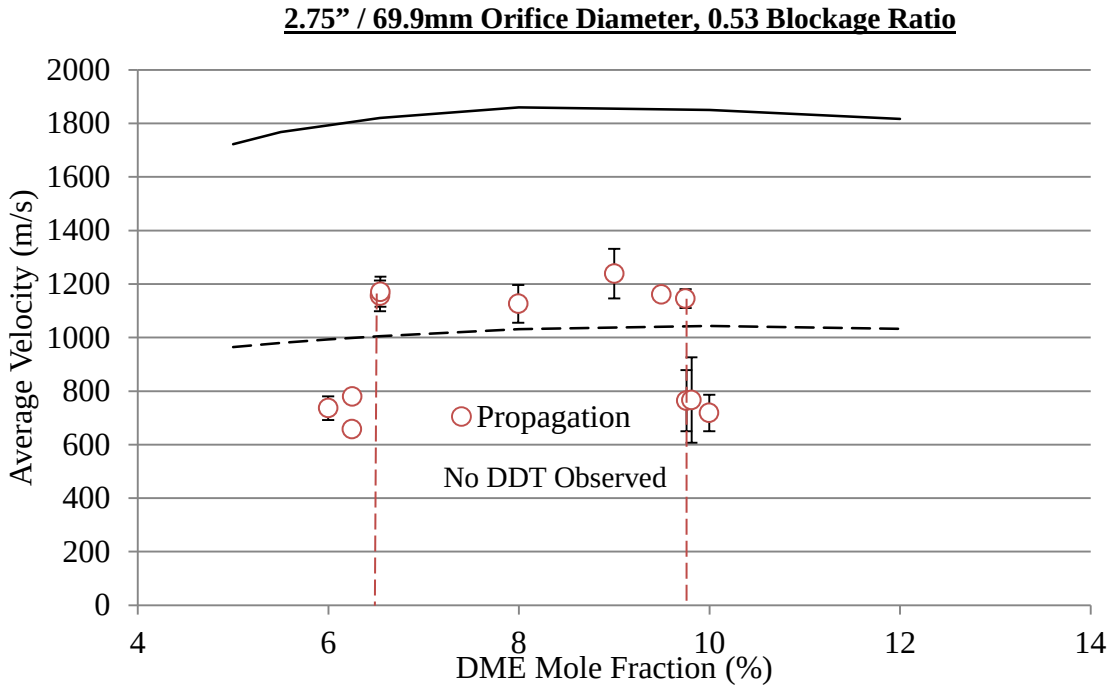

Figure A. 16: Average explosion front velocity for DME-air mixtures with 69.9 mm orifice plate

Propane-Air

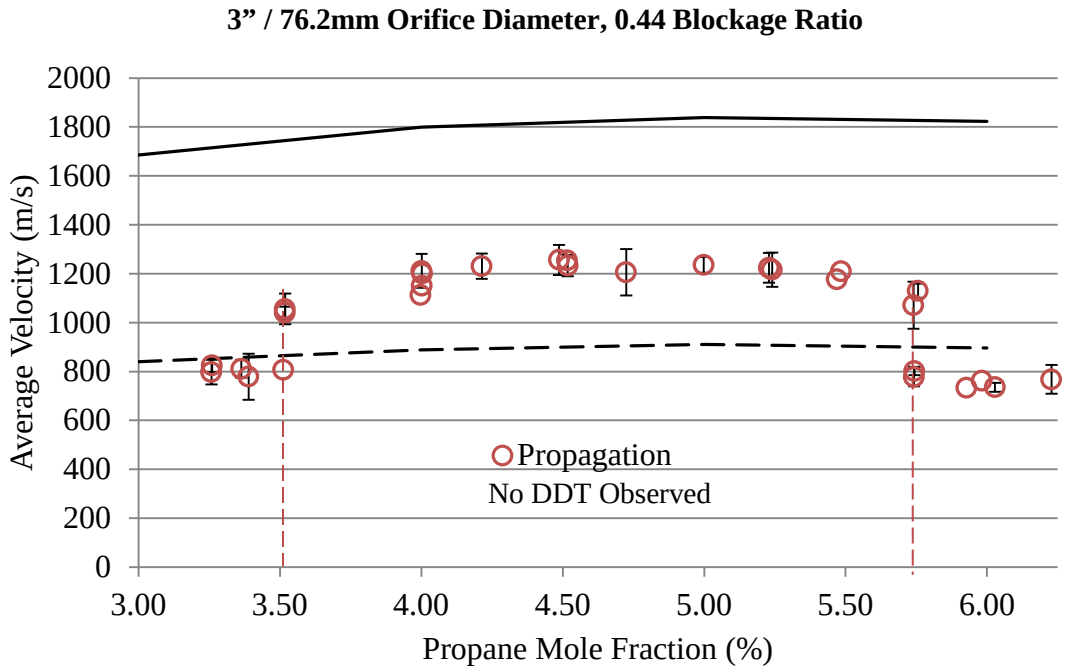

Figure A. 17: Average explosion front velocity for propane-air mixtures with 76.2 mm orifice plate

Summary of detonation propagation and DDT limits as a function of orifice plate BR

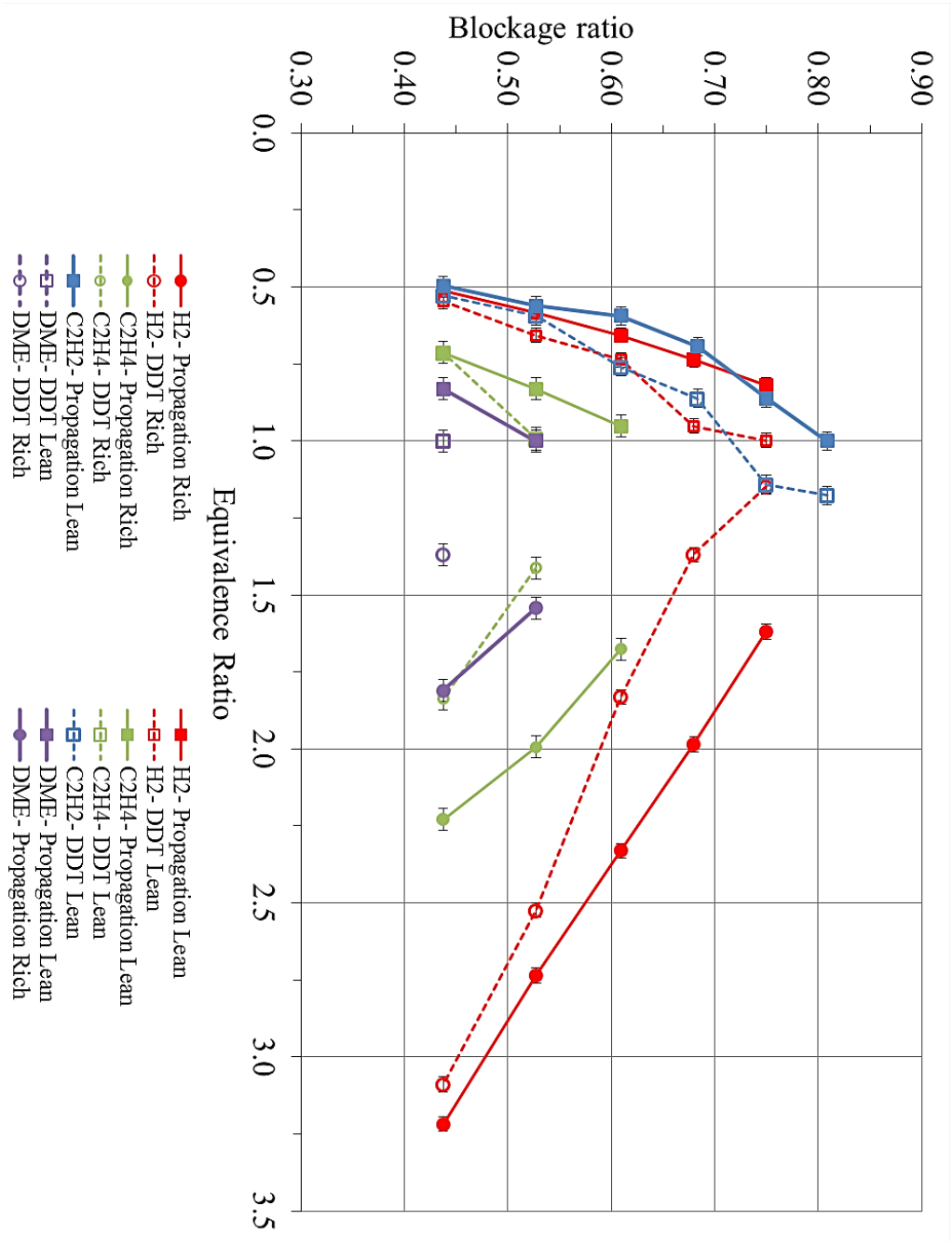

Figure A. 18: Detonation propagation and DDT limits as a function of orifice plate BR.

Flame front velocity as a function of orifice plate diameter for different stoichiometric fuel-air mixtures

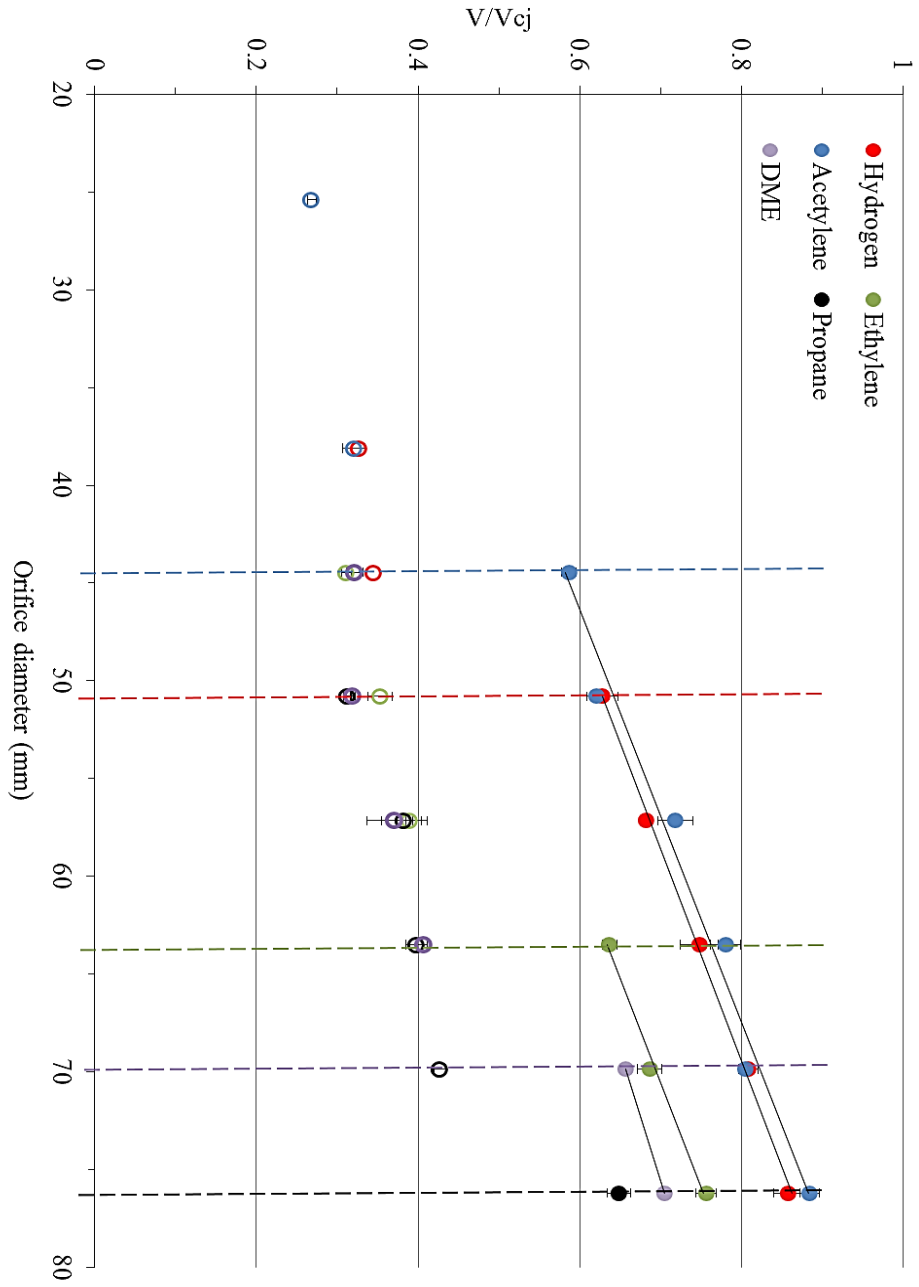

Figure A. 19: Flame front velocity as a function of orifice plate diameter for different stoichiometric fuel-air mixtures.

Appendix B: Uncertainty Analysis

In this section the uncertainty associated with various aspects of this project will be discussed. This project was based on a large quantity of experiment based data collection. As is to be expected, the sources of uncertainty with this type of project are more focused on instrumentation and procedure. Several sources of error are discussed, as well as the steps taken to reduce these uncertainties.

Mixing Chamber Pressure Transducer

An OMEGA PX209-060G5V solid state pressure transducer was used to measure the fill pressure of the mixing chamber. This transducer has a reported accuracy of 0.25% which is ideal for accurate measurement of mixture pressure. This corresponds to a manageable error of 1.025 kPa over the reported pressure transducer range, 0 – 60 psi (0 – 413.7 kPa). The method used to calibrate the transducer is discussed below.

Combustion Tube Pressure Transducer

An OMEGA PX219-015G5V solid state pressure transducer was used to measure the fill pressure of the combustion tube. Similar to the mixing chamber transducer it has reported accuracy of 0.25% which corresponds to a manageable error of 0.25 kPa over the reported pressure transducer range 0 – 15 psi (0 – 103.4 kPa). The method used to calibrate the transducer is discussed below.

Pressure Transducer Calibration

The transducer was calibrated using a standard two point calibration method. To obtain the first calibration point the vacuum pump was connected directly to the pressure transducer. This was done to minimize the system volume and the prospect of a leak. The pump manufacturer

specifies a vacuum condition of 2.0×10^{-4} kPa which is acceptable. The output voltage of the transducer was recorded using a multi-meter and was assumed to correspond to an absolute vacuum condition (0 kPa). This represents the first of the two calibration points. The second calibration point was obtained by exposing the transducer directly to atmospheric room pressure. The output voltage was recorded again at this condition and was assumed to correspond to the atmospheric pressure reported by The Weather Network in Kingston, Ontario. This procedure was repeated when necessary in order to maintain an accurate calibration throughout the experimentation period of the project.

Mixture Composition

Test mixtures were consistently created in the mixing chamber based the method of partial pressures. This method is best described by Equation B.1.

$$[Test\ Fuel] = (P_f - P_v)/P_{Total} \qquad \textbf{B.1}$$

Where the concentration of the test fuel is *[Test Fuel]*, the fuel pressure is P_f, the initial pressure at vacuum is P_v, and the total mixture pressure is P_{Total}. Based on a ratio of the mixing chamber and combustion tube volumes a total mixture pressure of 310kPa was specified. This value ensures that the pressure difference between the two volumes is enough to transfer the initial test pressure (101.3 kPa) to the larger tube volume.

To calculate the uncertainty associated with the creation of test mixtures a sample mixture of 30% fuel will be used. A maximum initial pressure after vacuum of 0.4 kPa and a total mixture pressure of 310 kPa were used.

$$0.3 = (P_f - 0.40)/310 \qquad \textbf{B.2}$$

Solving Equation B.2 for the fuel pressure, P_f, a total fuel pressure of 93.4 kPa will need to be added with the remaining mixture pressure being air. The associated uncertainty with the mixture composition can be determined using partial derivatives to propagate the effect of each variables uncertainty, Equation B.3 .

$$Derror = \left(\frac{DP_f + DP_v}{P_f + P_v}\right) + \frac{DP_{Total}}{P_{Total}} \qquad \textbf{B.3}$$

The total uncertainty of the mixture composition is given by Derror. DP_f and DP_v are the uncertainties associated with adding the test fuel and initial vacuum pressure respectively. These uncertainties are both 1.025 kPa calculated previously. Continuing with the same sample mixture as before, the total mixture composition error is calculated as shown in Equation B.4 .

$$Derror = \left(\frac{1.025 + 1.025}{93.4 + 0.40}\right) + \frac{1.025}{310} \qquad \textbf{B.4}$$

The result is a total mixture composition error of 0.025 kPa for this typical sample.

Combustion Tube

There is a notable source of error associated with loading the test mixture from the mixing chamber to the combustion tube. For experiments where the total specified fill pressure is equal to atmospheric pressure the mixture can be overfilled and vented back down to atmospheric pressure. In the case where the additional driver gas pressure must be considered there is a minor error due to the sensitivity of the pressure transducer (discussed previously).

A more significant source of error is due to the natural fluctuations in atmospheric pressure. In order to minimize this error the combustion tube pressure transducer was regularly calibrated, however this does not account for daily fluctuations between calibrations. Based on observed fluctuation on a day to day basis this inaccuracy is typically 1 kPa. It was noted that

more extreme atmospheric changes (seasonal changes) can cause this fluctuation to be as high as approximately 2 kPa.

Ionization Probe Output Signal

The uncertainty associated with manually processing the ionization probe signals is a large source of error in this project. The ionization probes are used to provide flame time of arrival measurements in the form of distinct voltage drops. The times associated with these drops in voltage are manually recorded using a data probe tool in LabVIEW to accurately select the point at which the drop occurs. A sample signal that is very distinct is shown in Figure B. 1

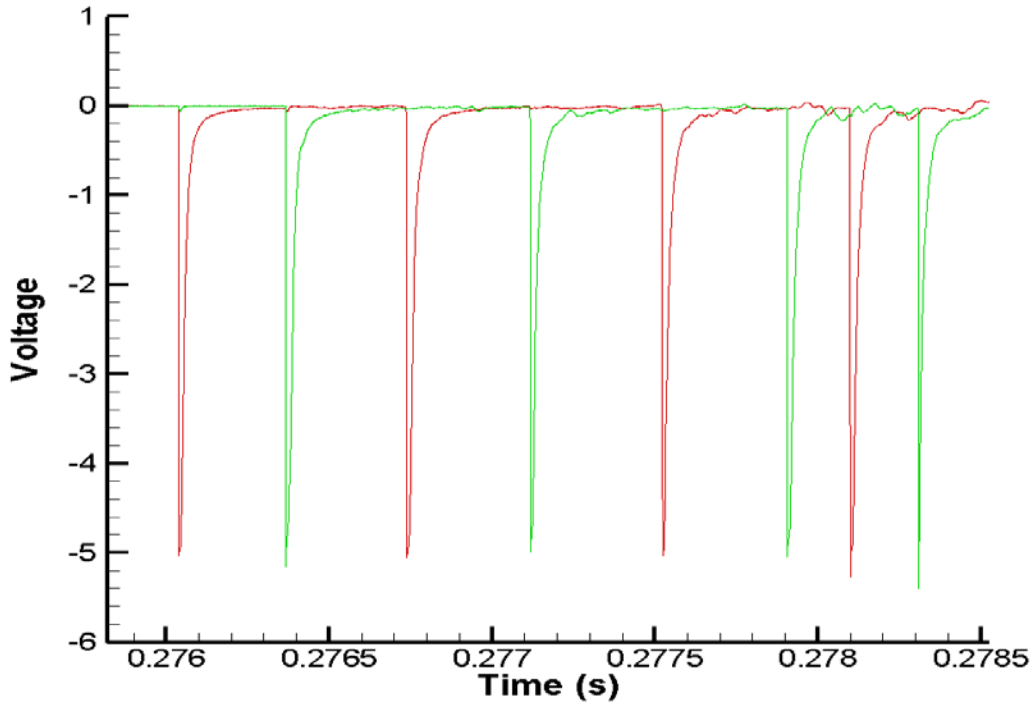

Figure B. 1: Distinct Ionization Probe signal (7.75% Acetylene Driver 3in orifice plates)

In test cases where the mixture is close to the propagation limit this signal is not always as distinct. An example of this is shown if Figure B. 2.

To remain consistent in the analysis of ion probe signals each signal is analyzed identically. The signal point for each probe is selected based on two criteria:

1. The signal is the strongest (largest and most immediate drop in signal if more than one drop is shown for an IP).
2. The start of the voltage drop (closest point to 0 V datum where the flame initially reaches the IP).

These two criteria are indicated on Figure B. 2. Based on these criteria a large amount of uncertainty with the analysis of IP signals can be mitigated. However, signals that are less regular than others will always provide a significant source of error. This type of error was quantified by taking several sets of measurements of the same signal and determining the standard deviation. This technique was used by Diakow et al. with IP signals in a similar experimental setup [45]. Using the IP signal from Figure B. 2 there is an uncertainty between repeated measurements of 0.31 %.

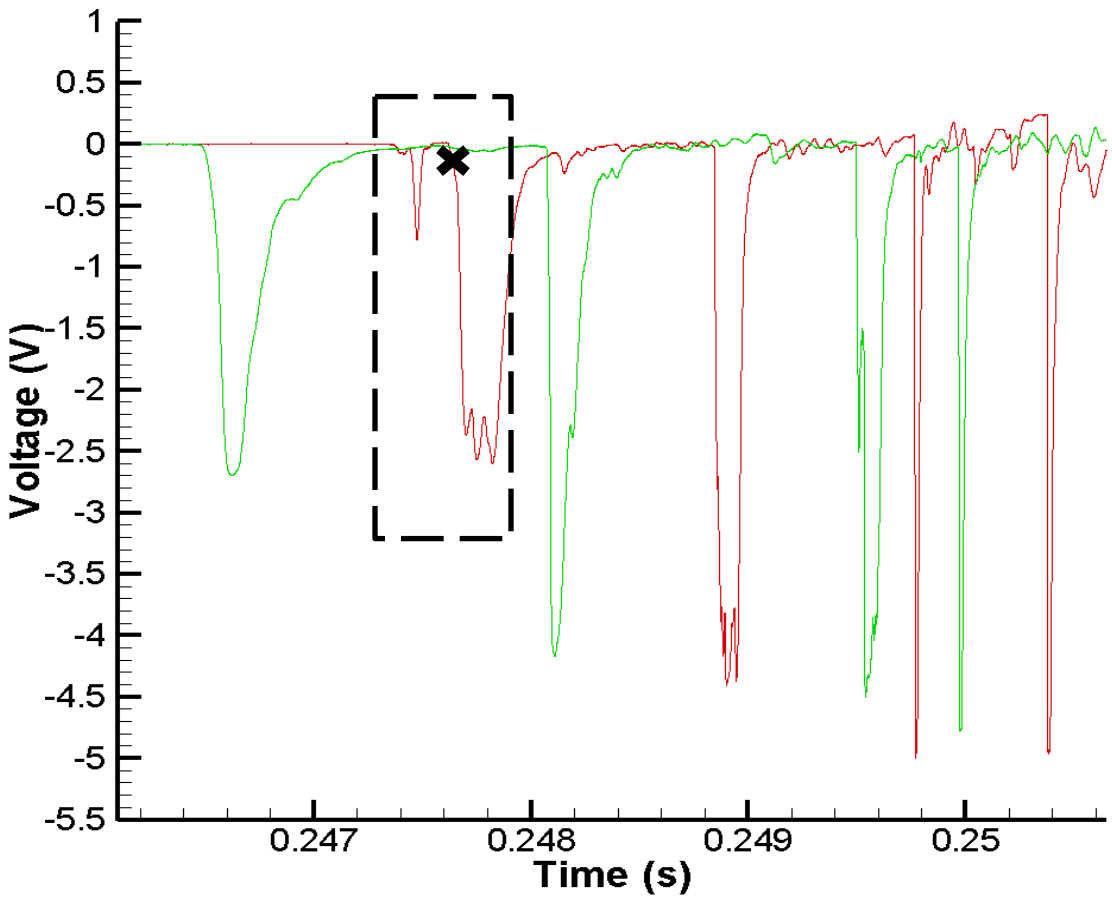

Figure B. 2: Indistinct Ionization Probe signal (8.75% DME DDT 3in orifice plates)

Determining Detonation Limits

The detonation limits shown graphically throughout this project were determined based on a "Go / No-go". That is to say if a single test is able to propagate at an average velocity above the isobaric speed of sound in the products it is considered able to propagate as a detonation. Average velocities are measured over a span of obstacles after a quasi-steady velocity is obtained in the obstacles. The plotted error bars represent the maximum and minimum velocity measured over the steady part of the velocity profile. For points with no error bars a velocity plateau was not achieved and the velocity based on the last two ionization probes was used. The total uncertainty associated with determining detonation limits is due to a combination of this quasi steady velocity and the mixture composition testing resolution. This testing resolution was limited

to a maximum of 1 % (Hydrogen Tests) and as little as 0.25 % for the remaining fuels. These testing resolutions were chosen based on the width of the detonability limits and are summarized in the results section of this report. Adding these two independent uncertainties together the total uncertainty associated with determining the detonation limits is approximately 1.25% by composition.

The validity of this experiment depends largely on the ability to consistently generate a planar CJ detonation wave prior to the orifice plate obstacle section. This aspect of the experiment was achieved by using a regulated amount of driver gas and measuring the wave velocity prior to the obstacle section. The specific amount of driver gas used for each fuel was determined by experimentation. Beginning with a small amount of driver gas the quantity was increased incrementally until a successful detonation was achieved prior to the obstacle section. This was done instead of recurrently using a large amount of driver gas to avoid interference with the combustion properties of the test mixture. This wave velocity was compared to a theoretically calculated CJ velocity, using STANJAN. If the two velocities were the same the test results could be considered valid. However, if the detonation wave was overdriven (velocity > theoretical CJ velocity) or under driven (velocity < theoretical CJ Velocity) the test data was void.